Annular Microfabricated Piezoelectric Tactile Sensor for Minimally Invasive Surgery

Nagarajan Narayanan Babu

A Thesis

In

The Department

Of

Mechanical and Industrial Engineering

Presented in Partial Fulfillment of the Requirements

For the Degree of Master of Applied Science at

Concordia University

Montreal, Quebec, Canada.

December, 2006

Your file Votre référence
ISBN: 978-0-494-28943-3
Our file Notre référence
ISBN: 978-0-494-28943-3

ABSTRACT

Annular Microfabricated Piezoelectric Tactile Sensor for Minimally Invasive Surgery

Nagarajan, Narayanan Babu

The commercially available endoscopic graspers are tooth like in order to grasp slippery tissues during a Minimally Invasive Surgery (MIS). However, they don't provide the tactile feedback to the surgeon during the operation. One of the most important requirements of a tactile feedback in MIS is softness sensing. This thesis presents the design, analysis, fabrication and testing of an annular microfabricated piezoelectric tactile sensor to determine the softness of tissues during MIS. This tooth-like sensor consists of an array of four sensors on each jaw of the endoscopic grasper. Each sensor consists of a rigid inner cylinder surrounded by a soft hollow cylinder. The sensor works on the principle of relative deformation between the inner rigid cylinder and the outer compliant cylinder. In this design Polyvinyledene Fluoride (PVDF) film is used as the sensing element.

The fabrication sequence of the sensor involves three steps, namely, fabrication of cylinders, PVDF film patterning and sensor assembly. The compliant cylinders are realized by micromolding of liquid silicone rubber. The PVDF film was patterned using photolithography techniques and the patterned portions are etched using commercially

available aluminium etchant. Different parts of the sensor are assembled under a stereomicroscope.

Different materials are tested under dynamic applied load and their modulus of elasticity has been found using the force ratio output from the PVDF sensing element. A 3D analysis in ANSYS has been done to compare the force ratios with the experimental values. It has been shown that good agreement exists between experimental and finite element results. A viscoelastic Kelvin model is employed for tissue characterization. A closed form expression is derived to express the relationship between the force ratio and compliance. Using the force ratios output from the experiments performed, the compliance of various soft materials in contact with the tactile sensor are obtained. These results are shown to be in close agreement with the manufacturer's value.

ACKNOWLEDGEMENT

The path to a Master's degree has been an exciting and winding one. The route was not always well illuminated, but there have been many people who provided guidance and support along the way. I am grateful for their time, friendship, and words of wisdom.

First I would start thanking my supervisors, Dr. Javad Dargahi and Dr. Muthukumaran Packirisamy for their invaluable support, suggestions at various junctures of this research work. The support which they offered both academically and financially will be remembered time and again. I would also like to thank Dr. Rama Bhat for his valuable inputs during the completion of journal works. I would also like to express my gratitude to the Mechanical Engineering support staffs, lab technicians and machinists for their timely assistance.

I have been fortunate enough to work with extremely talented and friendly members of the Tactile Sensors and Optical Microsystems Labs. I would like to express my sincere thanks to Mr. Ali Bonakdar, Mr. Saeed Sokhanvar, Mr. Reza Ramezani and Mr. Arvind for their assistance and friendly support during the length of my research work.

I will be whining for ever if I fail to thank my friends who have been with me through the times of good and crisis. I would like to thank all my friends with special thanks to Mr. Anand, Mr. Rakesh, Mr. Sujikumar, Ms. Uma, Ms. Hamsa and Ms. Ekta for their constant encouragement and making my stay in Montreal a pleasant one.

Last, but my no mean the least I would express my sincerest gratitude, love to my parents and my family for their continuous motivation and emotional support. I would like to thank my Mom Mrs. Bhuvaneswari, My Dad Mr. Babu Narayanan and My Uncle Mr. Bhaskaran Srinivasan who taught me the value of patience, hard work and commitment without which I couldn't have completed my Masters.

TABLE OF CONTENTS

LIST OF FIGURES

LIST OF TABLES

List of Acronyms and Symbols

LVDT	Linear Variable Differential Transformer
[k]	Element Stiffness Matrix
{d}	Element Nodal Displacement Vector
{D}	Electric Flux Density (C/m^2)
{E}	Electric Field Vector (V/m)
{F}	Force Vector for System
{f}	Element Nodal Force Vector
{S}	Strain Vector (Dimensionless)
{T}	Stress Vector (N/m^2)
{U}	Displacement Vector for System
°C	Degree Celsius
1-D, 2-D	One Dimensional, Two Dimensional
A/D	Analog to digital
AWG	American wire Gauge
B(t)	relaxation modulus in dilatation
C	Capacitance
c	Viscous Damping coefficient
d_{31}, d_{32}, d_{33}	Piezoelectric conistant
DAQ	Data Acquisition system
DC	Direct current
e	Piezoelectric Coefficient (C/m^2)

$\vec{E}$	Modulus of Elasticity
E1	Young's modulus of object under investigation
E2	Young's modulus of compliant cylinder
F1	Force carried by the inner rigid cylinder
F2	Force carried by the outer compliant cylinder
Fy	Force applied in Y direction
$G(t)$	shear relaxation function
g_{31}, g_{32}, g_{33}	Piezo Coefficient Related to the Voltage (V-m/N)
g_i	spring modulus
GPa	Gigapascal
Hz	Hertz
IC	Integrated Circuit
IR	Infrared
$J_1(t)$	creep compliance
$J_2(t)$	volumetric compliance
L	Length of membrane
lbf	Pound force
LIGA	X-Ray Lithography
LSR	Liquid silicone rubber
MEMS	Micro Electro Mechanical Systems
MIS	Minimal Invasive Surgery
MPa	Megapascal
MR	Magnetoresistive

MST	Micro-systems Technology
N	Newton
pC	Picocoulumb
PR	Photoresist
PVDF	Polyvinylidene Fluoride
PVDF-1	PVDF under the inner rigid cylinder
PVDF-2	PVDF under the outer soft cylinder
PZT	Lead Zirconate Titanate
Q	Charge
r	Density
R	Radius of rigid Cylinder
R1	Inner Radius of Compliant cylinder
R2	Outer Radius of Compliant Cylinder
s_0	step change of deviator stress
s_{ij}	deviator stress
SNR	Signal to noise ratio
t	time
T1	Thickness of sensed object
T2	Rigid and compliant cylinder height
UV	Ultraviolet
V	Voltage
V1	Voltage output of PVDF under Inner cylinder

V1	Voltage output of PVDF under the outer cylinder
VLSI	Very large scale Integrated circuit
W	Width of Piezoelectric crystal
X1	Deformation of sensed object over rigis cylinder
X2	Deformation of the compliant cylinder
δ_{ij}	Kronecker delta
ε_{ij}	strain
η	dashpot viscosity
μm	Micrometer
Ω	Ohms

1. CHAPTER

INTRODUCTION AND LITERATURE REVIEW

We use our hands every day to assess the size, shape, and texture of objects. We sense and interpret tactile stimuli from our environment and perform tasks with our hands in a nearly instinctual manner. The ability to discriminate among surface textures, sense incipient slip, and roll an object between fingers without dropping it can be attributed to the specialized mechanoreceptors in the hand. These touch receptors possess unrivaled range and acuity. They respond to both static and dynamic stimuli as well as temperature and pain. We are also equipped with reflexes and automatic responses (e.g., grasp force regulation) that allow us to make use of tactile information without expending cognitive effort. Despite the obvious importance of tactile cues in our everyday lives, the subject of tactile sensing for teleoperators, virtual reality, and more generally, its application in medical field has recently received significant impetus.

This thesis presents a novel method of tactile sensing. The goal of this research is to bring the level of tactile sensitivity and acuity that humans possess to telemanipulators and other medical applications especially in minimally invasive surgery. Since the designed sensor is tooth-like it is being developed for application in minimally invasive surgery after integration with the endoscope tools.

1.1 Minimally invasive Surgery

A decade ago, Minimally Invasive Surgery (MIS) was just being introduced in general and thoracic surgery. Today, MIS has become a standard surgical procedure, often replacing traditional open surgery and has also become widely accepted. Traditional surgery requires an incision large enough for the surgeon to see directly and place his or her fingers and instruments directly into the target operating site [1]. Most often, the damage done to skin, muscle, connective tissue, and bone to reach the region of interest causes much greater injury than the curative procedure itself. This results in more pain to the patient, longer recovery time, and complications due to surgical ordeal. The current trend is accelerating toward minimally invasive surgery (MIS), in which unnecessary trauma in conventional surgical procedures is limited by reducing the size of incisions to less than about 1 cm or by using catheters or endoscopes threaded through vessels, the gastrointestinal tract, or other tubular structures. In addition, they can even extend the surgeon's capability over great distances, via telesurgery.

The first endoscopic cholecystectomy which is the removal of the gallbladder was done in 1987. Gallbladder removals, along with appendectomies, are some of the most common minimally invasive procedures in practice. Keyhole approaches are used in a number of other fields - cardiology, urology, neurology, gastroenterology, gynecology, and many others. Companies have designed a number of endoscopes for specific operations. For instance, the laparoscope is used for surgery in the abdomen. Heart surgeons use a thoracoscope to examine the interior of the chest.

MIS is a procedure carried out by a surgeon through a small incision using specialized equipment and endoscopic or other visualization techniques not requiring direct access. Traditional surgical approaches have utilized incisions designed to provide the maximum exposure of the operative site. Minimally invasive surgical approaches, on the other hand, utilize small incisions through which cameras and instruments are passed to accomplish the operation from within a body cavity. The minimally invasive surgical approach offers several advantages over traditional open surgery. Surgeons skilled in minimally invasive surgical procedures regularly perform them as rapidly as they perform the equivalent open operations. Furthermore, the reduction in inpatient hospital stays results in an actual lowering of total hospital costs for many of the procedures performed. Figure1. below shows some of the minimally invasive surgical tools being currently used.

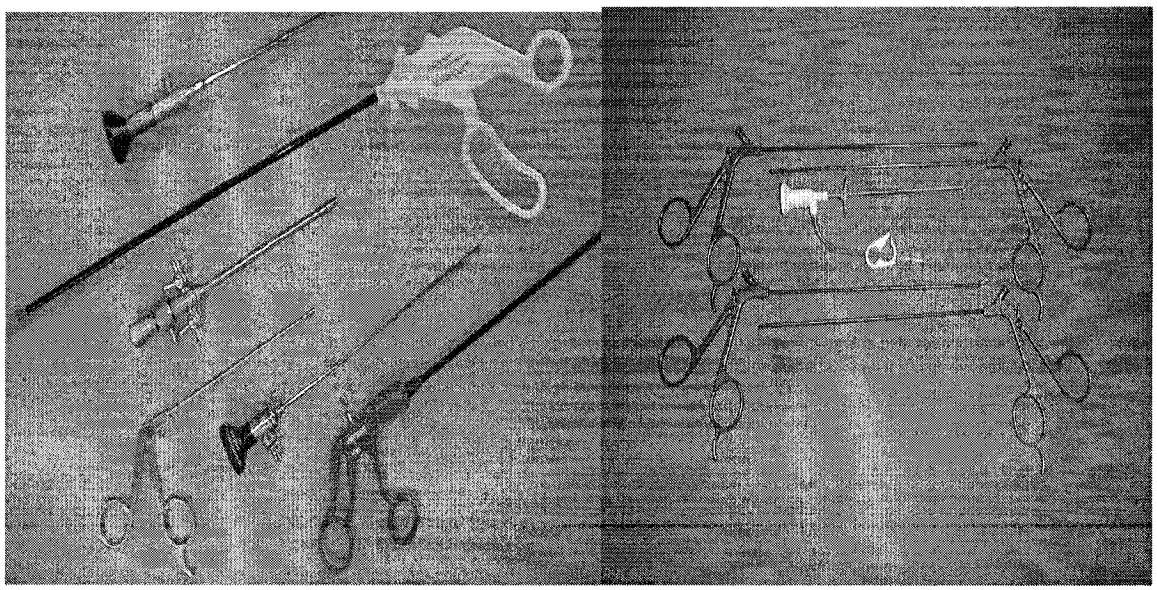

Figure 1-1Typical Minimally Invasive tools. A rod running the length of the instrument shaft connects the motions of the scissors grip handle with the jaws of the gripper. Internal tissues are grasped by passing the instrument through a small incision in the patient's body [2].

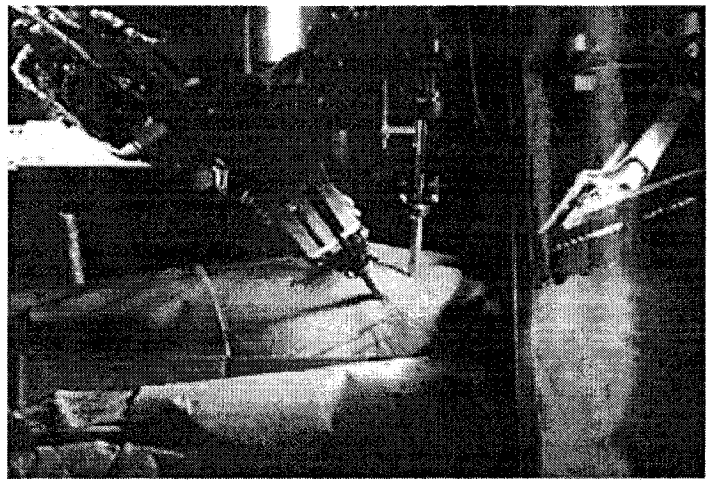

Figure 1-2 A typical Endoscopic Surgery Scene [3]

Some of the benefits of minimally invasive surgery are enumerated below [1].

1.1.1 Minimally Invasive Surgery Benefits

- Smaller incisions
- Less blood, less scarring
- Less pain during recovery
- Some procedure performed on an outpatient basis
- Faster recovery
- Quicker return to everyday activities
- Shorter hospital stays
- Better clinical outcomes
- Fewer complications due to infection

With MIS we can do the following operations which are done by traditional surgeries in a more effective way.

1.1.2 More Surgical Option

- General Surgery
- Gynecology
- Orthopedics
- Plastic Surgery
- Thoracic Surgery
- Vascular Surgery

The other side of MIS, unfortunately, from the surgeon's point of view, is the lack of tactile feedback that is used to apprise the surgeons about the tissues, bones, organs within the operative site. As a result of this loss, the surgeons will not be able to manipulate important properties of the tissues such as the softness, compliance, surface texture at the site of the operation.

1.2 Tactile Sensing

Tactile sensing is defined as continuous sensing of variable contact forces. The tactile sensation may be defined as sensing ability of human finger [4] (force, hardness, temperature, and roughness). Surgery is perhaps the most exciting and rapidly developing area where tactile sensing is actually of central importance. The reason that tactile sensing is so important in surgery is that, soft tissue can only be properly examined and identified by assessing its softness, viscosity and elasticity properties. The palpation of tissues and organs is an essential procedure that surgeons value highly.

Minimally Invasive Surgery is only 10 years old and now routinely used as the preferred choice for many operations. However, despite its advantages, MIS severely

reduces the surgeon's sensory perception during manipulation. Surgery is essentially a visual and tactile experience and any limitation on the surgeon's sensory abilities are most undesirable.

To perform the MIS more effectively, the surgeon should be able to feel the tissue, sense the pressure of blood vessels and ducts during the procedure. This ability is of great use during the manipulation tasks, such as, the grasping of the internal organs, gentle load transfer during lifting, suturing and removing tissues [5]. The need to feel the tissue and its softness is particularly important during operation. In MIS surgery, stereoscope vision and tactile information about tissue consistency are no longer available to the surgeon. To compensate for these sensory deficits, various tissues can be characterized with an electromechanical sensor that records their properties. In future, these sensors will be integrated into surgical instruments, providing the surgeon with information about tactile properties of tissue [6]. Advancement in this regard where there is an artificial process developed, which can restore the tactile feedback to the surgeon, will be of great benefit. Figures 3 and 4 describe the tactile sensor application in MIS.

In laparoscopy, long slender tools are inserted through small puncture openings in the abdominal wall and the surgeon uses a range of tip mounted instruments guided by video feedback images. As the instruments are rigid rods and effectively have fixed pivots at the entry points, the available degrees of freedom are restricted and therefore demand extra operator expertise. It is clear that tactile sensing is greatly needed in this area.

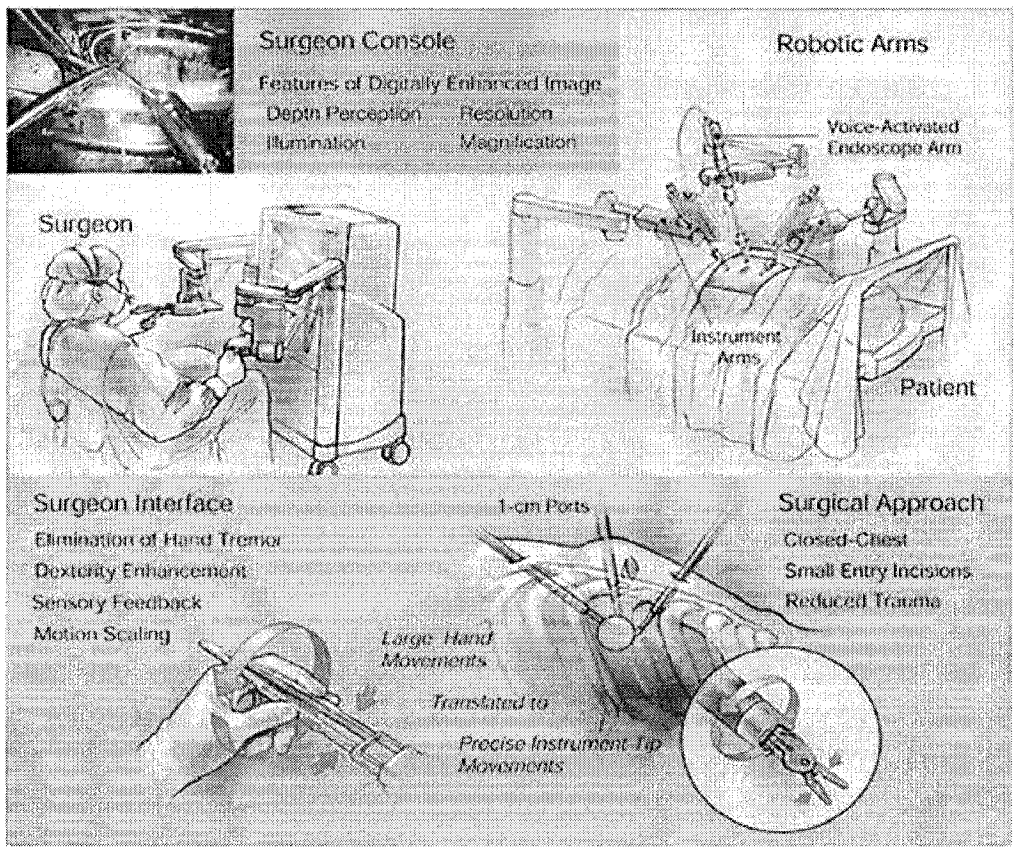

Figure 1-3Tactile sensor application in MIS and robotic surgery [7]

Surface texture and roughness perception of various tissues are also important for inspecting of texture of tissue by endoscopic grasper during MIS surgery. Texture perception is different from roughness. To find out the surface texture perception, the tactile sensor must be capable of measuring the roughness, compliance and viscoelastic behavior. Since tissue is viscoelastic and behaves non-linearly, sensor must be capable of measuring compliance as function of time so that the viscoelastic properties of the tissue can be ascertained [8]. Till now very little work has been done in the field of viscous behavior of tissue. A lot of work has been done for tactile perception of the tissue during minimal invasive surgery and perception of their elastic behavior.

The range of precision necessary for tactile sensing in minimally invasive surgery range from microns to few millimeters. The present day tactile sensors to be employed in a MIS must have small size, high sensitivity, low manufacturing cost, and the possibility of being disposable after a surgery. The thoughts of integrating all these aspects led to the utilization of microfabrication and MEMS in the field of tactile sensing and MIS.

1.3 MicroelectroMechanical System [MEMS]

The term MEMS is an abbreviation of MicroElecroMechanical System. "Micro Electro-Mechanical Systems" is a class of sensors, actuators and micromachines that are physically small. These systems have both electrical and mechanical components. The MEMS fabrication technologies include fabrication of different electrical and mechanical components on a single common substrate [9].

MEMS and microsystems have become increasingly dominant in every aspect of commercial marketplace as the technologies for microfabrication and miniaturization continue to develop. At present there are many major commercial markets for MEMS such as computer storage systems, automobiles, biomedical, Micro fluidics and genetic engineering. Many predict that biomedical industry will be the major user of Microsystems after the automotive industry [9]. The term **BioMEMS** has been used extensively by the MEMS industry and academe in recent years [10]. The applications of MEMS in different areas are represented by Figure.5.

The core element in MEMS generally consists of two principal components: a sensing element or an actuating element and a signal processing unit. Micro sensors are built to sense the existence and the intensity of certain physical, chemical, or biological quantities such as temperature, pressure, force, sound, light and chemical compositions.

Micro sensors have the advantage of being sensitive and accurate with minimal amount of required sample substance. They can be mass produced in batches with large volumes.

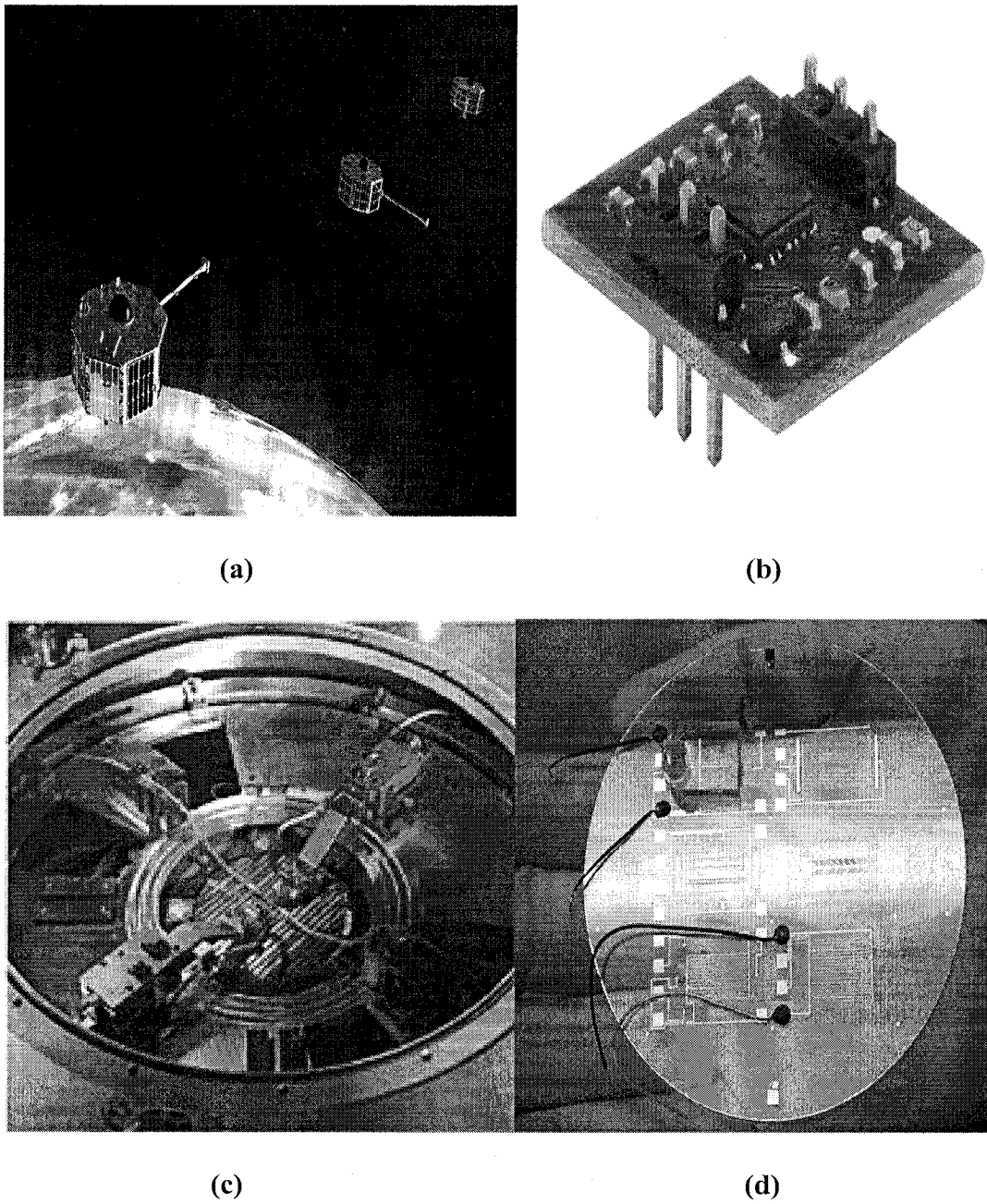

Figure 1-4Different applications of MEMS (a) Micro satellites [69] (b) Accelerometers [70] (c) RF MEMS [71] (d) Microfluidics [72]

There are many types of micro sensors developed for different applications and are widely used in industry [9]. Common sensors include biosensors, chemical sensors, optical sensors, thermal and pressure sensors. Biosensor and biomedical sensors will have significant share in the microsensors market in the near future [10]. Micro biomedical sensors are mainly used for diagnostic analysis and these sensors require minute amount of sample and produce significant results faster than the traditional biomedical instrument [9]

The MEMS fabrication technology can be applied in the field of tactile sensing to produce very tiny micro tactile sensors which can be manipulated according to the surgeon's convenience. These micro fabricated tactile sensors are creating revolution in the field of minimally endoscope surgery. The advantages of miniaturization of the sensors include improved dexterity of the surgical tools. Moreover, these sensors can be produced in batches, resulting in a low unit cost and also can be disposable.

1.4 Literature Review

Many researchers have done work on the grasper force and perception of the elastic behavior. In the following section previous works on this topic are discussed.

1.4.1 Minimally Invasive Surgery

Surgeons have been known to insert their fingers through the access openings during MIS simply to perform direct tactile exploration [11]. Dario's short but far-sighted review [12] cites medical applications in which the hardness of soft tissues is detected through palpation. However, Bicchi et. al.[13], have discussed capacitive tactile sensor

and associated tactile display unit for use in MIS. By correlating force against deformation, the system was able to identity five objects of different elastic properties.

A series of designs for endoscopic and laparoscopic tools are discussed by Cohn et al., [14] who intend incorporating their tactile telepresence apparatus. An interesting idea raised here is the possibility of using the capacitive tactile sensor, not to measure applied force, but to detect the varying dielectric permittivity of different tissue. Cohn et. al., suggest that water, fat, blood vessels, and cancerous tissue might all be discriminated by this means.

An experiment with a sensor for laparoscopic attachment has been described by Fischer et. al., [15]. A 64 point sensor of area 1 cm^2 was connected to a fingertip vibrotaction display.

Dizaji et al. [16] developed a new cancer diagnostic approach by ultrasonic imaging of tissues in which the tissue elasticity is measured and compared with the elasticity of normal tissues. The results of displacement estimation of normal and abnormal breast tissues under external stress are calculated using image registration technique. The work estimates not only the translation, but also the rotation and scaling parameters. The Youngs modulus calculated from displacement values was then used to identify tissue characterization. The work also showed that the above-mentioned procedure can successfully detect abnormal tissues. The latest developments in minimally invasive hapatic surgery were described by Guillaume et al. [17], a new deformable model based on non-linear elasticity and the finite element method was proposed. This model is valid for large displacements, invariant with respect to rotations and therefore improves the realism of the deformations and solves the problems related to the

shortcomings of linear elasticity that is only valid for small displacements. Problems associated with anisotropic behavior and volume variations were also addressed. Gladilin et al. [18] used a physical model based approach, where in a finite element based modeling scheme was implemented for static soft tissue prediction and muscle simulation. .

In their work, Tritto et al. [19] used vascular fractal geometries to describe the coupling between elastic network deformation and vascular branching pattern modification under simulated controlled skin expansion. The work also tested the role of elastic organization of the skin, the interrelation between skin tension, line orientation, pedicle axis and the apparently random proliferation of the branching vascular pattern.

1.4.2 Tactile Sensing

The ultrasonic tactile method is entirely non-destructive in its use as a sensor. A microrobot was designed for colonoscopy using a pneumatic inchworm propulsion method described by Dario et. al., [20]. The difficulties of adopting totally autonomous robotic systems in surgery are discussed by Howe et. al., [21] and an approach is developed where the surgeon maintains supervision and control but is constrained from driving the cutting tools outside force limited regions.

Silva et. al., [22] developed the strain gauge type tactile sensor for measuring finger force. It was constructed using metallic strain gauges. It is rugged, has linear response, good repeatability, resolution of 0.3 N, low hysteresis and sensitivity of 0.12 V/N.

Shinoda et. al., [23] design the acoustic cell ultrasonic sensing matrix which are placed face to face. They used this sensor for mounting on the robots finger with 5-D

deformation. Sensor measured 10μm displacement by 18.5 mm cell height and 0.001 rad change in surface inclination. This sensor can measure contact force and as well as slip of the grasped object.

Dargahi et. al., [24] developed the prototype for tactile sensing system with only three sensing element "PVDF". The magnitude and position of force is obtained by using triangulation approach combined with membrane stress. The lack of agreement between theoretical and experimental results could be attributed both to the experimental errors and the assumption in the theoretical analysis. Ohka et. al., [25] developed the optical tactile sensor equipped with an optical wave guide plate mounted on a robot manipulator. The experimental results confirmed that the tactile sensor is capable of detecting the distribution of three axis force and that the calculated and experimental results coincide well. This tactile sensor comprised a CCD camera, light source, an acrylic board and a silicon rubber sheet that are assembled into a casing. So the feasibility of using in miniaturization is very low. Providing light source with endoscope is a new problem to overcome.

Obana et. al., [26] designed a semiconductor strain gauge tactile transducer. It was designed with the goal of measuring finger force without affecting the hand dexterity. Semiconductor strain gage was used due to its small size, and high sensitivity, but it has high temperature sensitivity. The transducer has both dynamic and static responses, hysteresis is negligible and linearity is good. Force sensitivity was 0.05 V/N. This sensor is ideal for measuring the force applied on the tissue. But the problem is to find out the softness of tissue and to avoid tissue damaging. Howe et. al., [27] also designed capacitive tactile array sensor which is based on an earlier design of Fearing [28]. This

device measures the pressure distribution at the contact between the robot hand and the grasped object. Experiments confirm the system's ability to convey significant contact information.

Payandeh et. al., [29] designed haptic interface for endosurgery. The design consists of tunable spring based on the haptic and surgical requirements. Simulation and experimental results demonstrated the practicality of such design concept.

Petter et al. [30] developed a new tactile measurement system, which is capable of differentiating the hardness of various soft materials like living tissues. The system measures the mechanical frequency response of the tissue. It is intended to integrate this "vibrotactile sensor" inside the top of a tactile rod for endoscopic surgery, in order to provide the surgeon a substitute for the missing tactile feeling. Locating arteries hidden beneath superficial tissue is a difficult task in MIS. Ryan et al. [31] developed a system, that can find the paths of arteries using tactile sensing in MIS. The surgeon begins by using the surgical robot to place the tactile sensor instrument on a known artery location. Signal processing algorithms locate the artery from its pulsatile pressure variation. The problems with compliance in the system result in occasional loss of the artery path. To perform MIS effectively, surgeons should be familiar with the quantitative assessment of the biomedical properties of soft tissues. Many different layouts were proposed and designed for examining the tissue behavior while performing minimal invasive surgery. Yongping et al. [32] developed an ultrasound indentation system with a pen-size hand held probe that is used to obtain the indentation responses of lower limb soft tissues. A linear elastic indentation solution was used to extract the effective Young's modulus that ranged from 10.4 to 89.2 kPa for soft tissues. The Youngs modulus determined was

demonstrated to be significantly dependent on site, posture, subject and gender. No significant correlation was established between the effective Youngs modulus and the thickness of entire soft tissue layers.

1.4.3 Micro Tactile Sensors

Gray and fearing et. al., [33] have reported on an array of microtactile capacitive sensors for use as an endoscopic-surgery telemanipulator for sensing organic tissue on small scale. The eight by eight tactile capacitive array sensors were used for detection of sub-millimeter features and objects, where the entire sensor array is smaller than normal human spatial resolution of 1mm. The sensor has capability of detecting milliNewton force and good interpolation between elements. The sensors had severe hysteresis problems, but no detectable proximity effects. Due to hysteresis problem the results were not reliable.

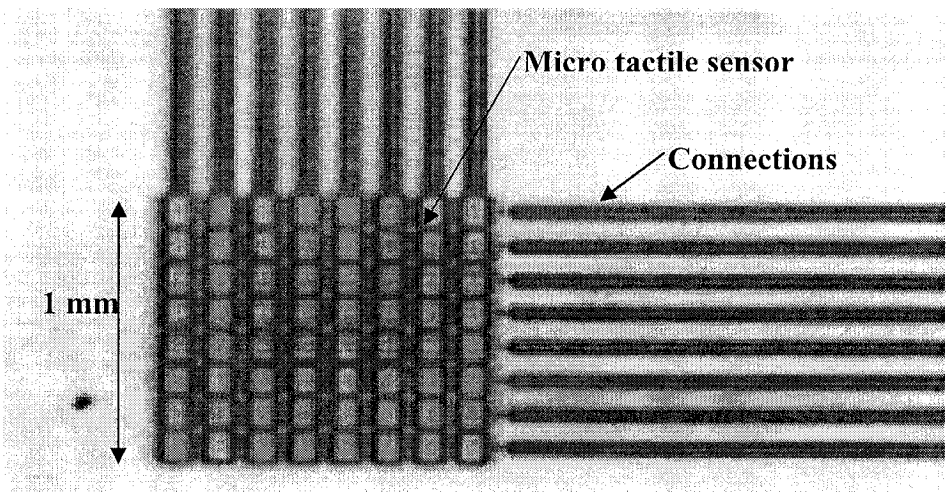

Figure 1-5 Microscope Photo of Entire 1 mm^2 Array [33]

Manish et al. [34] designed and fabricated a capacitive micromachined endoscopic teeth-like pressure sensor. But the sensor only measures a few grams of the

applied force and secondly there is no provision available to measuring compliance of tissue. Dargahi et. al. [35] have designed and fabricated a micro machined robust piezoelectric endoscopic tooth like tactile sensor with good linearity and a high dynamic response. Sensor may be damaged due to application of shear stress along the sensor while handling the tissue. The sensor lacks DC response due to the nature of the PVDF films. Dario et. al., [36] have constructed a tactile sensor, which can discriminate amongst various complaint objects.

Recent studies have focused on the development and control of a microgripper based on flexure joints, fabricated by LIGA and instrumented with semiconductor straingauge force sensors [37]. Straingauge sensors located at the tip of the micro-gripper provide useful information for force control of the microgripper in biomedical applications. Majority of tactile sensor technologies have focused on silicon based sensors that use piezoresistive [38, 39] or capacitive sensing [40, 41] and polymer-based approaches that use piezoelectric polymer films [42, 43] for sensing. Engel et al. [44] developed a polyimide-based two-dimensional tactile sensing array realized using a novel inverted fabrication technique. This is the first tactile sensor array based solely on polymer micromachining and thin-film metal resistors. The main advantages of this approach include increased robustness, decreased fabrication cost and complexity, low-temperature processing and improved strain transfer from membrane to strain gauges [45]. Shinoda et al. [46] have developed ultrasonic emission tactile sensor that is capable of quick localization of touch and detouch, sensation of texture under movement and detection of precursor.

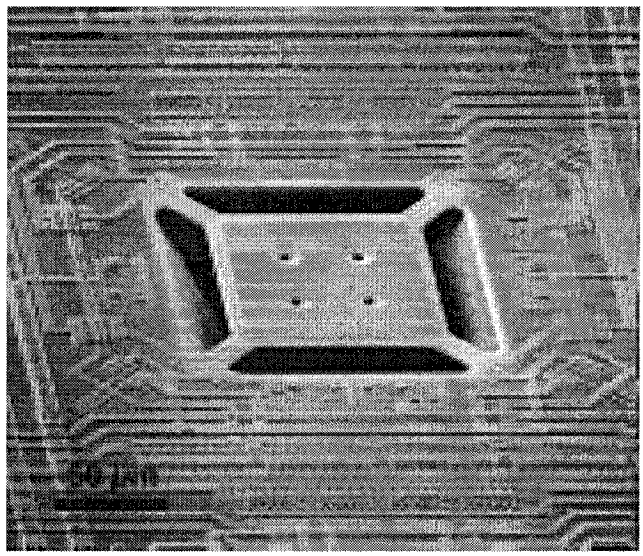

Figure 1-6 canning electron micrograph of a single traction stress sensor consisting of a suspended plate / bridge structure with four embedded polysilicon resistors [53].

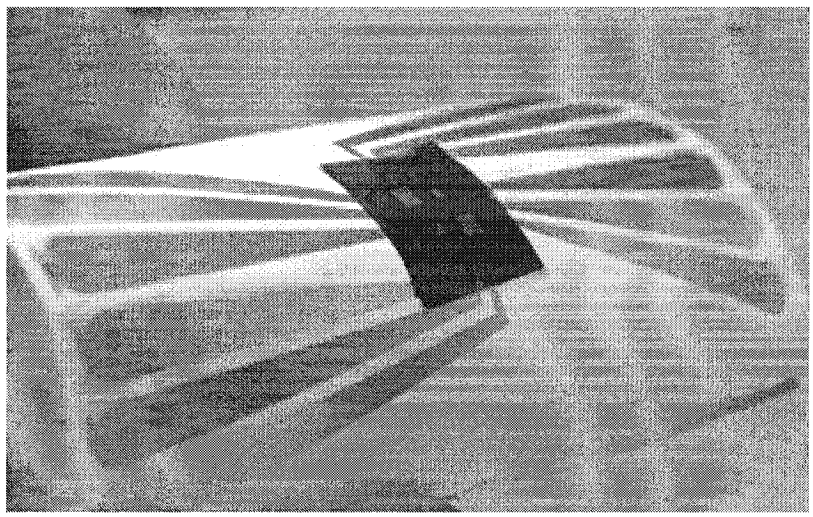

Figure 1-7 A flexible polymer tactile sensor [54].

Although technology has rapidly progressed in the area of robotic end effector sensors, few researchers have attempted to specifically address the problems associated with tactile sensing in a clinical setting. Recent technological advances have provided small and thin sensors having promise for use in directly measuring individual finger

forces during normal grasping activities. However, conventional force measurement sensors are inadequate for measuring hand forces produced during manual work activities and activities of daily living.

Reston and Kolesar [47] have constructed a 5X5 robotic tactile sensor based on piezoelectric polyvinylidene fluoride (PVDF) film coupled to an integrated circuit. Although the array provided a linear output, its limited range and inability to measure static forces makes it a poor choice for a finger mount tactile sensor. Germagnoli *et al.* [48] developed a fingertip 8X6 array sensor sensitive to all six independent stress tensors by careful orientation of PVDF sensing elements. The sensor sensitivity is low and requires amplification close to the sensor to achieve an adequate signal-to-noise ratio. The Lord Industrial Automation (Covy, NC) [49] sensor is a commercially available optical force sensor. However, the sensors are too thick (28.4 mm) to be useful in finger-mounted applications.

Suzuki et al. [50] developed a silicon tactile imager based on an array of capacitive cells. Samaun et al. [51] developed an early piezoresistive-pressure sensor which could be catheter mounted. Lee and Wise [52] developed a silicon capacitive pressure sensor. Tanigawa et al. [53] developed a silicon pressure sensor with on-chip signal processing. Kane and Kovacs report a tactile sensor capable of high-resolution imaging. The sensor uses a CMOS compatible process and can resolve both normal and shear stress. However, all of these sensors have a thin diaphragm and most target the problem of tactile imaging and are, thus, unsuitable for measuring finger and hand forces in clinical applications.

Atkinson et al. [54] have fabricated a MEMS tactile sensor using a novel high temperature piezoelectric polyimide material which can measure the tactile information over a non planar geometry. These devices have the potential to offer high temperature tactile sensor performance than conventional fabricated sensor

Tao Mei et al. [55] have developed a robust MEMS integrated three-dimensional tactile sensor with soft contact surface and large force range. The sensor uses an over-stop design to increase the robustness for overloading and has CMOS integrated piezoresistive sensing elements and on-chip data-reading circuitry to reduce total sensor volume.

1.5 Objective and Scope of Research

Although many tactile sensing systems based on different technologies were designed and tested, very little work has been done in the field of viscoelastic analysis of tissue behavior during tactile sensing. This thesis presents the design, analysis, fabrication and testing of an annular micromachined piezoelectric tactile sensor to determine the softness of tissues during MIS. This tooth-like sensor consists of an array of four sensors on each jaw of the endoscopic grasper. Each sensor consists of a rigid inner cylinder surrounded by a soft hollow cylinder. The sensor works on the principle of relative deformation between the inner rigid cylinder and the outer compliant cylinder. In this design Polyvinyledene fluoride (PVDF) film is used as the sensing element.

A viscoelastic Kelvin model is employed for tissue characterization. A closed form expression is derived to express the relationship between the force ratio and compliance. The model of tissue was assumed as the soft rubber object with different

compliance. The viscoelastic behavior of tissue was not taken into consideration while testing sensed object. The objectives of the research are summarized below as:

1. Design of the piezoelectric tactile sensor with good sensitivity and linearity for measuring force and compliance of tissue.
2. Develop an analytical model to understand viscoelastic properties of tissues.
3. Develop Micro- fabrication techniques and test prototype tactile sensor.
4. Compare the theoretical and experimental results.

1.6 Overview of the Thesis

Chapter 1 gives an overview of minimally invasive surgery, tactile sensing and microelectromechanical systems. It enumerates the various contributions by different people in the field of tactile sensing and minimally invasive surgery over the last decade. Further it states the objective and the scope of the research as enumerated in the subsequent chapters.

Different force measuring devices are discussed in the Chapter 2. The selection and decision for using the piezoelectric sensor also are discussed at the end of the chapter. It also discusses the design of the sensors. The single sensor design and four sensors mounted on the grasper with common base are discussed along with the properties of materials used.

Chapter 3 discusses the microfabrication of the sensors. It also briefs on how the different parts of the sensor are realized and are assembled together.

Chapter 4 deals with the analysis of the sensors. The 2D and 3D design of the single sensor were discussed using mathematical approach and simulation in ANSYS,

respectively. The results of force ratio variation with different material softness also are presented.

In Chapter 5, the experimental setup, calibration of the instruments and procedure used for the data acquisition are discussed. At the end of the chapter, the experimental and theoretical results are compared. The comparison of single sensor, common base sensor is also compared pictorially.

In Chapter 6, the conclusion and summary of the theoretical and experimental work are presented. The drawbacks of sensors with future suggestion and recommendation are also discussed.

At the end of thesis, an appendix is provided for covering the details of the related work. The Appendix I discusses about the properties and behavior of the PVDF materials. Finally, Appendix II discusses about the sensor characteristics i.e. SNR, sensitivity, temperature drift etc that are presented in this section.

2. CHAPTER

SENSOR DESIGN

2.1 Technologies for Tactile Sensor

There are many physical principles that can be exploited for the development of tactile sensors. As the technologies involved are very diverse, this chapter considers only the generalities of the technology involved. The development in tactile sensing technology is application driven and the operation of a tactile sensor is dependent on the material of the object being grasped.

2.1.1 Capacitive sensors

Capacitive sensors make use of the change in capacitance between two electrodes. The membrane electrode deflects when pressure is applied, which causes the distance between the two electrodes changed. The capacitance change is the measure of the pressure exerted on the membrane. Despont et al. [56] had designed a silicon based capacitive pressure sensor. The electrodes in this are made of a planar comb structure. The sensor element comprised of two parts: first, a movable elastic structure that transforms a force into a displacement, and second, a transformation unit consisting of electrodes that transform the displacement into a measurable change in capacitance. By separate measurement of the capacitance changes on sides, high linearity and sensitivity were obtained. Compared to piezoresistive sensors, capacitive sensors have better long term stability, higher sensitivity and no hysteresis. However, the advantages of capacitive

pressure sensors go along with more complex signal processing and higher production costs.

2.1.2 Conductive Elastomer sensor

Compliant materials that have a defined force resistance characteristic have received a lot of attention in tactile sensor research. The basic principle of conductive elastomer sensors lies in measuring the resistance of a conductive elastomer or foam between two points. The majority of sensors use an elastomer that consists of a carbon-doped rubber. Fig 2.1.shows the schematic of a conductive elastomer sensor.

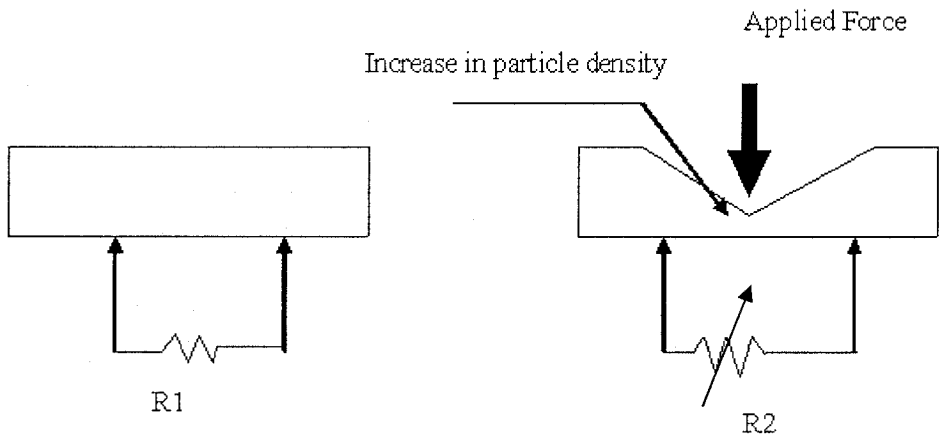

Figure 2-1 Schematic of a conductive elastomer

In the above sensor, the deformation due to the applied force changes the particle density and thereby changing the resistance of the elastomer.

2.1.3 Magnetic based sensor

A magneto resistive or magneto elastic material is a material whose magnetic characteristics change with an externally applied physical force. Magneto elastic sensors have a number of advantages such as, high sensitivity and dynamic range, no measurable mechanical hysteresis, a linear response, and physical robustness. Of the two approaches to designing of tactile sensors based on magnetic transduction, the first one is based on the principle that the movement of a small magnet by an applied force will cause the flux density at the point of measurement to change. The observed change in flux density can then be measured using Hall effect or by a magneto resistive device. The second approach involves the fabrication of the core of a transformer or inductor from a magneto elastic material that will deform under pressure and cause the magnetic coupling between the transformer windings to change. If a very small permanent magnet is held above the detection device by a complaint medium, the change in flux caused by the magnet's movement due to an applied force can be detected and measured. The field intensity follows an inverse relationship, leading to nonlinear response, which can be easily linearized by processing. A tactile sensor using magneto elastic a material consists of material bonded to the substrate, and is used as a core for an inductor. As the core is stressed, the susceptibility of the material changes, which is measured as a change in the coil inductance.

2.1.4 Optical Sensors

The rapid expansion of optical technology in recent years has led to the development of a wide range of tactile sensors. The operating principles of optical-based

sensors are well known and they fall into two classes: Intrinsic, where the optical phase, intensity, or polarization of transmitted light are modulated without interrupting the optical path and Extrinsic, where the physical stimulus interacts with the light external to the primary light path.

Intrinsic and extrinsic optical sensors can be used for touch, torque, and force sensing. For industrial applications, the most suitable will be that which requires the least optical processing. For robotic touch and force-sensing applications, the extrinsic sensor based on intensity measurement is the most widely used due to its simplicity of construction and subsequent information processing.

Touch and tactile optical sensors have been developed using a range of optical technologies. The force sensitivity in the optical sensor is determined by a spring or elastomer. To prevent cross talk from external sources, the sensor can be constructed around a deformable tube, resulting in a highly compact sensor. A Schematic of an optical sensor is shown in Fig 2.2.

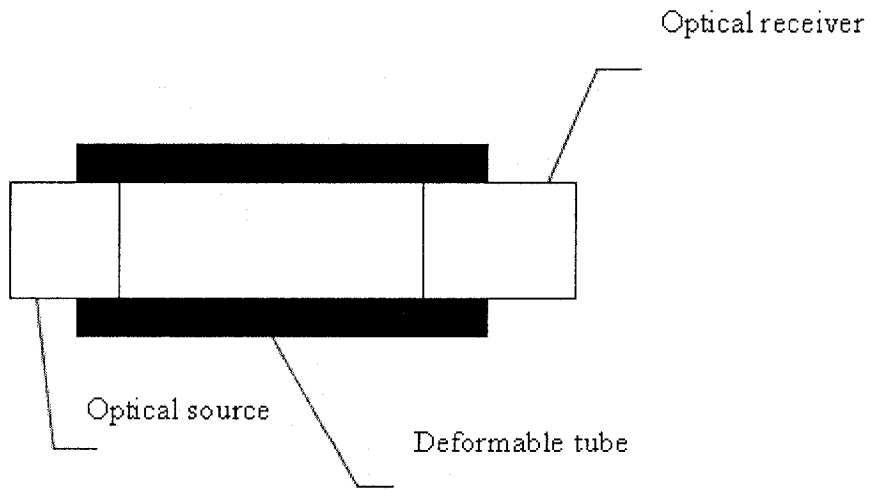

Figure 2-2 Optical Sensors

2.1.5 Strain Gauge Sensor

Strain is the amount of deformation undergone by a body due to an applied force. More specifically, strain (ε) is defined as the fractional change in length. There are several methods of measuring strain and the most common being the use of a strain gauge which is a device whose electrical resistance varies in proportion to the amount of strain in the device. The most widely used gauge is the bonded metallic strain gauge. The metallic strain gauge consists of a very fine wire or, metallic foil arranged in a grid pattern. The grid pattern maximizes the amount of metallic wire or foil subject to strain in the parallel direction. The cross sectional area of the grid is minimized to reduce the effect of shear strain and Poisson Strain. The grid is bonded to a thin backing, called the carrier, which is attached directly to the test specimen. The strain experienced by the test specimen is transferred directly to the strain gauge, which responds with a linear change in electrical resistance. Strain gauges are available commercially with nominal resistance values from 30 to 3000 Ω, with 120, 350, and 1000 Ω being the most common.

2.1.6 Piezoelectric Sensors

A Piezoelectric material may be defined as one that produces an electrical discharge when subjected to a mechanical deformation or undergoes a mechanical deformation when subjected to an electrical input. Polymeric materials that exhibit piezoelectric properties are suitable as tactile sensors. Polyvinylidene fluoride (PVDF) is a classical example of a polymer that is now widely being tested for use as tactile sensors. PVDF is available in sheets that are 5 microns to 2 mm thickness. It has good mechanical properties and can be molded to an appropriate shape with little difficulty. Metallization

is used to apply a thin layer of metal on both sides of the PVDF sheet to form electrodes an collect the charge accumulated. As mentioned earlier, deformation caused by an external force results in an electrical charge that is a function of the applied force. This charge results in a voltage V= Q/C , where Q is the charge developed, and *C* is the capacitance of the device.

Piezoelectric crystals act as transducers that turn force or mechanical stress into electrical charge which in turn can be converted into a voltage. A Schematic of a piezoelectric sensor is shown in the Fig 2.3.

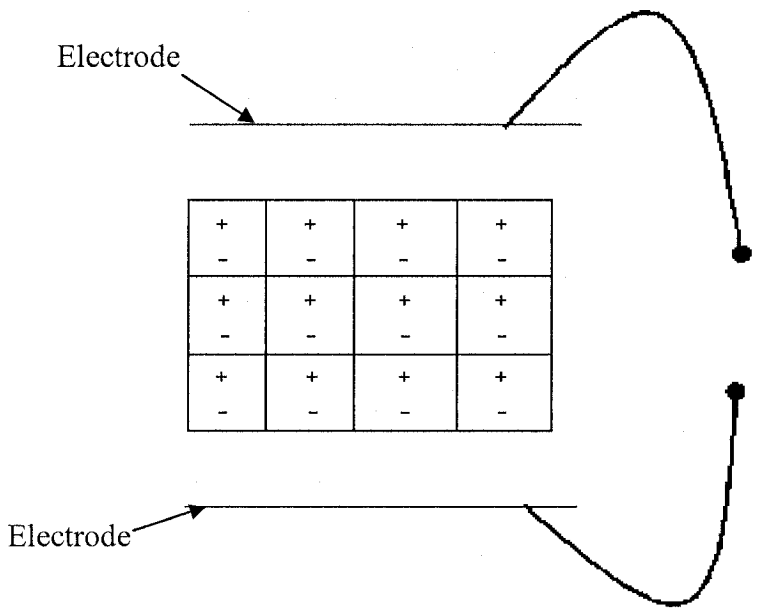

Figure 2-3 Schematic for a Piezoelectric Sensor

Before choosing the technology for the tactile sensor, the advantages and the disadvantages of the different technologies should be compared. All the previous discussion on transduction method for force measuring devices is given in the Table 2.1

Table 2-1 Comparison of Different Sensor Technologies used for Measuring Force [57]

Sensor Type	Advantage	Disadvantage	Purpose
Capacitor Type	• Simple construction • Static and dynamic Response • Small Size and Mass • Excellent Response • continuous response in DC, Digital	• High Impedence • Temperature Drift • complex circuit is required	Used for measuring Small forces
Conductive polymers	• Inexpensive • Easy to install	• High hysteresis • Low accuracy • Not viable for small force measurements • Nonlinear variation	Used for Measuring Force
Inductive Sensor	• Continuous Resolution • Static and Dynamic Response • High Output Response • High SNR • No temperature Drift	• No High Frequency Response • Large Displacement • Input required • External Magnetic Field influence • Miniaturization impossible	Used for Measuring Large Displacement
Magneto Resistive Sensor (MR)	• Highly Sensitive • Good Frequency Response	• Cumbersome Electrical connection	Used for position, current sensor,

		• Non Linearity	speed
Optical Sensors	• Low signal attenuation • Flexibility and no electromagnetic interference problem • High sensitivity • Smallsize, rugged, inexpensive and light weight • Compatible for bioinstruments	• Extremely Fragile • Sensitive to vibration • Requires light emitter and receiver • Miniaturization for force sensor is difficult	Used for cardiac catheters, teleoperation and robotics
Strain Gauge Sensor	• High accuracy • Static and Dynamic response • Insensitive to shock and vibration • Reliability	• Low stability • Limited strain range • Nonlinear • Low dynamic Range • Hysteresis Problem	Used to measure strain caused by force, shear, pressure and torque
Piezoelectric Sensor	• High accuracy • Static and Dynamic response • Insensitive to shock and vibration • High resolution • Readily Miniaturized	• High Temperature Drift • Low frequency Response	Used as a force sensor and temperature sensor

2.2 Selection and Decision of Sensing technology

From the Table 2.1 it is clear that capacitor, conductive polymers, magnetoresistive (MR), inductive and optical sensor requires some input source. Capacitive and piezoresistive sensors have high level of sensitivity but also show noise problem. Silicon strain gauges are fragile and they are difficult to align while gluing. Optical sensor is good preference for the measurement of very minute force but it could not be achieved easily (requires emitter and receiver).

Secondly, two tasks in design of a single tactile sensor should be considered: one is measuring force and the other is finding the compliance of tissue. Calculation of the compliance of the tissue is based on the relative deformation in two parts of the sensor.

The actual measurement of the sensor depends on the stress-strain relationship and changes in electrical properties. For higher sensitivity of the sensor, small stress-strain change with large coupling coefficient (a dimensionless number related to the effectiveness of electrical to mechanical energy conversion in non-resonant piezoelectric devices) is required. PVDF film is one of those materials that its electrical properties change with small change in strain. PVDF film also has low modulus of elasticity and coefficient of coupling as compared to ceramic. PVDF films do not require any activation current, which is highly undesirable in medical applications.

Piezoelectric polymer polyvinylidene fluoride (PVDF) film exhibits extremely large piezoelectric and pyroelectric response, making it attractive for the design of highly sensitive sensors for use in a wide variety of applications. The piezo-and pyroelectric applications of the PVDF film vary from robotic (i.e. matrix sensors, displacement measuring transducers), medical instruments (i.e. blood flow detectors and ultrasonic

echography) to military applications (i.e. hydrophones and IR detectors). The application of PVDF extends to transportation, sports, acoustical sensors, optical and electrical sensors. Recent state of the art surveys suggests that piezoelectric principles have been the most attractive amongst research in the field of tactile sensors. PVDF film exhibits many advantages; it is light, rugged, and potentially low cost. It can be prepared between 6μm to 2 mm in thickness be formed into complex surfaces. In addition, PVDF has bandwidth ranging from near D.C. up to the megahertz range. Piezoelectric polymers present an interesting avenue for the development of a tactile sensing system that can mimic the skin response of a human hand [58].

2.3 Sensing Material

In the designed and fabricated tactile sensor, we use 0.025mm metallized and poled piezoelectric PVDF film as the sensing element. The details of the piezoelectricity property are discussed in the Appendix 1 at the end of this thesis. The Table 2.2 discusses the property of the PVDF films used in the sensor fabrication.

Table 2-2 Properties of Polyvinylidenefluoride[PVDF] Film [59]

Property	Value
Material	Bi-Axial
Thickness	25μm
Piezo Coefficient – d31 pC/N	18-20
Piezo Coefficient – d32 pC/N	2
Piezo Coefficient – d33 pC/N	≈ -20
Piezo Coefficient – g31 Vm/N	0.15
Piezo Coefficient – g32 Vm/N	0.015
Piezo Coefficient – g33 Vm/N	≈ -0.15

2.4 Design of micro machined PVDF tactile Sensor

2.4.1 Single Sensor Design

The single sensor structure consists of four different parts, as shown in the Figure.2.4 and Figure. 2.5, namely rigid and the compliant cylinders, the sensing element and the substrate. The rigid cylinder is machined from plexiglas with dimensions of 3mm in diameter and 1mm thick. The purpose of the rigid cylinder is dual. It not only acts as major sensing element but also increases the friction between the grasper and the sensed object. The second cylinder is the compliant cylinder which surrounds the rigid cylinder. The compliant ring shaped cylinder is micro molded from liquid silicone rubber. For the demonstration purposes, the outer diameter of the compliant cylinder is 6 mm and the inner diameter is 4 mm. The thickness of the cylinders is 1 mm. Due to fabrication limitations, a gap of 0.5 mm used between the rigid and the compliant cylinders. This gap can be reduced further with more precise fabrication process.

A 25 μm bi-axially oriented, metalized and poled PVDF film is sandwiched between the cylinders and the substrate. The piezoelectric sensing element has the strain coefficients of d_{31}, d_{32} and d_{33} of 20, 2 and -20 pC/N, respectively [60-61]. The PVDF film contains patterned aluminum electrodes right underneath the rigid and the soft cylinders. The patterned PVDF films are attached to a 0.5 mm thick silicon substrate. The output charges from both the PVDF are fed to data acquisition system through electrical connections.

One of the important advantages of this design is the thermal insulation provided to the PVDF films by the rigid and the compliant cylinders. Due to this when the grasper is in contact with different objects at different temperatures there are no spurious output

and hence the pyroelectric effect is not a problem in this specified design. During the actual testing, the object is assumed to have viscoelastic behavior.

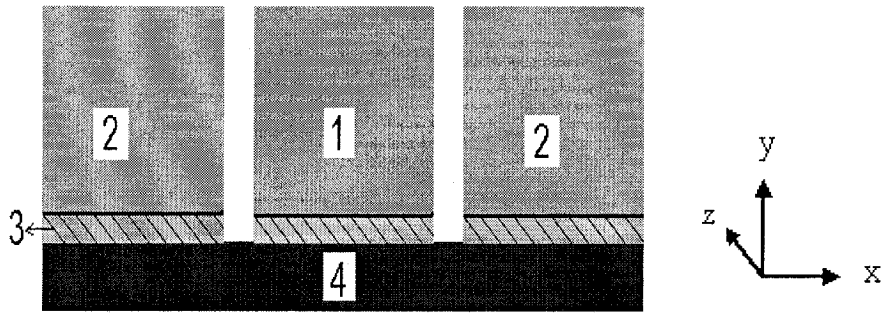

Figure 2-4 Cross sectional view of the sensor

1. Rigid cylinder 2.Compliant cylinder

3. PVDF 4. Substrate

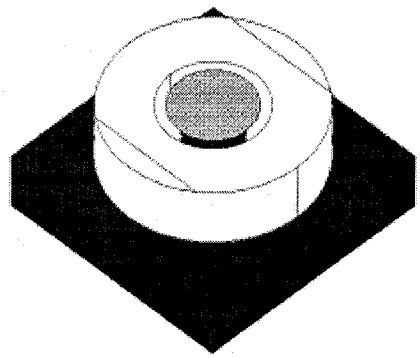

Figure 2-5 Isometric view of the sensor

2.4.1.1 Design of Base Substrate

Sensor design consists of a square base plate. It is made up of copper. The modulus of the copper lies between the 50 GPa to 100 GPa. In our analysis we used 70 GPa and Poisson ratio of 0.3. The base plate has size of the 6 x 6 x 0.5 mm. The properties of the plate material are as given in Table. The schematic diagram of the plates is shown in the Fig 2.6.

Table 2-3 The Properties of the copper

Properties of Copper used as base plate for sensor	
Young's Modulus	70 GPa
Density	1190 Kg/m3
Poisson Ratio	0.3
Dimension of Plate	6 x 6 x 0.5 mm

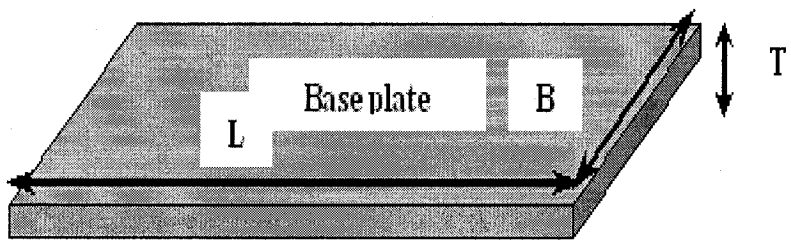

Figure 2-6 Design of Base plate for the Sensor

2.4.1.2 Design of PVDF Films

Piezoelectric substances are new materials used for sensors and actuators with the help of microelectromechanical systems technology. When external force is applied to piezo-materials, it generates charge on the surface, which is proportional to applied mechanical force. The converse effect is also there,(i.e) applied voltage generates deformation in the materials. Piezoelectricity relates to the crystalline ionic structure. PVDF films in shape of circular cross section are used for measuring the force on the rigid cylinder and soft cylinder of the sensor. Circular and ring shaped PVDF films are under the rigid and the soft cylinder, respectively, and are named as PVDF-1 and PVDF-2, respectively. The design of the PVDF-1 and PVDF-2 are discussed below.

A single layer of PVDF film was taken and was patterned using lithography process according to the required design and dimension. The PVDF-1 which is circular with 3mm diameter is sandwiched between the base plate and the rigid cylinder. This PVDF-1 film measures the force acting on the rigid cylinder.

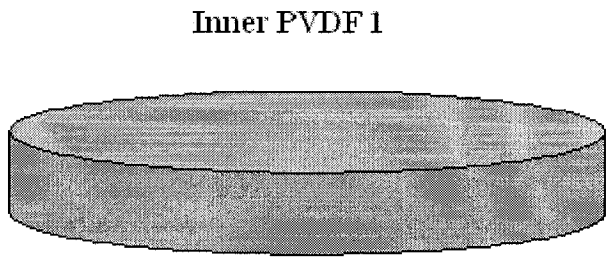

Figure 2-7 Design of PVDF 1

The other PVDF film which is in the shape of a ring with inner radius of 2 mm and outer radius of 3mm. Both the PVDF films have the same materials properties see (Table 2.2) PVDF-2 film is sandwiched between the soft cylinder and base plate. This PVDF film measures force on the outer soft cylinder. Both the rigid and the soft cylinders are attached to the PVDF using non-conductive glue.

PVDF film is anisotropic in nature. Film used in the sensor is polarized in 'Z' direction and the charge developed is taken from two electrodes on the face of the aluminium of the PVDF film. During the analysis of the forces, it was assumed that there was no shear forces in the sensor and only Z direction force and deformation was taken into account.

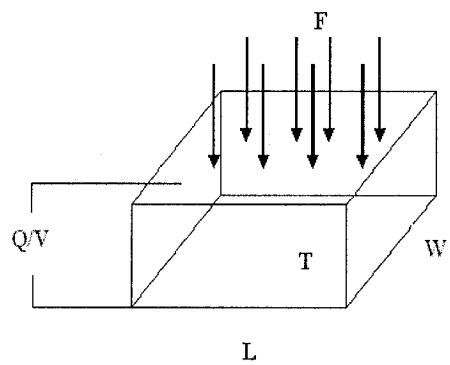

Figure 2-8 Polarization of a PVDF film

PVDF-2 was used as sensing element under the rigid cylinder. For defining the properties of PVDF we have to concentrate on its structural and electric behavior. Four parameters are required for analysis of the piezoelectric behavior, i.e. density, anisotropic array, permittivity and piezoelectric matrix. These parameters are supplied by the manufacturer. All the parameters for PVDF film are defined in the Appendix I under piezoelectricity.

2.4.1.3 Rigid Cylinder Design

The rigid cylinder is made of plexiglass. The plexiglass polymer was used as rigid cylinder because of it non conductive nature with good rigidness. It has good mechanical properties, with a modulus of elasticity of 70GPa and Poisson ratio of 0.3. The electrical resistivity offered by the rigid cylinder is quite high. This rigid part of the cylinder acts as the teeth in sensor. When the force is applied on the sensor compliant cylinder experiences more compression as compared to the rigid cylinder. As a result of this compression the rigid part protrudes relative to the complaint part. This provides the gripping effect to the tissue. The diameter, D of the cylinder is 3mm and height of cylinder, T_2 is 1 mm and shown in Fig. 2.8.

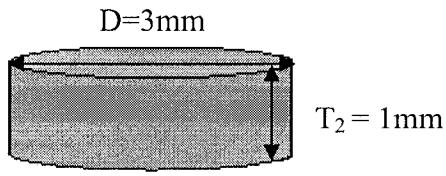

Figure 2-9 Rigid cylinder made up of Plexiglass Size: R1.5 mm x 1 mm

2.4.1.4 Compliant Cylinder Design

The rigid cylinder is surrounded by the complaint cylinder. The size of the complaint cylinder is R_1 = 2 mm, R_2 = 3mm and height of the cylinder is 1mm. The rubber material used for this cylinder is Liquid Silicone Rubber (LSR) sylgard 184 purchased from Dow Corning with modulus of elasticity 7.1MPa.

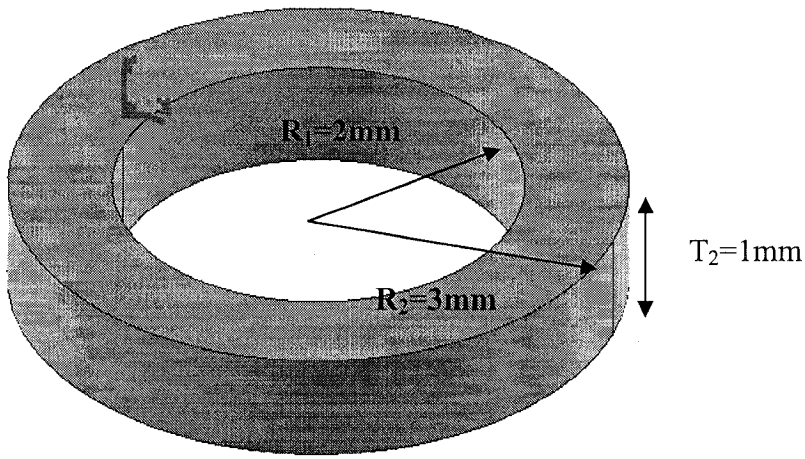

Figure 2-10 Compliant cylinder is made up of soft rubber

2.4.1.5 Sensed Object Design

The tissue behaves like the visco-elastic material. Viscous behavior makes tissue to change its deflection and stress with time. This behavior is not considered in our experimental study. The tissue is considered as rubber specimen with different modulus of elasticity. The Modulus of Elasticity, range of samples used varies from 10MPa to 200MPa. The size of sample is kept similar to the base plate size. The thickness T1 is varied for different samples and similarly the length is varied. The linear materials with isotropic properties were considered. Figure 2.11 and 2.12 shows the sensed object design.

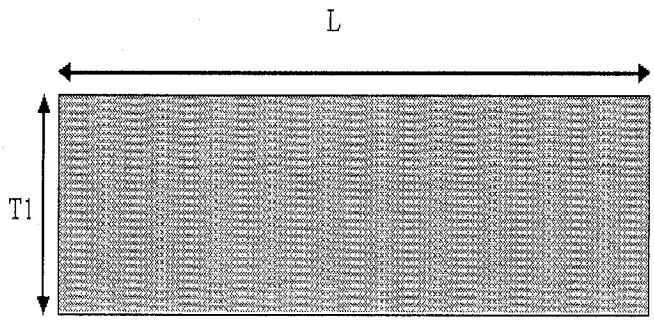

Figure 2-11 sensed object design

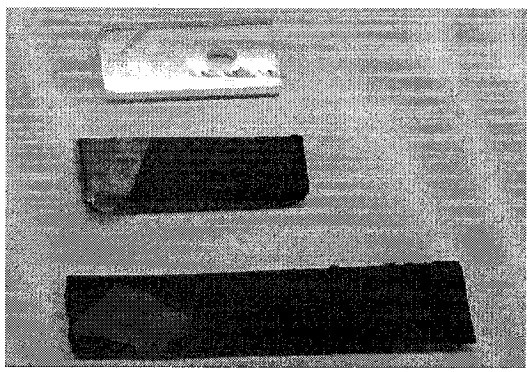

Figure 2-12 Sensed object design

2.4.2 Four Sensor Design

The single sensor used for study will not serve the purpose of the endoscope grasper mounting. Endoscope grasper required number of small micro machined tactile sensor mounted in the form of array. In practical application on the endoscope grasper these sensors could be in number of 4 to 6 in a regular pattern of array. Even though, there could be different arrangements for assembling the sensor on the endoscope, we limited our approach and focus on only one type of sensor designs.

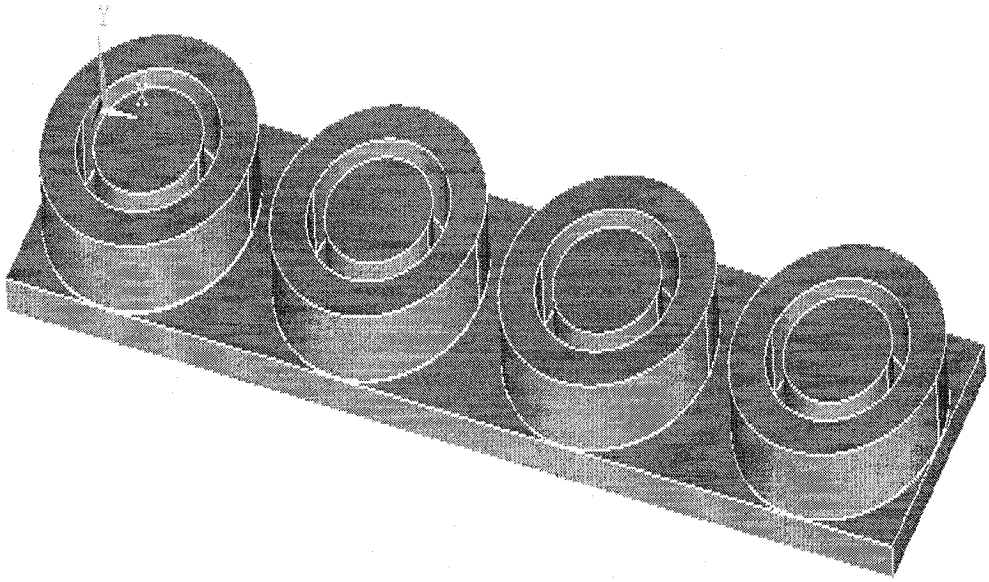

Figure 2-13 Array of sensor on a common base

Figure.2.13. shows the arrangement of four sensors on a substrate. In this design we have a common substrate for all the four sensors and it is integrated to the grasper jaw with a help of a dovetail fix that will slide into the grasper teeth. In total there are eight sensors combining both the teeth's. The object is grasped by both the jaws with the sensors and the output from the eight sensors is fed to the data acquisition system and is calibrated to visualize the softness of the different objects being grasped. Once the objects are tested by the sensors the dovetail fix can be conveniently removed from the grasper teeth. The following figures will display the technicalities of the grasper design as well as the dovetail fix.

The base plate used for the array of sensor changes in dimension. The dimensions of the base plate are 40X10X0.5 mm. A fixture of the required dimension is machined to and the copper substrates along with the sensor are mounted to the endoscopic grasper. Fig. 2.14 gives the complete details of the endoscopic grasper mounting and also its isometric view with the sensors.

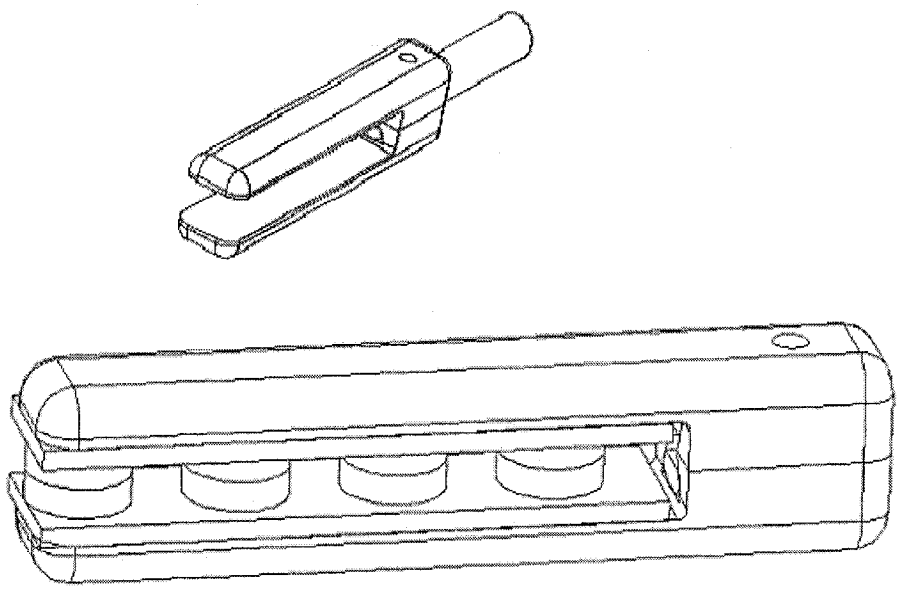

Figure 2-14 AutoCAD drawing of endoscope grasper mounting with the sensors

3. CHAPTER

FABRICATION OF SENSOR

This Chapter describes the basic microfabrication processes used to fabricate the piezoelectric tactile sensor. The assembly of the sensor is also discussed.

3.1 Micromachining

Semiconductor sensors are transducers that convert mechanical signals into electrical signals that are widely used for the measurement and control of physical variables. The list of applications of semiconductor devices is humongous and discussion of the same is out of scope of the following work. Over the past twenty years, interest in semiconductor sensors has been greatly fuelled by the application of microelectronic technology to the fabrication of mechanical devices. Micromachining technology takes advantage of the benefits of semiconductor technology to address the manufacturing and performance requirements of the sensor industry

In general, there is no single technology that can allow for fabrication of a wide variety of sensors. There are however two classifications in silicon micro-sensor technology namely Bulk Micromachining and Surface Micromachining. Bulk-micro machined sensors are made by accurate machining of a relatively thick substrate while Surface-micro machined sensors are fabricated from stacked thin films. Both technologies however, use materials and processes borrowed from VLSI technology. The

three processes of deposition, lithography, and etching are sufficient to construct a wide variety of mechanical structures required for specific sensors.

Surface micromachining is the fabrication of micromechanical structures by deposition and etching of thin structural and sacrificial films. Surface micromachining relies on encasing specific structural parts of a device in layers of a sacrificial material during the fabrication process. The sacrificial material is then dissolved in a chemical etchant that does not attack the structural parts. In surface micromachining, the substrate wafer is used primarily as a mechanical support on which multiple, alternating layers of structural and sacrificial material are deposited and patterned to realize micromechanical structures. Surface micromachining enables the fabrication of complex, multicomponent, integrated micromechanical structures that would be impossible with traditional bulk micromachining. Thus, simple microstructures like beams or membranes as well as complex structures like linkages or encapsulated resonators can be fabricated on top of a silicon substrate.

3.2 Sensor Microfabrication Process

The tactile sensor consists of a silicon substrate with a PVDF film sandwiched between the silicon substrate and the rigid and soft cylinders. The geometrical size of the sensor was selected from the design calculations performed. Two designs, one a single sensor and other one with four sensors were realized. Both the designs had a silicon substrate as the base. Silicon substrate, PVDF, plexiglass and liquid silicone rubber were the materials involved in the fabrication of the sensor.

The microfabrication process sequences of the sensor are described below.

3.2.1 Silicon Wafer Cleaning Process

The material that is used for the substrate only for the photolithography process is silicon. Silicon is used because it is more compatible for Microfabrication processes. The silicon wafer was cleaned to eliminate unwanted impurities like dust, sodium, aluminum and native oxide. First it is diced to the required dimension and then cleaned. The cleaning process carried out is described as follows:

A double sided polished silicon wafer is first immersed in acetone and rinsed carefully for about 5 mins. Once the wafer is rinsed it is placed in an atmosphere of nitrogen so that any moisture that is present in the silicon is completely blown away. Then the diced wafer is kept in a hotplate and heated at 50°C for 5- 10 mins so that all the moisture is completely dried. Thus we have a silicon wafer devoid of any impurities. Once the microfabrication process is done, PVDF is removed from silicon and copper is used as the substrate because of its conductivity.

3.2.2 Fabrication of cylinders

A) Micro molding of outer cylinders

The next process is to get the outer hollow cylinder of the compliant rubber material. The fabrication of the outer hollow cylinder with a compliant object is a difficult process. This can be achieved by the process called micromolding . The material that is used for micromolding is liquid silicone rubber (SYLGARD 184) which was purchased from Dow corning Inc.

- The soft cylinder is fabricated by the process of micro molding of LIQUID SILICONE RUBBER (LSR) [85]. The desired shape is a hollow cylinder.
- To start with we have to create a mold cavity of the required shape and size of 6mm outer diameter, 4mm inner diameter and 1mm depth. This cavity in the shape of hollow cylinder was achieved by very high precision machining.
- Once the cavity is created the LSR which comes as a combination of base (Octamethylcyclotetrasiloxane) and curing agent (Dimethyl, methylhydrogen siloxane) is mixed thoroughly in a beaker in a ratio 10:1. During mixing of the base and curing agent a lot of bubbles will be created. To get rid of these bubbles the base-curing agent mixture is deaerated with the help of vacuum pump to remove the bubbles. This process is repeated until all the bubbles are completely removed.
- Once the bubbles are removed the base-curing agent mixture is carefully poured into the mold cavity which was created by high precise machining. A few drops of teflon was sprayed around the mold cavity for easy removal of the cured rubbers.
- Then the mold cavity along with the LSR mixture is cured in an oven at a temperature of 150°C for 15Mins. The general curing temperature and the time for Sylgard 184 LSR is defined in the following table.

Table 3-1 Curing time-temperature chart for Sylgard 184 [62]

Curing Temperature	Curing Time
Room temp	48 hours
100°C (212°F)	45 minutes
125°C (257°F)	20 minutes
150°C (302°F)	10 minutes

- Once the curing process is over, the ring shaped liquid silicone rubber structures are released from the cavity. Thus the final shape is realized which is of the order of 1 mm height as shown in Fig. 3.1

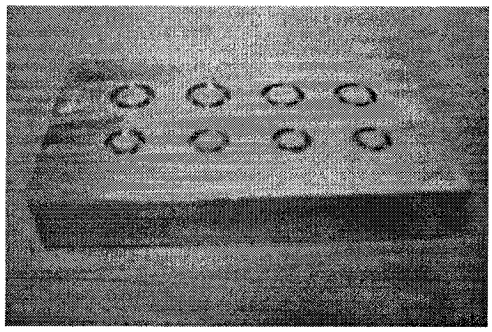

Figure 3-1 Mold Cavity

B) Inner rigid Cylinder

The inner rigid cylinder is made of plexiglass which is machined to the required diameter of 3mm and 1mm height by high precision machining.

3.2.3 Patterning of PVDF films

This is the process of patterning the PVDF film for getting the required shape. UV light is directed through a mask to selectively expose photosensitive materials. Patterned regions can be manipulated by various processes (E.g.: Etching). In this process the PVDF film was patterned to get the required cylindrical shape. This section describes in detail the standard photolithography process.

Overview of the Photolithography Process

Photolithography plays an important role in the fabrication of all micromechanical devices. During microelectronics device fabrication, there arises a need to selectively subject a portion of the sample to a variety of fabrication steps, leaving the rest of the sample untouched. Photolithography enables one to accomplish this. Patterning of geometry with extremely high precision has been a major challenge for engineers. Photolithography or microlithography has been the only viable solution for producing high precision patterns on substrates at micro scale.

The photolithography is conducted in room illuminated yellow in color to reduce the adverse effects of light on the photosensitive resist material. In this process, photoresist (PR) is applied on a wafer by spin coating. The coated wafer is then dried in an oven, exposed to UV light and then developed using a developer. The purpose of the photo resist is to protect chosen regions of the wafer for subsequent fabrication steps. A schematic depicting of the process of photolithography is shown in the Fig.3.2.

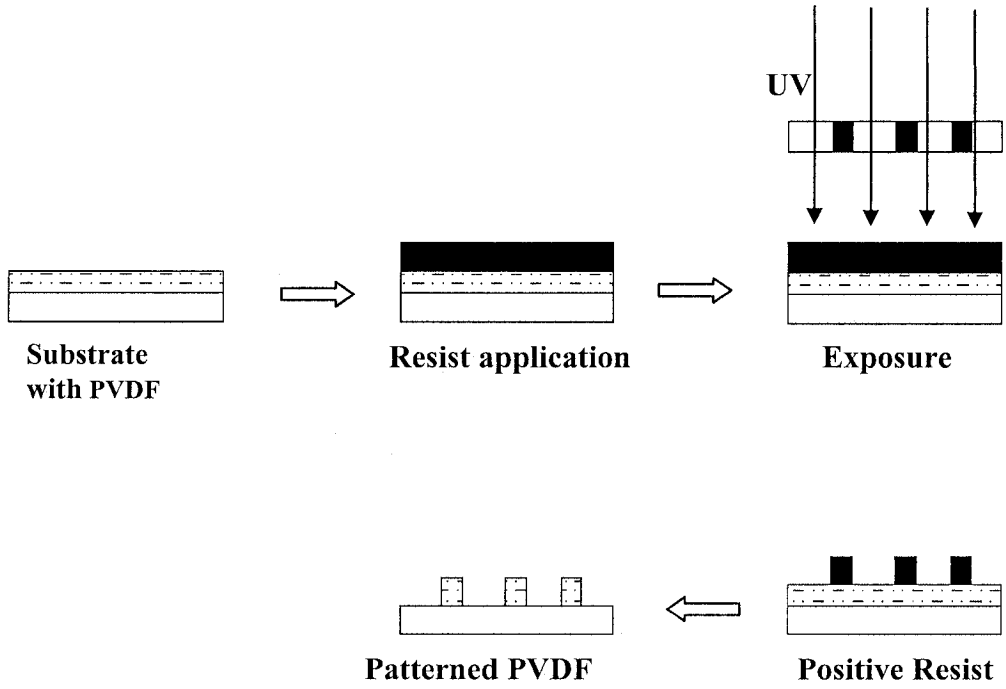

Figure 3-2 Photolithography process

This section describes the photolithography process employed for our sensor fabrication.

a. Surface Preparation

b. Coating (Spin Casting)

c. Pre-Bake (Soft Bake)

d. Alignment

e. Exposure

f. Development

g. Post-Bake (Hard Bake)

h. Stripping of PR

a) Surface Preparation:

In this process the PVDF film is glued onto a silicon wafer using the photo resist (PR). A bare silicon wafer was first cleaned as described in the Section 3.2.1 and photoresist was spin coated on it. The photoresist here acts as glue for the PVDF on the silicon wafer. Then the PVDF film of the required size was cut and placed over the surface spin with photoresist. It was pressed so that the PVDF film gets glued to the substrate. Then the substrate along with the PVDF was soft baked for 30 sec at 75°C on a hot plate. Thus the PVDF was glued to the silicon substrate.

b) Spin coating:

There are number of photoresists that can be utilized in photolithography. Photoresists are generally classified as positive photoresist and negative photoresists. Positive photoresists are more sensitive to ultraviolet rays while the negative photoresists are less sensitive to X-ray exposure but more sensitive to electron beams. Generally positive resists provide more clear definition of the patterns. Hence we use a positive photoresist Shipley S1818 in our lithography process. Silicon wafer along with the PVDF film is held on a spinner chuck by vacuum and photoresist is coated to uniform thickness by spin coating. Seven to eight drops of photoresist was dropped onto the PVDF film and the chuck was spun at a speed of 500 rpm for 15 sec and then at 3000 rpm for 30 seconds. By this method of spinning we ensure that the photoresist is coated uniformly over the PVDF film. The resist thickness is set primarily by resist viscosity and by spinner rotational speed. Fig. 3.3 and Fig.3.4 shows the schematic and picture of a spin coater setup

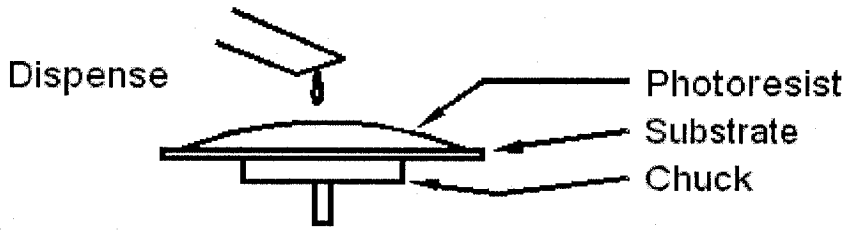

Figure 3-3 Schematic of Spin coating set-up

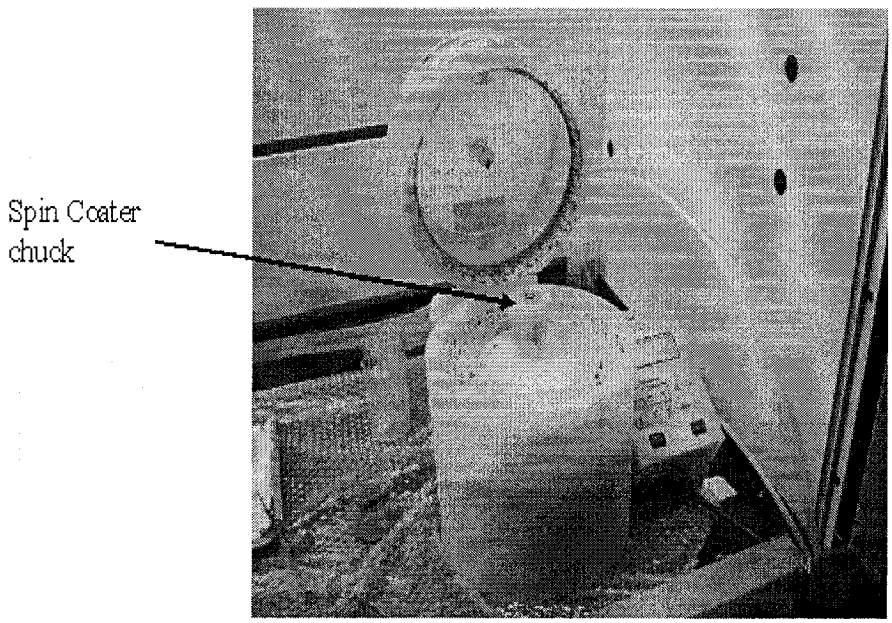

Figure 3-4 Spin coater set-up

c) Soft Bake:

Once the PR is spun on the PVDF film the very next step is to soft bake it in an oven. This process is done to evaporate the coating solvent and to densify the resist after spin coating. Typical thermal cycles are

- 50°C for 40 min. in an oven
- 75-85°C for 45 sec. on a hot plate

Once the sample is soft baked, the next procedure is to expose it to UV light through the predefined light field mask. Fig. 3.5 shows the photolithography set-up used to pattern PVDF

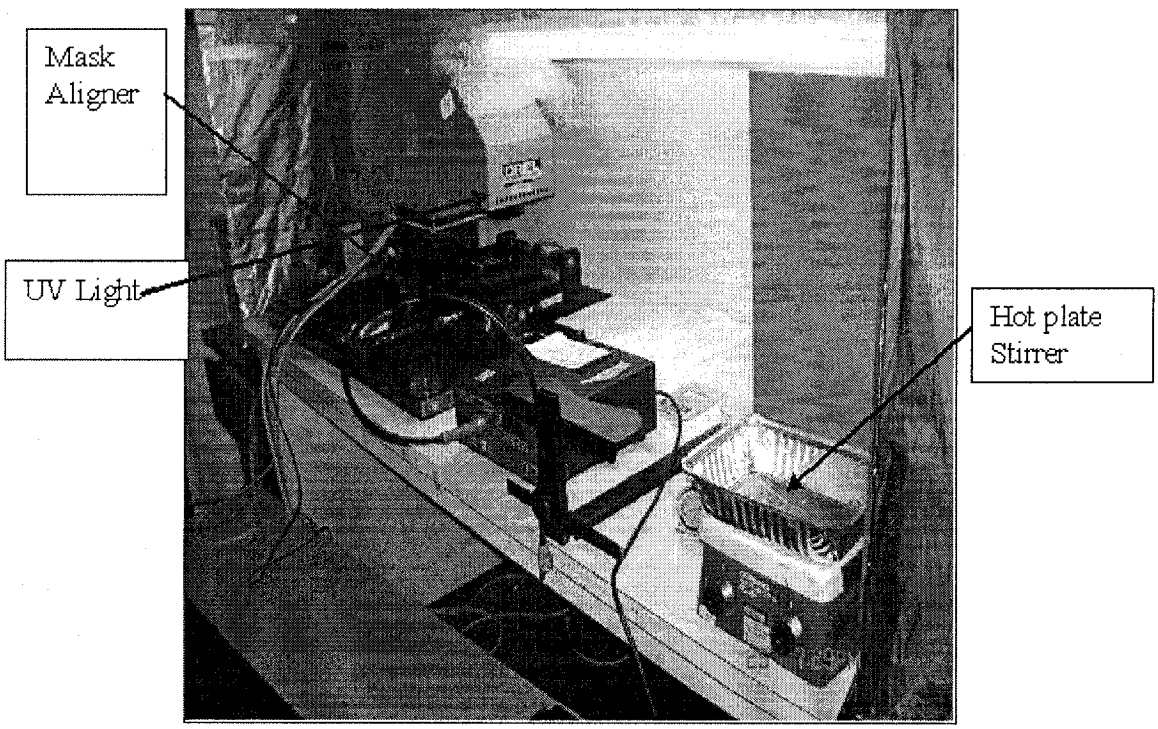

Figure 3-5 Photolithography Set-up

d) Mask Alignment and Exposure:

Initially the mask for patterning aluminium electrodes on the PVDF film is designed in the AutoCAD and it is transferred on to a transparent sheet as shown in Fig.3.6 and Fig. 3.7. For our design we need a light field mask as the aluminium electrodes have to be etched on a specific region. Once the Mask is aligned with the wafer using the alignment marks, the resist is exposed to the UV light through the mask. The exposure time for this sample is 23 sec.

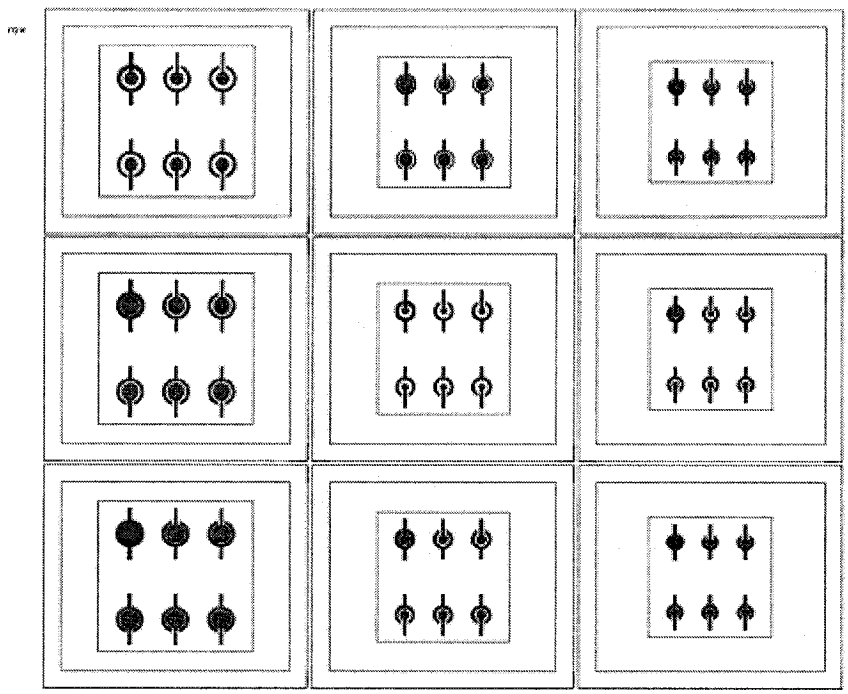

Figure 3-6 Mask Layout for Patterning

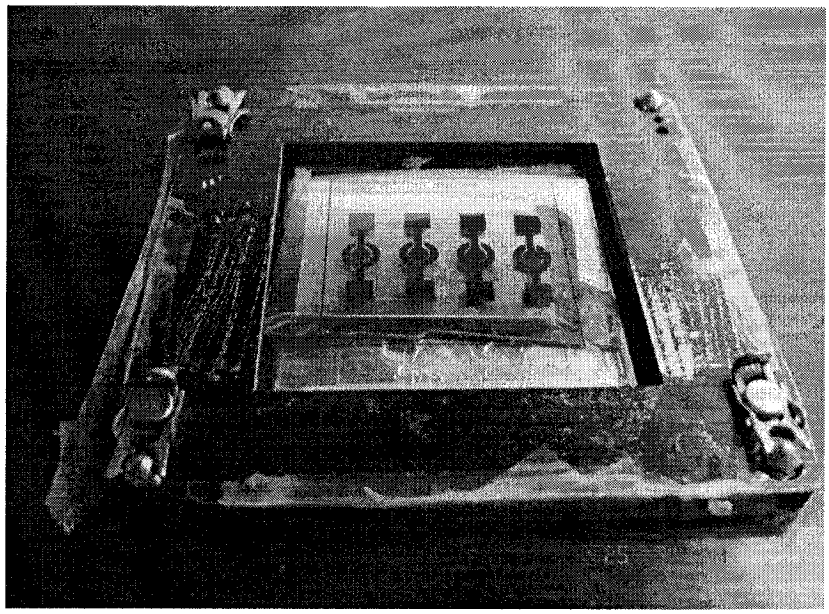

Figure 3-7 Mask for Patterning

e) Photoresist Removal:

Once the sample is exposed to the UV light source the next step is to develop the exposed sample in the developer solution. The sample is dipped in the developer solution and rinsed continuously until a clear pattern is visible. All the exposed regions of the sample will be completely removed by the developer solution. Once the sample is clearly developed it is rinsed in the distilled water for few seconds. After the sample is rinsed in water an atmosphere of nitrogen is passed through it to dry the sample.

f) Post Bake:

Post bake removes any remaining traces of the coating solvent or developer. This step is necessary in order to harden the photoresist and improve adhesion of the photoresist to the wafer surface. This eliminates the solvent burst effects in vacuum

processing. Post bake introduces some stress into the photoresist. Some shrinkage of the PR may occur. Longer or hotter post bake makes resist removal much more difficult. Usually the post bake is done at temperature of 115°. But for PVDF it is done at 50°C for 30-40 min.

3.2.4 Etching

Once the PR is stripped off, the PVDF sample is dipped in a commercial aluminum etchant TRANSENE ALUMINIUM ETCHANT A, which anisotropically etches the aluminium on the PVDF sheet without affecting the PVDF. In order to prevent under etching of the PVDF sample glued to the silicon wafer, photoresist is applied along the edges of the PVDF film and it was baked till the photoresist hardens. Thus, the, under etching of the aluminium electrodes of the PVDF film is prevented. The etchant is heated in a water bath at 50°C. Once the etchant attains the required temperature the sample is dropped into the etchant and is left for 20-30 min. Then the sample is removed from the etchant and is rinsed in distilled water and is dried using an atmosphere of nitrogen. Thus the patterned aluminium electrodes are etched using a commercially available etchant as shown in Figure 3.8

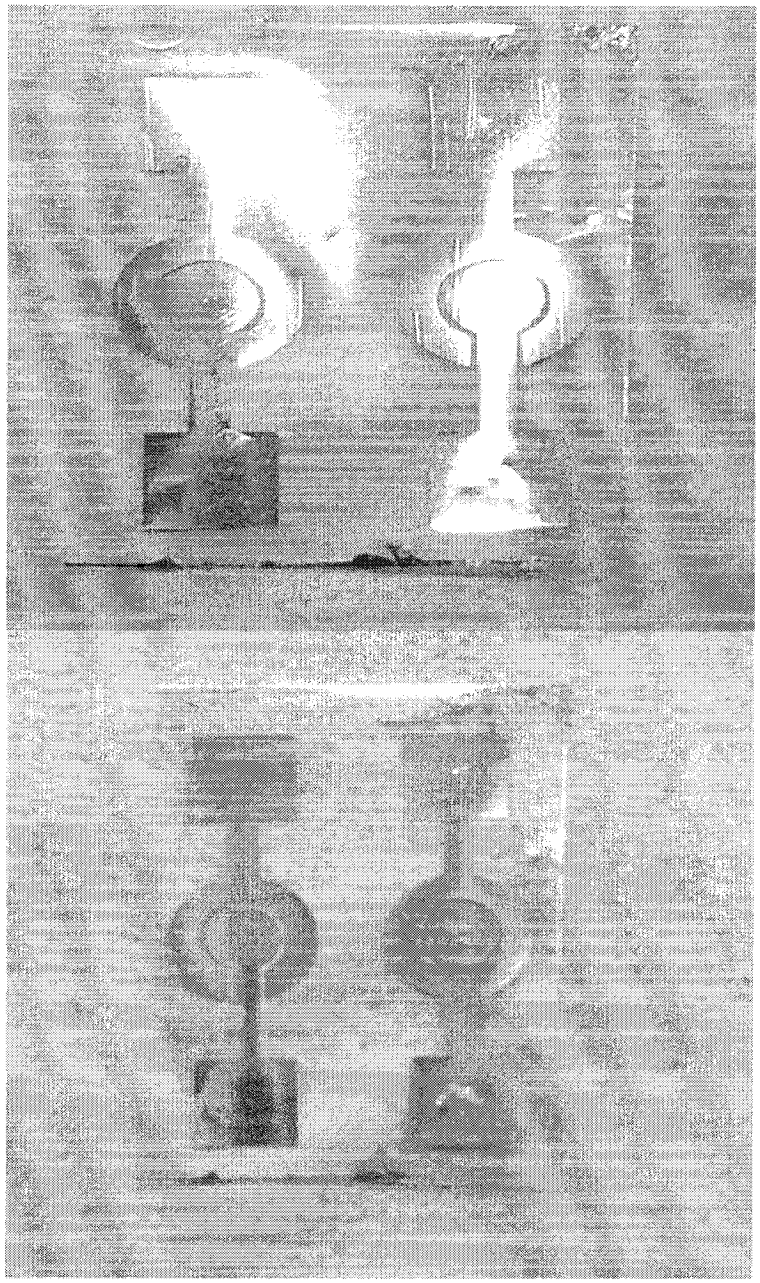

Figure 3-8 Pattern after Etching

3.3 Single Sensor Assembly

Once the different parts of the sensor are realized by different procedures, the next step is to assemble them. The following steps are followed to assemble the sensor. A thin layer of nonconductive epoxy is applied to the patterned side of the PVDF. Working under a stereo microscope and using the alignment marks, the rigid and the compliant cylinders are glued over the patterned PVDF films. This assembly was uniformly pressed using a compression block to ensure even adhesion and is cured inside an oven at 50°C for 1 hr. Then electrical leads are attached to the PVDF. This is done by soldering AWG 30 copper wires to the PVDF. The complete assembled sensor is shown in Fig. 9.

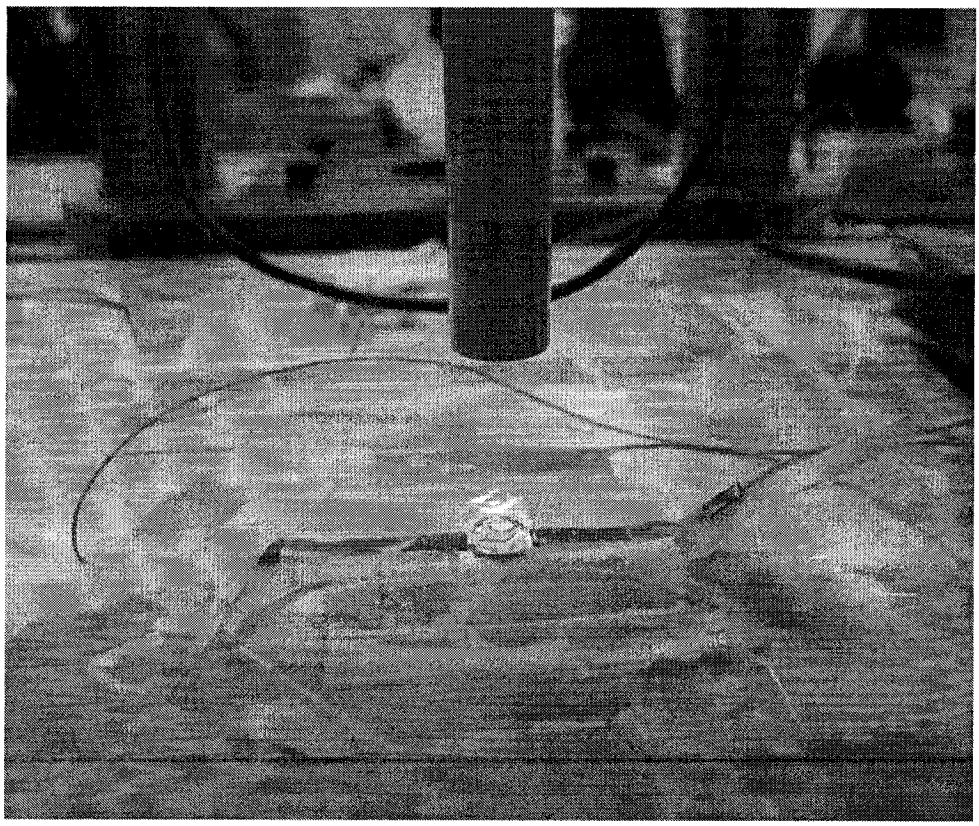

Figure 3-9 Sensor assembly under the probe

3.4 Four sensor assembly

The fabrication procedure for a single sensor and four sensors are almost the same except for the etching time. To increase the etching rate, the temperature of the etchant is increased from 50°C to 65°C. The four sensor array after fabrication was assembled in the same way as the single sensor and it is integrated to the grasper with a help of a dovetail jaw. The dovetail jaw which was designed using the AutoCAD was machined in the Concordia university machine shop. The sensor assembly along with the substrate was attached to the dovetail jaw using an epoxy so that it is rigid enough during grasper operation. The Figure 3.10 below shows the four sensor assembly and its integration with the grasper.

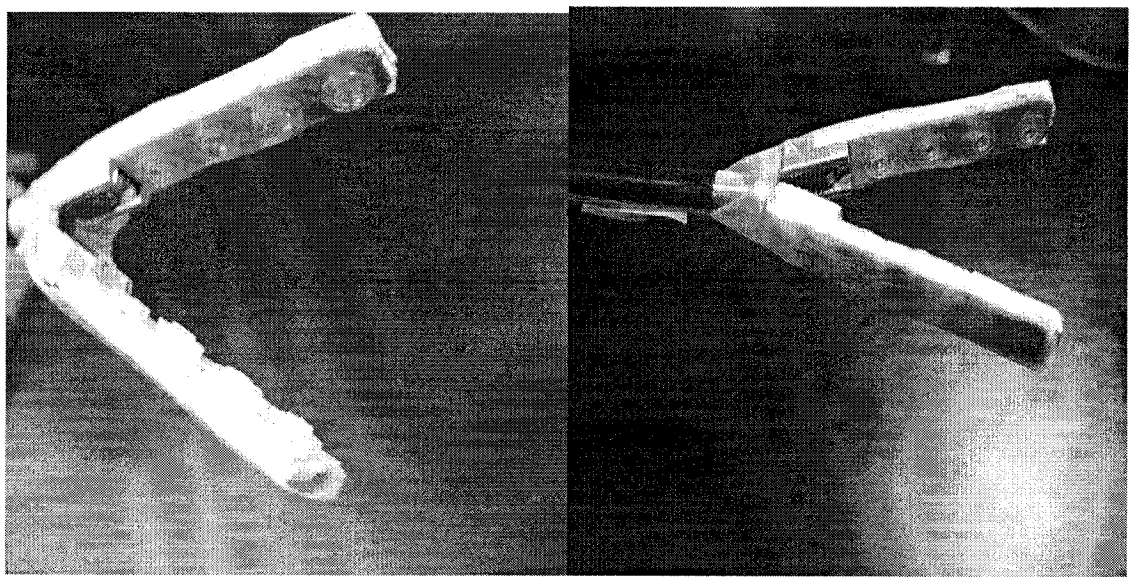

Figure 3-10 Array of sensor after integration with grasper

4. CHAPTER

ANALYTICAL AND FINITE ELEMENT MODELING

This chapter deals with analytical and finite element modeling of a tactile sensor. The sensor was modeled using Kelvin-Voigt Model [68] and the variation of force ratio with the modulus of elasticity was analyzed. Finite element analysis was done using ANSYS 9.0 for different materials and its force ratios were obtained.

4.1 Modeling the Tactile Sensor System

For simplicity, a single sensor is modeled and carefully analyzed using a spring-damper system. Since the tissues are viscoelastic in nature, the sensed object was modeled based on this viscoelasticity to analyze the sensor's behaviour. Mathematical equations are developed to determine Young's modulus values of the sensed objects.

4.1.1 Analytical Modeling

Compliance is achieved by measuring both force (stress) and the resulting deformation (strain) in an object using two different methods. The first is to measure the deformation of the entire object when a force or stress is applied. The second is to measure the relative deformation between adjacent parts of the object. We have adopted the latter method for our experiments. Because it is suitable for objects of any size, whereas the first method is suitable only for objects that can be placed within the sensor element of the device.

4.1.2 Viscoelasticity

Viscoelastic material models are frequently used to describe the behavior of human tissue, plastics, soil, etc. Commonly used viscoelastic models are the Kelvin, Kelvin-Voigt and Maxwell. Each model can be represented by springs and dashpots set in combinations of series and parallel elements [63].

A viscoelastic solid can be described by the following constitutive relationships [64, 65] between deviator stress and strain, s_{ij} and e_{ij}:

$$s_{ij}(t) = 2\int_0^t G(t-t')\frac{\partial e_{ij}(t')}{\partial t'}dt' \quad (1)$$

$$2e_{ij}(t) = \int_0^t J_1(t-t')\frac{\partial s_{ij}(t')}{\partial t'}dt' \quad (2)$$

The function $G(t)$ is the shear relaxation function, or time dependent shear modulus, which specifies the stress response to a unit step change of strain; the function $J_1(t)$ is the creep compliance, which specifies the strain response to a unit change in stress. In the theory of elasticity, J_1 which is time independent, is defined as $1/G$, where G is the shear modulus. Equation (1) is expressed in terms of the relaxation function $G(t)$ and can be regarded as the superposition of the stress responses to a sequence of small changes of strain $de(t')$ at times (t'). Similarly, Equation (2) expresses the total strain response to a sequence of step changes in stress. Deviator stress and strain can be expressed in terms of:

$$s_{ij} = (\sigma_{ij} - \delta_{ij} I_\sigma / 3)$$

$$e_{ij} = (\varepsilon_{ij} - \delta_{ij} I_\varepsilon / 3)$$

where σ_{ij} and ε_{ij} are stress and strain respectively. In addition, I_σ and I_ε are the first stress and strain invariants, respectively, which can be expressed as sum of principal stresses and strains as follows:

$I_\sigma = (\sigma_1 + \sigma_2 + \sigma_3)$ and $I_\varepsilon = (\varepsilon_1 + \varepsilon_2 + \varepsilon_3)$

Alternatively, the dilatation stress-strain relation [64, 65] is expressed as:

$$\sigma_{ii}(t) = 3\int_0^t B(t-t')\frac{\partial \varepsilon_{ii}(t')}{\partial t'}dt' \tag{3}$$

$$3\varepsilon_{ii}(t) = \int_0^t J_2(t-t')\frac{\partial \sigma_{ii}(t')}{\partial t'}dt' \tag{4}$$

where $B(t)$, the relaxation modulus in dilatation or time, is dependent on bulk modulus and $J_2(t)$ is the volumetric compliance [65].

The constitutive principle [66] can also be written as:

$$\sigma_{ij}(t) = \int_0^t [2G(t-t')\frac{\partial \varepsilon_{ij}(t')}{\partial t'} + \delta_{ij}\lambda(t-t')\frac{\partial \varepsilon_{kk}(t')}{\partial t'}]dt' \tag{5}$$

where $\lambda(t) = (3B(t) - 2G(t))/3$.

The time dependant Young's modulus and Poisson ratio [67] are then given by:

$$E(t) = [9G(t)B(t)]/[3B(t) + G(t)], \quad \upsilon(t) = [E(t)/2G(t)] - 1 \tag{6}$$

In the following analysis, idealized Kelvin viscoelastic materials are assumed [68] which includes a spring of modulus 'g' parallel to a dashpot of an equivalent viscous damping co-efficient 'c'. For the Kelvin model, the constitutive equation is expressed as:

$$c\dot{e}(t) + ge(t) = s_0 \tag{7}$$

The creep response to a step change in stress s_0 is given by:

$$e(t) = 0.5J_1(t)s_0 = \frac{1}{g}(1 + \exp(-t/T)s_0 \tag{8}$$

where $T = g/c$

The Kelvin-Voigt model, also called the Voigt model, can be represented by a purely viscous damper and elastic spring connected in parallel as shown in Figure 4.1.

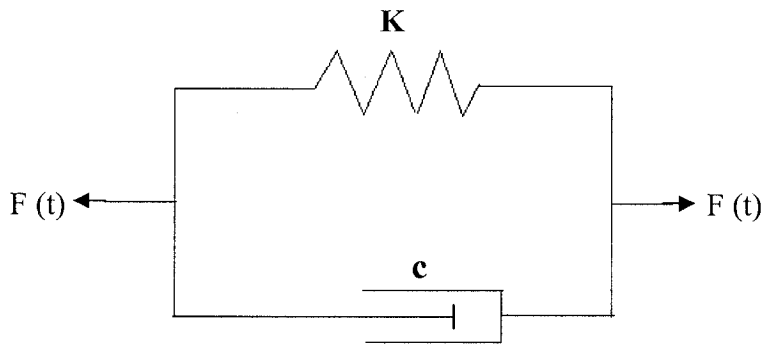

Figure 4-1 Schematic representation of the Kelvin-Voigt model.

If we connect these two elements in series, we get Maxwell model. In a Kelvin-Voigt model, stress σ, strain ε and their rates of change with respect to time t are governed by equations of the form:

$$\sigma(t) = E\epsilon(t) + c\frac{d\epsilon(t)}{dt}$$

where E is the modulus of elasticity and c is damping coefficient. This equation can be applied either to the shear stress or to the uniform tension in a material.

4.1.3 Modeling of the Sensor system

Figure 4.2 shows the proposed analytical model of sensor-object configuration.

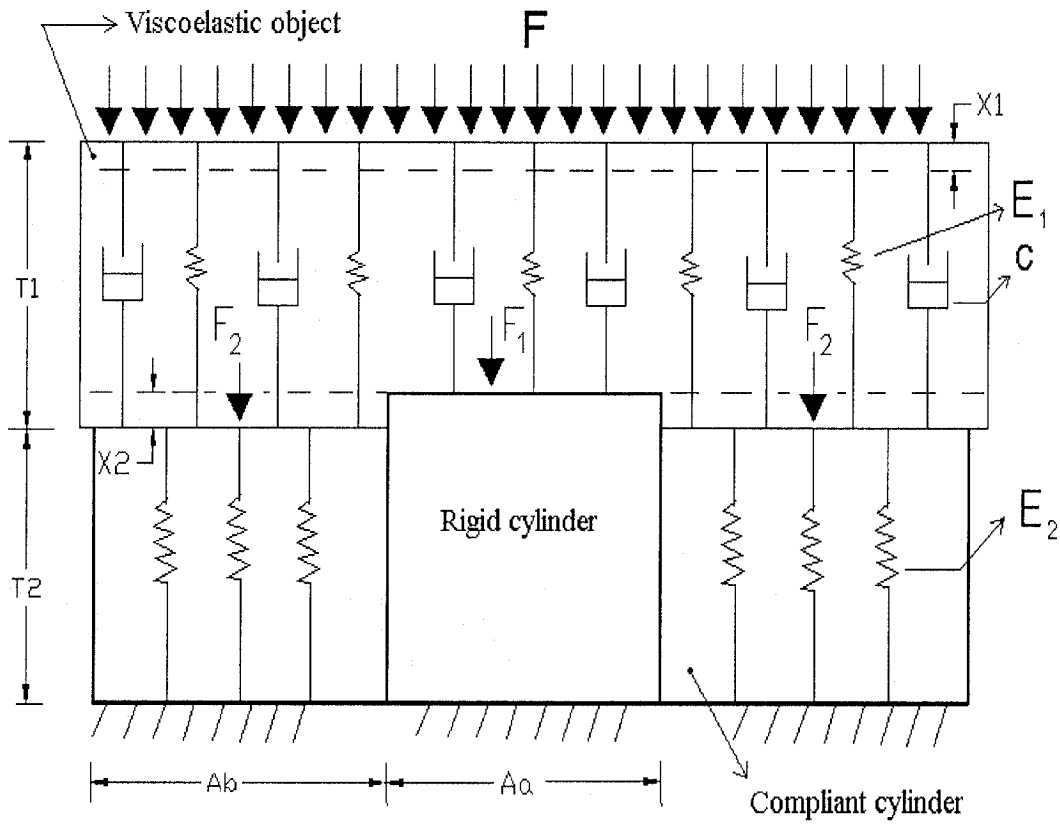

Figure 4-2 Analytical model of sensor-object configuration

Where,

A_a: Area of the rigid cylinder, A_b: Area of the compliant cylinder, T_1 and E_1 are the thickness and Young's modulus respectively of the modeled object under investigation, T_2 and E_2 are the thickness and Young's modulus respectively of the compliant cylinder and c is the damping coefficient of the modeled object.

As can be seen, the viscoelastic object is pressed to the sensor with known force, a part of which flows through the rigid cylinder and the rest through the compliant cylinder of the sensor. In this way, the parts of the object in contact with each element of the sensor are deformed to different extents.

It is assumed that the viscoelastic object can not take any bending load and hence the rigid cylinder experiences the load applied on the viscoelastic object just above it only. The same assumption holds good for the compliant cylinder.

Considering Equation (7), the force F_1 carried by the rigid cylinder can be written as:

$$F_1 = A_a\left(\frac{E_1 X_1}{T_1} + c\dot{X}_1\right) \tag{9}$$

where X_1 is the deformation of the sensed object over the rigid cylinder and X_2 is the deformation of the compliant element of the sensor. Deformations X_1 and X_2 are independent of each other and there is no shear force in either the sensor or sensed object.

The force F_2 carried by the compliant cylinder is:

$$F_2 = A_b\left[\frac{E_1(X_1 - X_2)}{T_1} + c(\dot{X}_1 - \dot{X}_2)\right] \tag{10}$$

Since part of the force, F_2, flows through the object, it can also be written in terms of sensor element deformation as:

$$F_2 = \frac{E_2 A_b X_2}{T_2} \tag{11}$$

The total force applied on the viscoelastic object is $F=F_1+F_2$.

The Force Ratio F_1/F_2 is given by:

$$\frac{F_1}{F_2} = \frac{A_a(\frac{E_1 X_1}{T_1} + c\dot{X}_1)}{\frac{E_2 A_b X_2}{T_2}} \tag{12}$$

Multiplying by T_1T_2, we get:

$$\frac{F_1}{F_2} = \frac{E_1 A_a X_1 T_2 + c A_a \dot{X}_1 T_1 T_2}{E_2 A_b X_2 T_1} \tag{13}$$

Now Equating (10) & (11) we get:

$$A_b[\frac{E_1(X_1 - X_2)}{T_1} + c(\dot{X}_1 - \dot{X}_2)] = \frac{E_2 A_b X_2}{T_2} \tag{14}$$

Rearranging the above equation we get:

$$c\dot{X}_2 + [\frac{E_1}{T_1} + \frac{E_2}{T_2}]X_2 = c\dot{X}_1 + \frac{E_1 X_1}{T_1} \tag{15}$$

Equation (15) is of the form $a\dot{y} + by = c\dot{x} + cx$, which must be equal to a constant since both the x and y variables are time dependent and are independent. Hence from Equation (15) we can assume:

$$\frac{[\frac{E_1}{T_1} + \frac{E_2}{T_2}]}{c} = \alpha \text{ And } \frac{[\frac{E_1}{T_1}]}{c} = \beta \tag{16}$$

Hence Equation (15) can be simplified as:

$$\dot{X}_2 + \alpha X_2 = \dot{X}_1 + \beta X_1 = \omega \tag{17}$$

The general solution for the above equation is:

$$\begin{aligned} X_2 &= K_2 \exp(-\alpha t) + \omega/\alpha \\ X_1 &= K_1 \exp(-\beta t) + \omega/\beta \end{aligned} \tag{18}$$

where K_2, K_1 and ω are constant values.

Now substituting the above solutions into Equation (13) we get:

$$\frac{F_1}{F_2} = \frac{E_1 A_a T_2 [K_1 \exp(-\beta t) + (\omega/\beta)] + A_a T_1 T_2 c[\omega \exp(-\beta t)]}{E_2 A_b T_1 [K_2 \exp(-\alpha t) + (\omega/\alpha)} \tag{19}$$

Initial conditions: When $t=0$, $X_1=X_2=0$. Hence from Equation (18), after applying initial conditions, we get:

$$\begin{aligned} K_1 &= -\omega/\beta \\ K_2 &= -\omega/\alpha \end{aligned} \tag{20}$$

Substituting K_1, K_2 values in Equation (19) we get:

$$\frac{F_1}{F_2} = \frac{E_1 A_a T_2 [(-\omega/\beta)\exp(-\beta t) + (\omega/\beta)] + A_a T_1 T_2 c[\omega \exp(-\beta t)]}{E_2 A_b T_1 [(-\omega/\alpha)\exp(-\alpha t) + (\omega/\alpha)]} \tag{21}$$

Eliminating ω we get:

$$\frac{F_1}{F_2} = \frac{E_1 A_a T_2 [\frac{1-\exp(-\beta t)}{\beta})] + A_a T_1 T_2 c \exp(-\beta t)}{E_2 A_b T_1 [\frac{1-\exp(-\alpha t)}{\alpha}]} \tag{22}$$

Multiplying by $\alpha \times \beta$ we get:

$$\frac{F_1}{F_2} = \frac{E_1 A_a T_2 \alpha [1-\exp(-\beta t)] + A_a T_1 T_2 c \alpha\beta \exp(-\beta t)}{E_2 A_b T_1 \beta [1-\exp(-\alpha t)]} \tag{23}$$

Substituting the values of α and β from Equation (16) into Equation (23), we get:

$$\frac{F_1}{F_2} = \frac{\left[E_1 A_a T_2 \left(\frac{E_1}{T_1} + \frac{E_2}{T_2}\right)(1-\exp(-\beta t))\right]/c}{\left[E_2 A_b T_1 (1-\exp(-\alpha t))\left(\frac{E_1}{T_1}\right)\right]/c} + \frac{\left[A_a T_1 T_2 \left(\frac{E_1}{T_1} + \frac{E_2}{T_2}\right)\left(\frac{E_1}{T_1}\right)\exp(-\beta t)\right]/c}{\left[E_2 A_b T_1 (1-\exp(-\alpha t))\left(\frac{E_1}{T_1}\right)\right]/c} \tag{24}$$

Equation (24) is reduced to:

$$\frac{F_1}{F_2} = \frac{A_a}{A_b}\left[1 + \frac{E_1 T_2}{E_2 T_1}\right]\left[\frac{(1-\exp(-\beta t)) + \exp(-\beta t)}{1-\exp(-\alpha t)}\right] \tag{25}$$

Assuming that $A_a = A_b$ we get:

$$\frac{F1}{F2} = \left[1 + \frac{E_1 T_2}{E_2 T_1}\right]\left[\frac{1}{1 - \exp(-\alpha t)}\right] \tag{26}$$

Figures 4.3, 4.4 and 4.5 show the indirect variations of the force ratio with modulus of elasticity and the viscosity of the tissue at different times.

As shown in Figure 4.3, the force ratio increases rapidly to a very large magnitude and then decays very quickly. With increase in the loading and unloading time, the force ratio reduces to a lower magnitude as shown in Figure 4.4 and Figure 4.5. It means that faster loading and unloading times give more accurate results when determining viscoelastic properties.

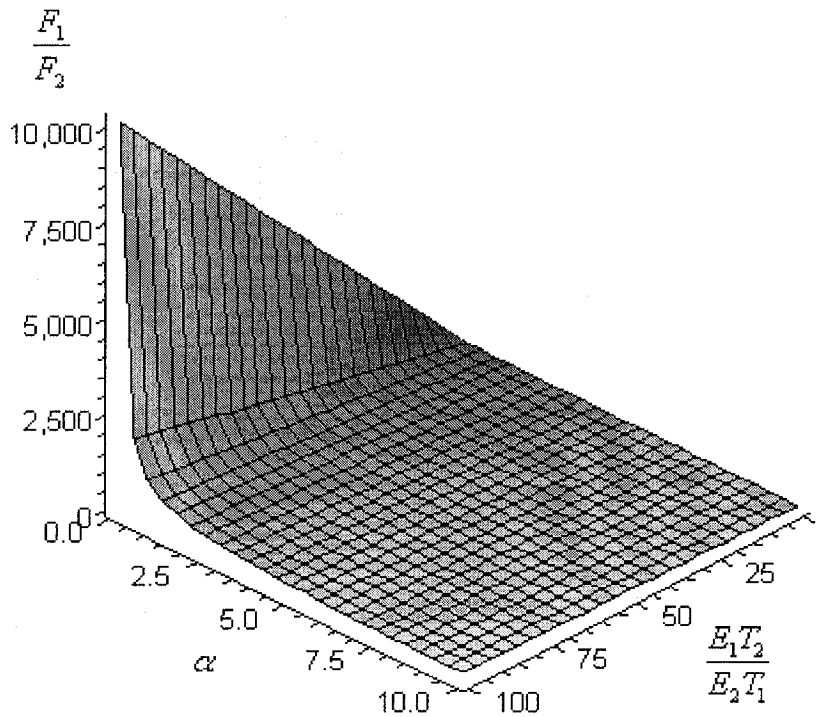

Figure 4-3- Variation of force ratio with modulus of elasticity and viscosity of the Kelvin Model at a loading-unloading time of 0.1 sec

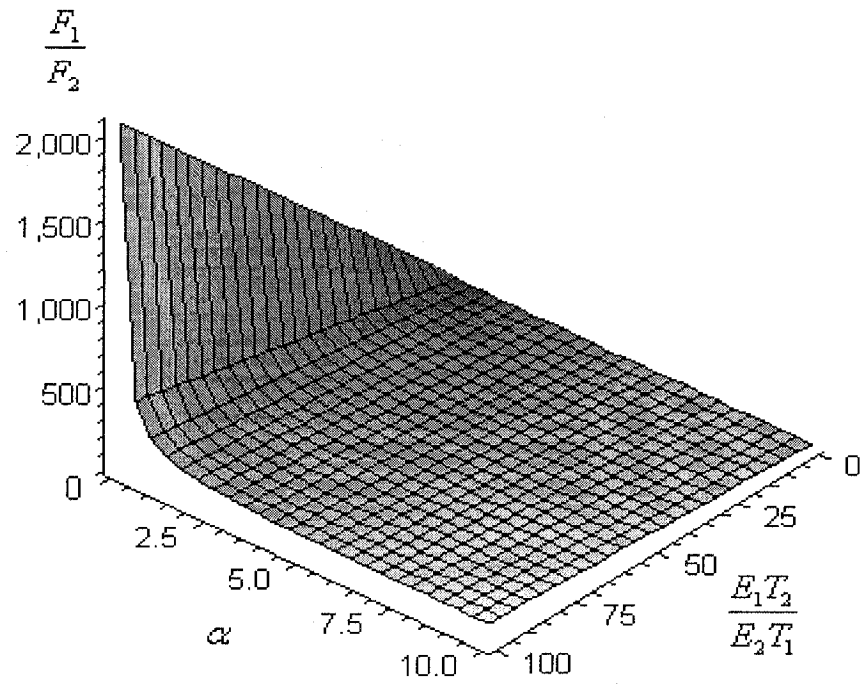

Figure 4-4 Variation of force ratio with modulus of elasticity and viscosity of the Kelvin Model at a loading-unloading time of 0.5 sec

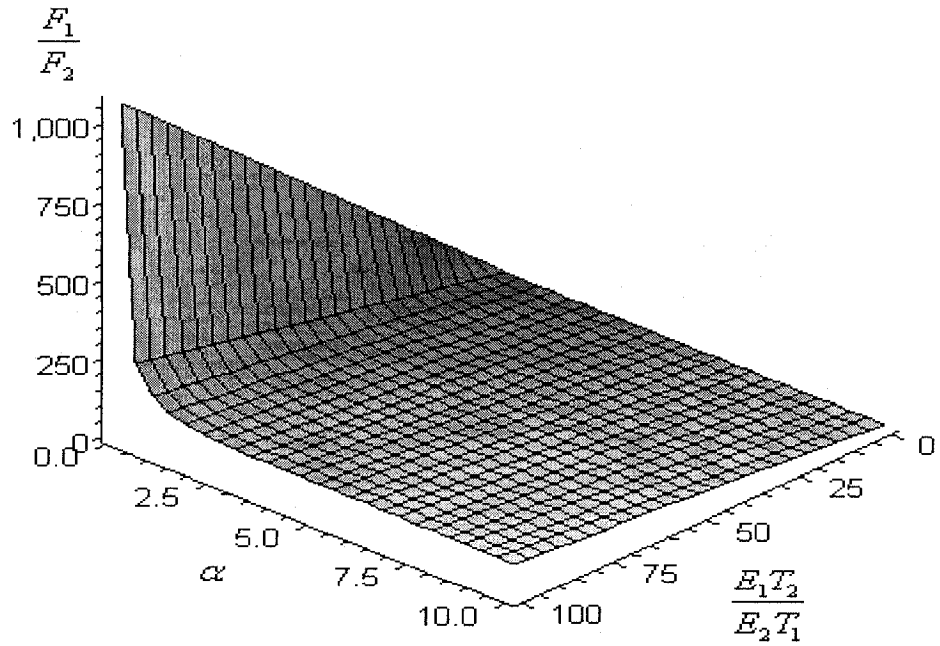

Figure 4-5 Variation of force ratio with modulus of elasticity and viscosity of the Kelvin Model at a loading-unloading time of 1 sec

From Equation (16), when we put $c = 0$, $\alpha \to \infty$ and the equation reduce to:

$$\frac{F1}{F2} = \left[1 + \frac{E_1 T_2}{E_2 T_1}\right] \tag{27}$$

If $A_a \neq A_b$ then equation 25 becomes:

$$\frac{F1}{F2} = \frac{A_a}{A_b}\left[1 + \frac{E_1 T_2}{E_2 T_1}\right] \tag{28}$$

Equation (28) relates to elastic behavior of the sensor.

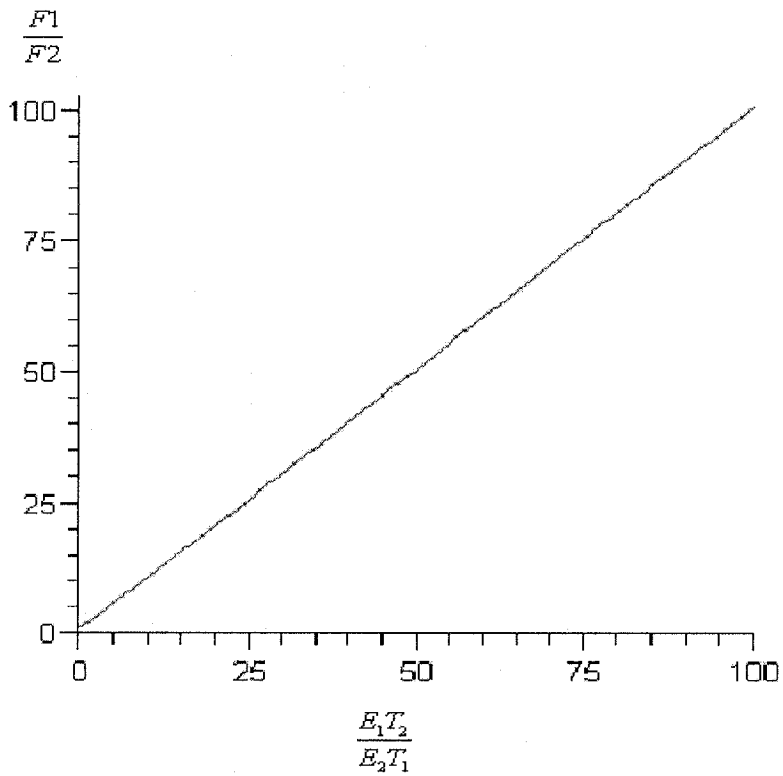

Figure 4-6 Variation of force ratio with modulus of elasticity in an elastic model

Let us consider $\frac{E_1 T_2}{E_2 T_1} = \alpha$, a dimensionless constant. The results obtained for the force ratio (it is the ratio of the force experienced by the rigid cylinder to the force experienced

by the soft cylinder) with the α variation at different area ratio (where A denotes the area ratio between the rigid and the outer compliant cylinder) from Equation 25 are shown in Figure 4.8

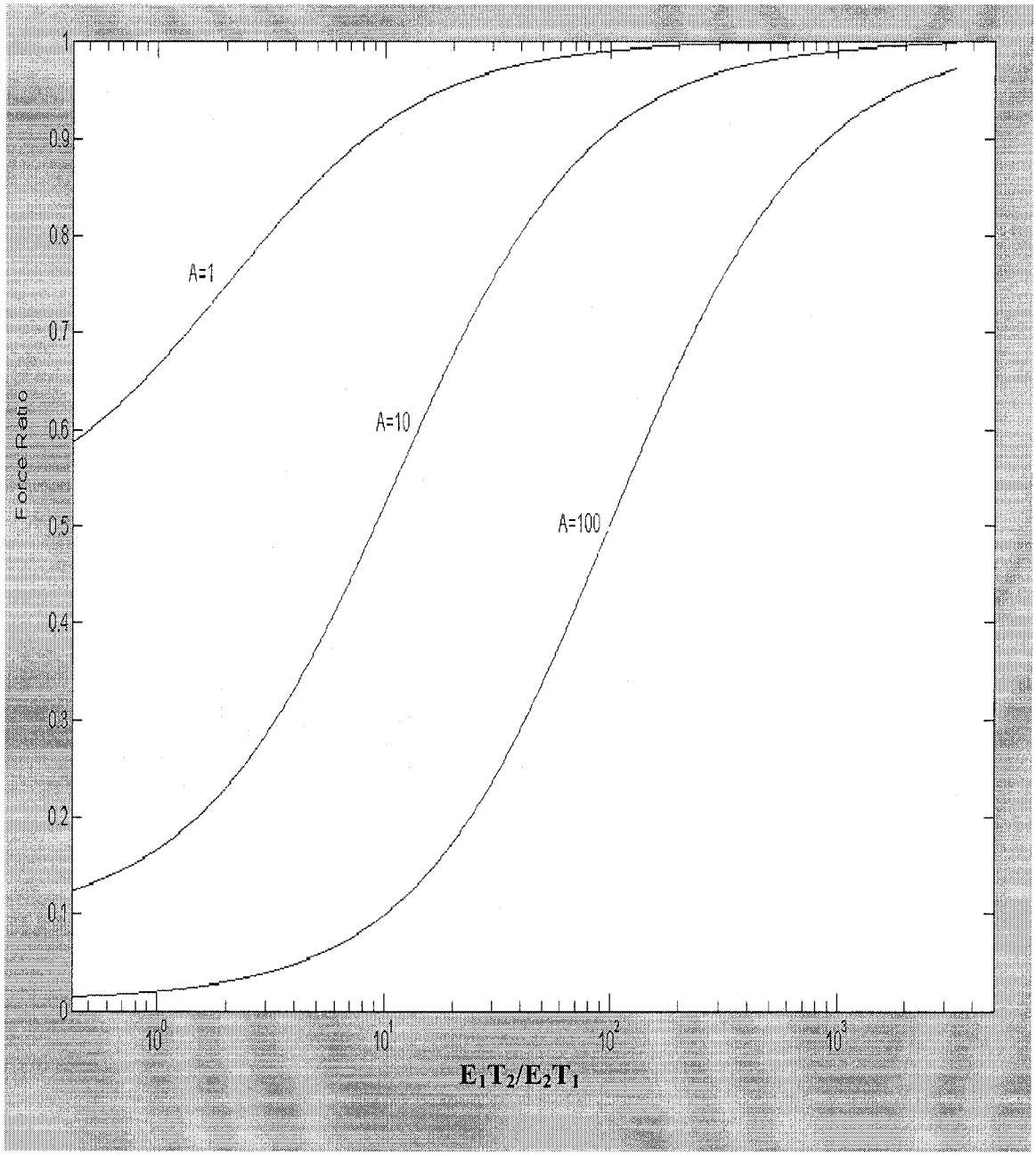

Figure 4-7 - Logarithmic Variation of force ratio with $\frac{E_1T_2}{E_2T_1}$ (α) function

It is clear from Figure 4.8 that as the dimensionless constant α increases, the sensed object becomes stiffer than the compliant element of the sensor. It is also interesting to note that in the limit where the sensed object has higher modulus of elasticity, the force ratio approaches unity. So, when the stiffness of the sensed object nearly equal to that of the rigid cylinder, only the rigid cylinder carries all the force applied meaning that the deflection between the rigid and the compliant element is not significant. When the sensed object is softer compared to the compliant cylinder, the outer compliant cylinder carries most of the forces, thus the force ratio decreases since this is directly proportional to the voltage ratio generated at the two different PVDF films.

As shown in Figure 4.7, the larger the area ratio, the larger the variation in the ratio of two forces thereby enabling a better estimation for the compliance of the object and force ratio obtained for area ratios ranging from 1 to 10. The curve tends to incline more for area ratios beyond 10.

4.2 Analysis in ANSYS

This section discusses details of modeling and analysis. In order to compare the results obtained above from the analytical symmetrical model, commercially available software can be used, such as, NATRAN, CATIA and ANSYS. The finite element analysis software ANSYS was used in our work with which modal, static and transient analysis can be carried out. With the help of advanced software geometrics, different load sets and materials properties can be analyzed. The ANSYS software used in our research was version 9.0 and was used to construct a complete geometric model for the compliance and force sensor. This model was used to predict the force ratio, stresses developed at the different location of the sensor for a given load.

4.2.1 Overview of ANSYS steps

When using ANSYS, all operations are performed using sequential steps. A flow chart, as shown in Figure 4.8, is the basic approach to find a solution. We can use ANSYS in two different modes; either the programming mode or graphical mode but the latter is much easier to use.

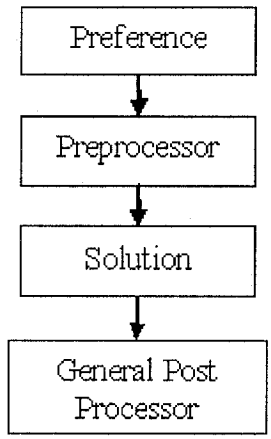

Figure 4-8 Overview of Ansys Steps [69]

4.2.1.1 Preference

The first step of ANSYS is to describe the nature of problem and to decide the method to be used for solving the problem which, in our case, is of a structural nature. Different modules are available for performing the analysis such as h or p methods. We used the h method for solving our problem.

4.2.1.2 Preprocessor

This is main body of modeling the problem and defining the element type, materials properties and real constant. In this section, we first defined the element type and its materials properties since the selection of the element is the main process in modeling. The modeling and meshing were performed in the next step. The main operation performed in the Preprocessor is given in the flowchart shown in Figure 4.9.

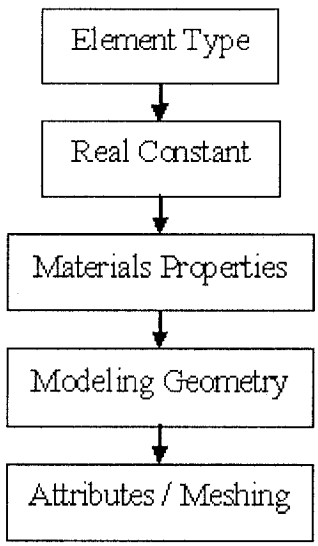

Figure 4-9 - Flow chart of processes in the Preprocessor

4.2.1.2.1 Elements type

In the following steps we describe our problem in ANSYS. First, we defined the problem in terms of structural and electrical aspects and it is only these properties that are considered during the whole modeling of the sensor. The next step was to define the different element types, depending on its purpose, used in meshing this model.

The Different elements performed different function in meshing and obtaining the results. The elements with different nature and different degree of freedoms help in making problem more suitable for results. The number of nodes per unit element also plays a significant role in obtaining good results. The elements and its properties are discussed in the following sections.

a) Solid 92

Solid 92 is a three dimensional tetrahedral structural solid element with 10 nodes. It has a quadratic displacement behavior and is suitable for a model that has irregular meshing. Each node has three degrees of freedom in x, y and z directions. Orthotropic material directions correspond to the element coordinate directions [69] element coordinate system orientation is as described in coordinate system. This element is for meshing the irregular and curved parts of sensor. The cylindrical parts were meshed with this element. The rigid and compliant cylinder was meshed using this element.

b) Solid 98

Solid 98 is a tetrahedral coupled field solid with 10 nodes with up to six degrees of freedom at each node [69]. This element behaves similar to solid 5 but has good meshing properties for irregular geometries. The element has quadratic displacement behavior and is well suited to models having irregular meshes. The three-dimensional

magnetic, thermal, electric, piezoelectric, and structural field capability is similar to that described for Solid 5 and was used for meshing the circular PVDF films. In the next section real constant and materials properties of the parts are defined.

4.2.1.2.2 Real constant

Our next step is to define a real constant for the defined element. In our problem, we are dealing with solid geometry so we require a solid element for our analysis but, in practice, solid elements do not require a real constant.

4.2.1.2.3 Material Properties

In the fourth step, we defined the material properties of all the individual parts of the sensor as per the material specification, as detailed in chapter 2. The rigid cylinder, substrate has the same material properties as discussed in the chapter dealing with sensor design. For these materials, we define the isotropic properties and the Poisson ratio. Similarly, for the compliant cylinder and sensed object, the isotropic properties and Poisson ratio are defined as 7.1 MPa and 0.45 respectively. The PVDF films have anisotropic behavior and electrical properties. The piezoelectric strain constant, d, for the material was defined with permittivity of the material. All materials described in the problem were numbered accordingly. The sensed object materials were assigned the material property similar to the samples being tested experimentally. The sensed object properties were changed for Material#1, Material#2, Material#3 and the ANSYS results were simulated. The sensed object properties are assigned as per the Manufacturer's data.

4.2.1.2.4 Modeling

In this section a quarter model of the sensor with the tissue is made with the exact dimensions of the sensor design, due to the issues with difficulty in meshing the full sensor as shown in Figure 4.11. The whole structure was created from different parts which are suitably positioned and glued. The dimension of each part is shown in the design section of Chapter 2.

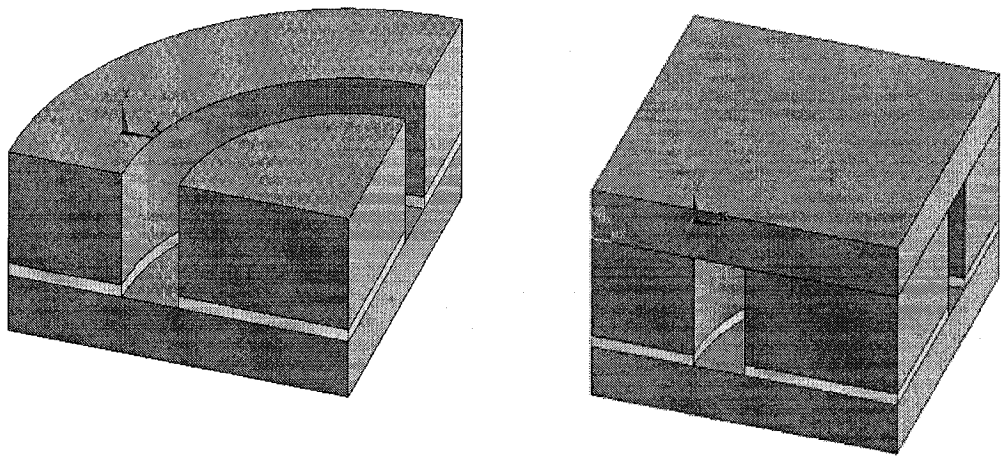

Figure 4-10 - Sensor structure with and without the sensed object

4.2.1.2.5 Attributes and Meshing

This is final stage of the preprocessor before starting the computational iteration for finding the solution. In this stage, each parts of the sensor are linked to their respective materials and elements and were meshed. The Elements meshing can be refined depending upon requirement of the results. Due to the unavailability of nodes for meshing, the model was meshed at a refine level of 4 as seen in Figure 4.12.

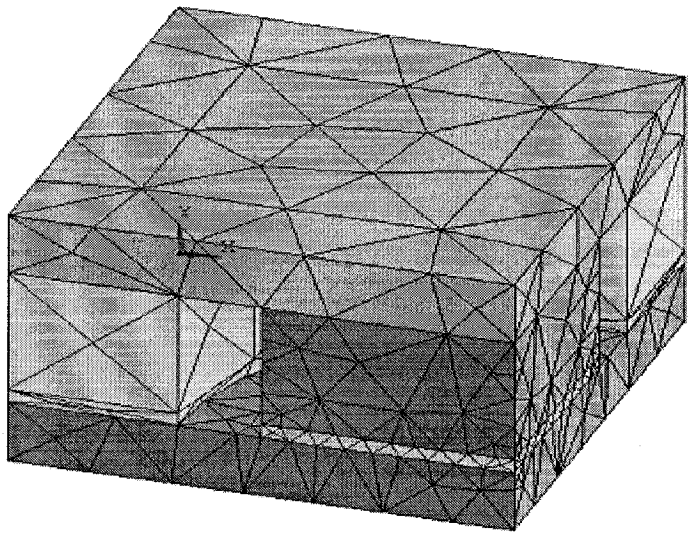

Figure 4-11- Meshed structure of a quarter model sensor with the sensed object

4.2.1.3 Solution

In this section, the ANSYS solution of modeled problem is carried out by using the flow chart shown in Fig 4.10. The first required entry is to define the analysis types such as static, harmonic, dynamic. Apply loads require entry of boundary conditions that apply to our model. The last step is to solve the meshed model.

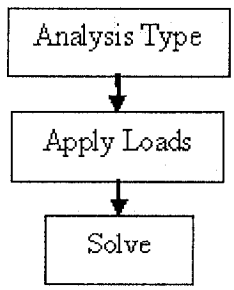

Figure 4-12 Steps for solving ANSYS model

Before continuing, the type of solution, such as static or dynamic needs to be defined. The load was applied on the surface of the sensed object in a uniformly distributed manner as shown in Figure 4.13. The boundary conditions were fixed for the sensor whose base substrate was assumed to be fixed. The boundary conditions are applied to a sensed object to make it a zero displacement in the XY plane and a load was applied on the sensed object. The program was then run to get the results during which warning conditions of aspect ratio were displayed that showed the longest to shortest side of element. These warnings are necessary because PVDF films can be as thin as $25X10^{-6}$m. Once a solution is shown, it is necessary to portray the results visually and is discussed in Section 4.2.1.4.

The Figure 4.13 below shows the load applied on different node numbers on top of the sensed object. A load of 10N was applied on each node and the force ratios obtained at the PVDF under the inner and outer cylinders were determined.

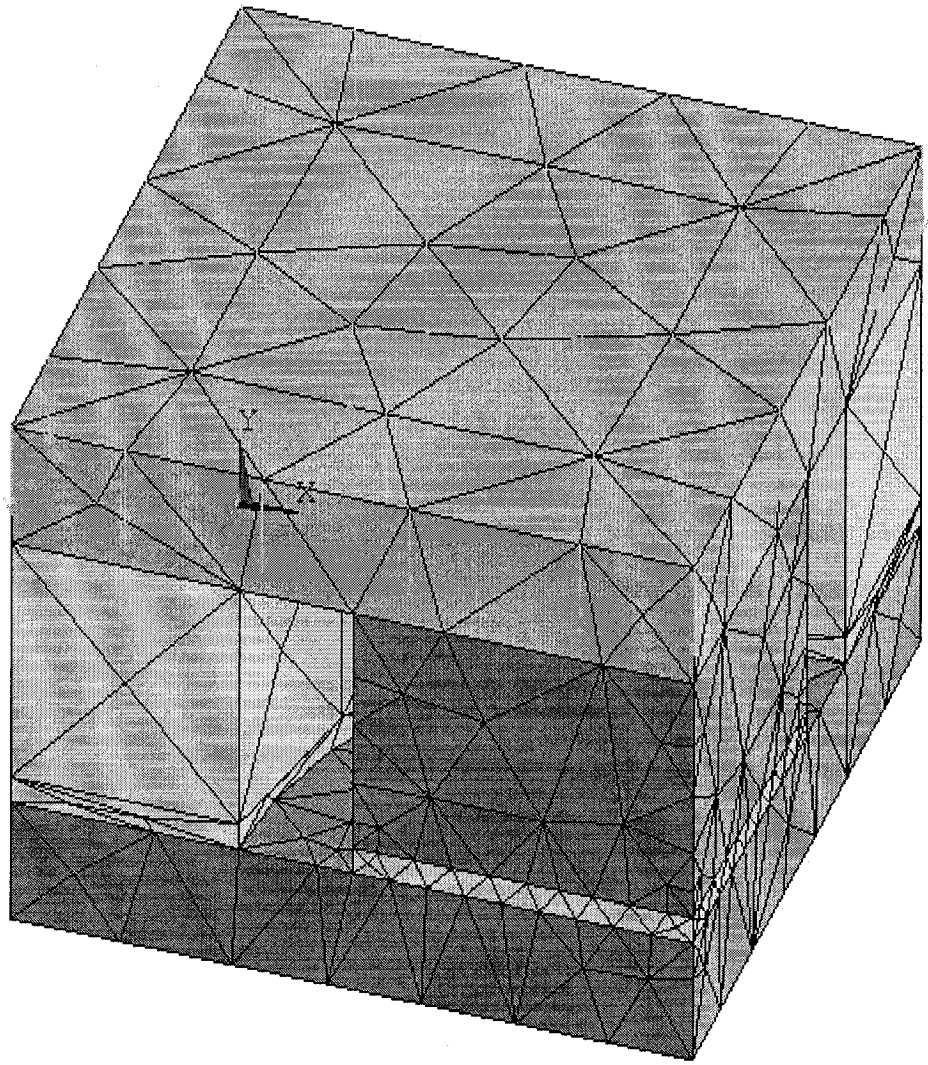

Figure 4-13 Uniform Load application on all top nodes

4.2.1.4 General Post Processor

In this section, data obtained as part of the solution section are reviewed using the many options available to see these results. Plot section and list section provide the results in the graphical presentation and numerical values, respectively. Any results such as stresses, strains, reactions at any point can be visualized using graphs.

Deformed shapes of sensor were plotted for checking geometrical deformation in the sensor. Stress distributions were also plotted. The material properties assigned for the sensed object were changed during the simulation according to the sample being tested. The thickness of the sensed object was considered as being the same as the one tested experimentally. But our main focus is to determine the effect on the rigid cylinder and voltage generated by PVDF films.

Since the voltage ratio is equal to the force ratio in our sensor design, the reaction force at all the nodes under the inner PVDF and the outer PVDF were found and an average value of these forces was calculated. The force ratio of inner and outer PVDF values are calculated and are compared to the voltage ratio found experimentally in Chapter 5.

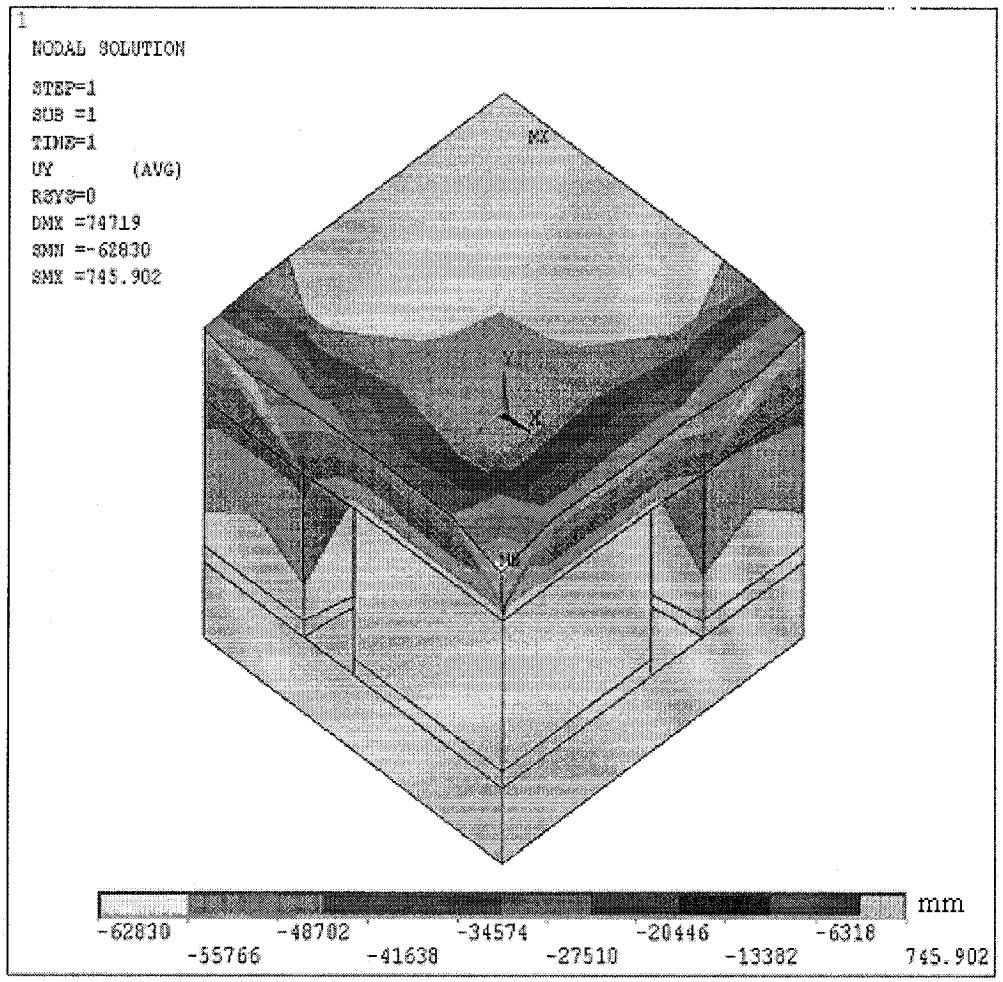

Figure 4-14 The deflection of the sensor structure after the application of load

Figure 4.14 shows the deflection of the sensor when the load is applied. The sensed object comprises a hard material (Material#1). It can be seen that the maximum deflection occurs in the rigid cylinder, which means that there is more force on the inner PVDF than on the outer PVDF.

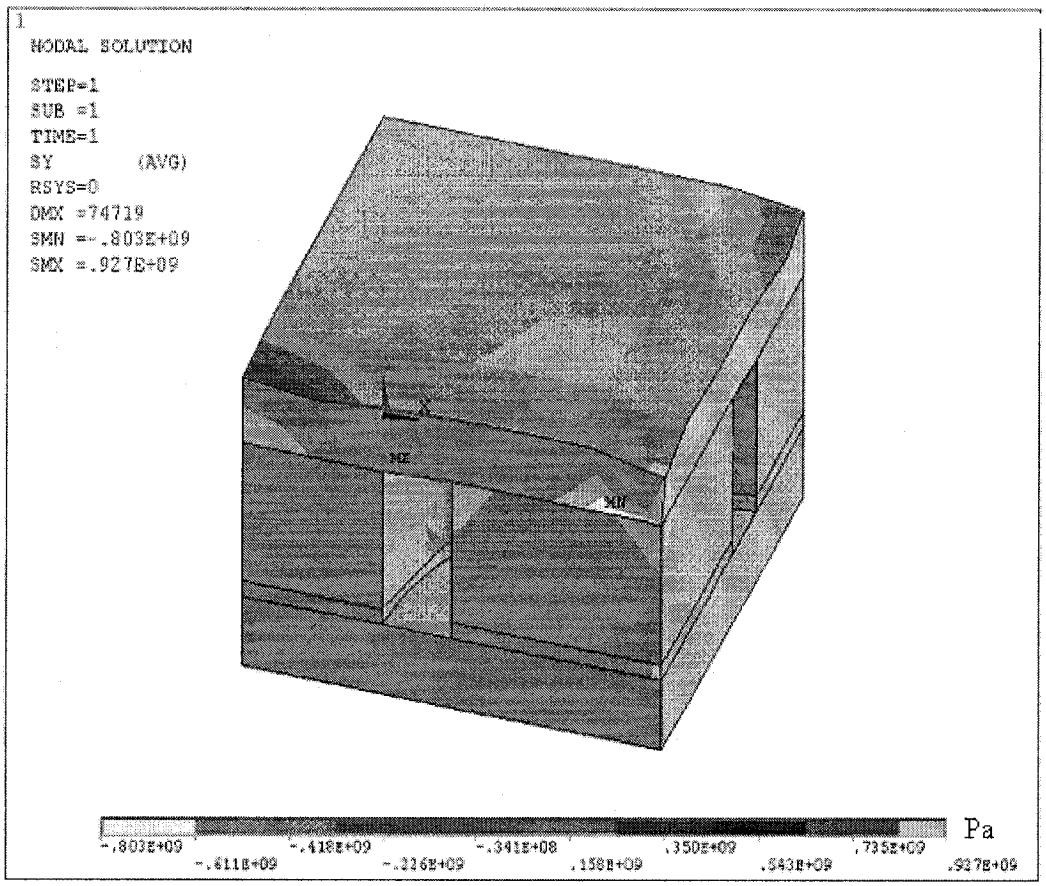

Figure 4-15 Stress distribution in the Y direction over the sensor structure

Figure 4.15 shows the stress distribution in the Y direction along the structure of the sensor for the sensed material (Material#1). It again shows that the maximum stress distribution occurs along the rigid cylinder. The maximum value is .927e9 Pa.

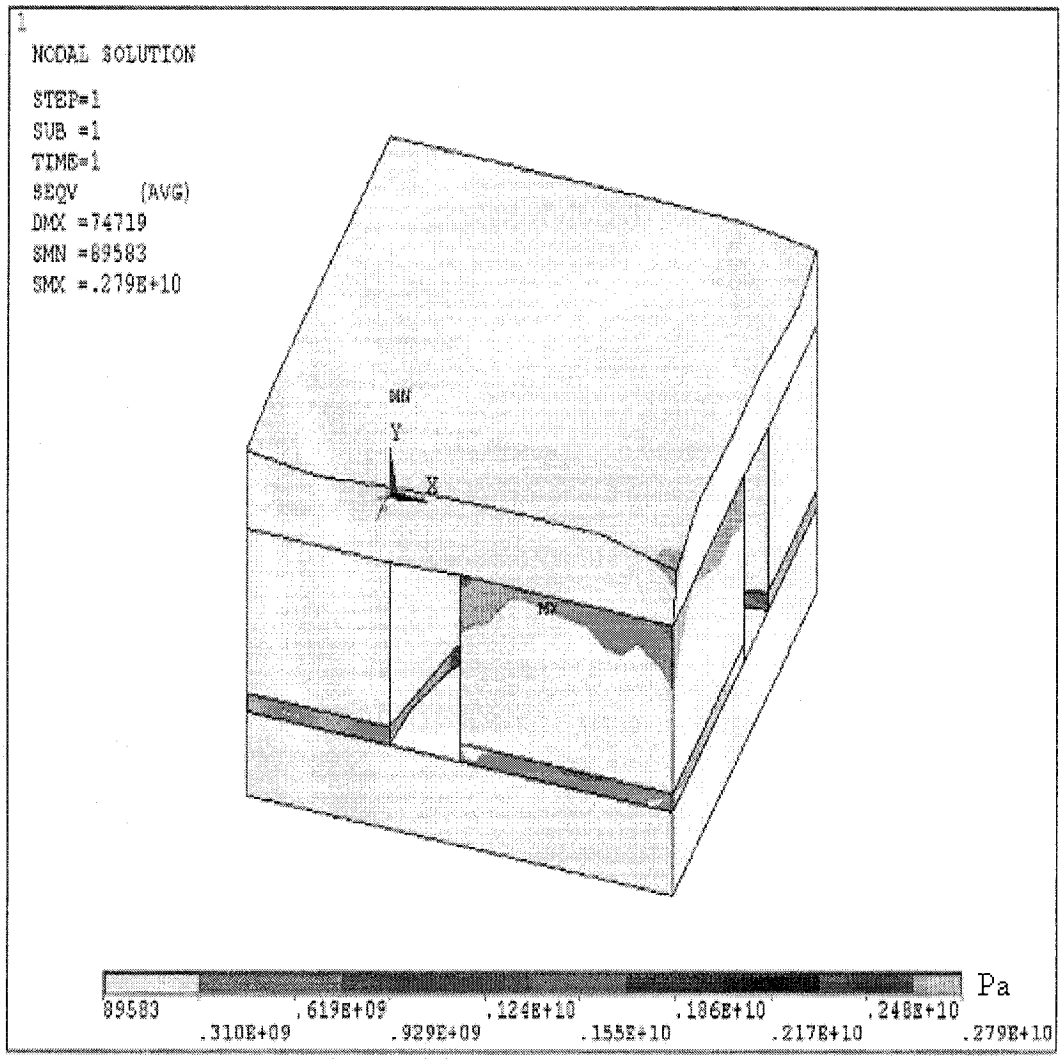

Figure 4-16 Von-Mises Stress distributions over the sensor structure

Figure 4.16 shows the Von-Mises stress distribution across the sensor for Material#1.Finally, the reaction force at the nodes under the inner PVDF and outer PVDF were tabulated and the force ratios obtained as shown in Table 4.2. This force ratio, which is equal to the voltage ratio, is compared to the experimental value. The tables below shows the force values at inner PVDF and the outer PVDF for all the three materials. The maximum stress is 0.279e10 Pa

Table 4-1 Reaction forces at the Inner and Outer PVDF for Material#1

Force on the inner PVDF under the rigid cylinder	Force on the outer PVDF from the compliant cylinder
N	N
3.72	0.92
3.73	0.68
3.99	0.85
3.87	0.88
5.87	1.08
5.17	1.13
6.32	1.26
6.09	1.58
4.67	0.80
6.31	1.25
AVG = 4.974	AVG = 1.073

From Table 4.1, we obtain the average force F_1 from the PVDF under the rigid cylinder and the average force F_2 from the PVDF under the compliant cylinder as F_1 = 4.974 N and F_2 = 1.073 N. Hence the force ratio for Material#1 from ANSYS is 4.63.

Table 4-2 Reaction forces at the Inner and Outer PVDF for Material#2

Force on the inner PVDF under the rigid cylinder,	Force on the outer PVDF from the compliant cylinder,
N	N
5.67	3.56
6.23	6.65
8.18	5.98
4.65	4.88
3.12	6.27
6.32	4.28
4.89	5.54
4.55	3.65
3.78	6.76
5.36	4.33
AVG = 5.275	AVG = 5.19

From Table 4.2, we get the average force F_1 from the PVDF under the rigid cylinder and the average force F_2 from the PVDF under the compliant cylinder as F_1 = 5.275 N and F_2 = 5.19 N. Hence the force ratio for Material#2 from ANSYS is 1.016.

Table 4-3 Reaction forces at the Inner and Outer PVDF for Material#3

Force on the inner PVDF under the rigid cylinder	Force on the outer PVDF from the compliant cylinder
N	N
3.13	5.76
3.65	6.65
3.89	7.85
8.88	2.55
4.56	5.48
6.96	4.89
1.55	7.21
5.49	6.53
6.56	4.39
8.75	5.91
AVG = 5.342	AVG = 5.722

From Table 4.3, we get the average force F_1 from the PVDF under the rigid cylinder and the average force F_2 from the PVDF under the compliant cylinder as F_1 = 5.342 N and F_2 = 5.722 N. Hence the force ratio for Material#3 from ANSYS is 0.933.

5. CHAPTER

EXPERIMENTAL TESTING AND RESULTS

5.1 Introduction

The smart endoscopic grasper test system consists of an array of tactile sensors and data acquisition cards as important components. The sensor is tested for dynamic force inputs and each has two analog voltage outputs which are generated from the forces applied by the load cell to the object. These voltages are proportional to the softness of the grasped object and are interfaced using a data acquisition card via connectors and an electronic system. Using the data acquisition card, the signals are amplified, filtered, digitized and finally processed by a computer. The connection of the sensors to data acquisition card initially created some technical problems due to high impedance, which were overcome by adding electronic components, as will be detailed in following sections.

The sensor design has been fully described in previous chapters but basically consists of a rigid cylinder surrounded by a compliant cylinder as shown in Figure 5.1. A PVDF (Polyvilidene Fluoride) sensing element is positioned under both the rigid and compliant cylinders as shown in Figure 5.2. When an object is in contact with the sensor, a load is applied to these cylinders. The softer the contact object, the more the transfer of load from the rigid to compliant cylinder increases.

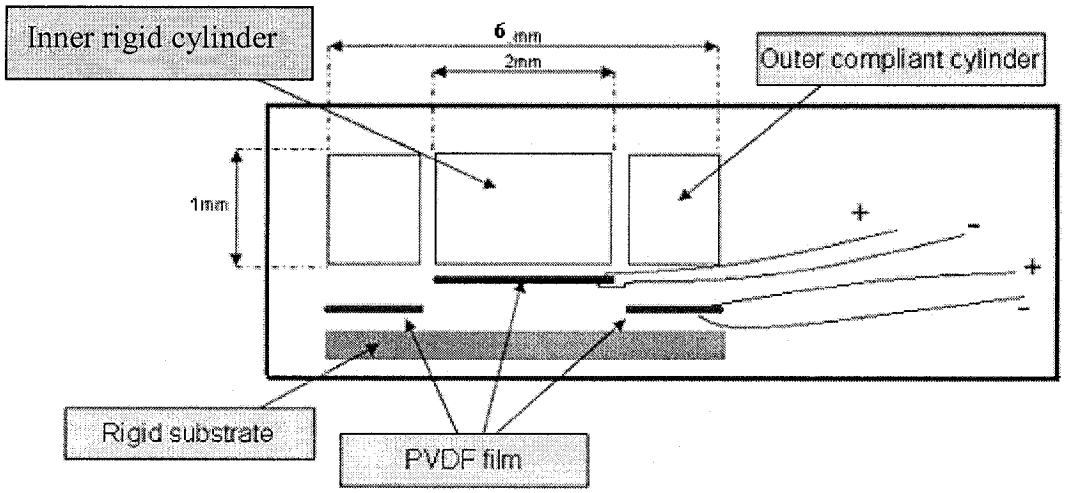

Figure 5-1 Cross sectional exploded view a sensor unit

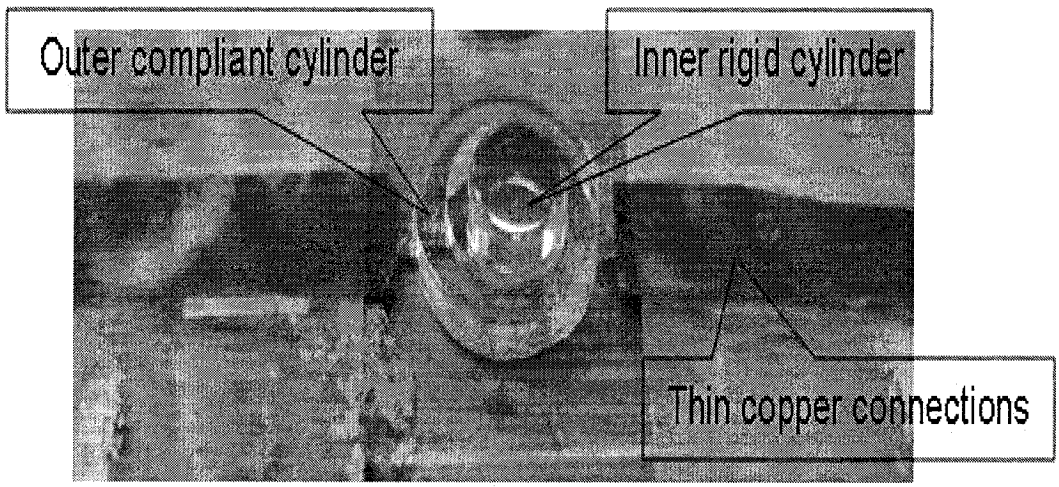

Figure 5-2 Sensor and electrical connections

5.2 Experimental set-up

The schematic diagram of the experimental measurement setup, developed to analyze the performance of the sensor, is shown in Fig.5.3.

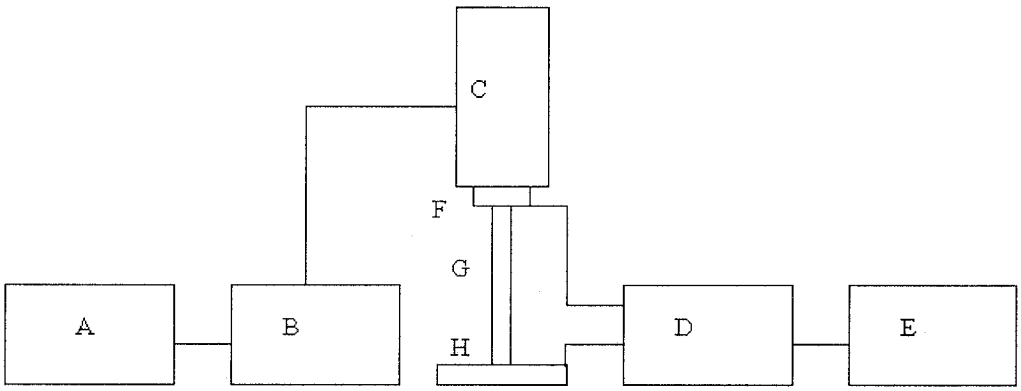

A-Power Amplifier	E- Computer
B- Signal Generator	F-Force Transducer
C-Vibrator	G-Probe
D- A/D Converter	H-Sensor

Figure 5-3- Experimental Set-up

A cylindrical probe, driven by a vibration unit (Ling dynamic model V203), was used to apply a sinusoidal force at about 10Hz. The vibration unit itself was activated by a signal generator (Agilent 33220A). The magnitude of the applied force was determined by a force transducer (Kistler, Type 9712B50) inserted between the probe and the vibration unit. The charge generated by both inner and outer PVDF films was amplified and the output was measured on the computer. Channel 1 (CH1) of the data acquisition system was used to measure the output of the PVDF right under the rigid cylinder. Channel 2 (CH2) was used to measure the output of the PVDF under the outer cylinder.

The amplification factor of these outputs, F_1 and F_2 respectively, was 10mv/lbf. Another output from the force transducer was also amplified by another charge amplifier (Kistler Instrument, model 504E). Another channel in the data acquisition system is arranged to measure this signal, which was used to verify that the probe made proper contact with the test system.

Three kinds of objects were tested. A dynamic sinusoidal load was applied to the test object. The peak to peak voltage and frequency values from the three channels were captured by the data acquisition and interface system, as detailed in the following section.

Below is a list of all the equipment and their specifications used in the experimental measurement setup and test process:

- Dual Mode Power Amplifier: Model 504E, Kistler Instrument Corp.
  Useful Amplifier factor: 1V/lbf

- Signal Generator: Agilent 33220A
  20MHz Function/Arbitrary Waveform Generator

- V203 Vibrator: made by Ling Dynamic Systems LTD. Main specification,
  Sine force peak: 17.8N;
  Useful frequency Range: 5 ~ 13000Hz;
  Velocity sine peak: 1.49m/s;
  Amplifier rating: 0.048kVA;
  Displacement pk-pk: 5.0mm;

- Charge Amplifier: Type 2634.
  Amplifier factor: 10mv/lbf

- Oscilloscope: Agilent 54624A Oscilloscope, 100MHz 200MSa/s;
  Controller interface: RS-232
- Force Transducer: Type 9712B50, Kistler Instrument Corp.
  Sensitivity: 92.9mv/lbf;

Measuring range: 50lbf;

Temperature: -50~120°C.

- Probe: Aluminum bar, connected with force transducer, passing force to tactile sensor.
- Tactile Sensor: see Figure 2.6 in the sensor design section.

5.3 Data acquisition system

The Data Acquisition System (DAQ) contains all the necessary hardware to take the analog signals from the sensor and digitize them. The DAQ (Type: NI PCI-6225 from National Instrument Company), was used in this testing.

Because the PVDF in the sensor does not have a common ground connection with the data acquisition card, and because the input impedance of that card is very high, it was necessary to use bias resistors to connect the sensor output to the card. To reduce the loading effect on the sensor output, the values of these resistors needed to be very high. Such high resistance is achieved by the dynamic resistance of a pair of diodes, which are connected to each other with opposite polarity, as shown in Figure 5.4.

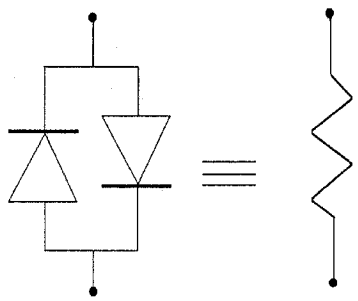

Figure 5-4 Bias resistor using two diodes

The input voltage from the inner and outer PVDF sensing elements of each individual tactile sensor unit is read. Since the grasper consists of eight sensing units, as shown in Figure 5.5, a total of 16 analog input voltages are registered. In order to reduce the 60Hz line noise, which was induced into the system due to the presence of PVDF film, the DAQ main amplifier was used in differential mode. Hence, in order to read 16 input voltages, 32 channels from the DAQ were utilized.

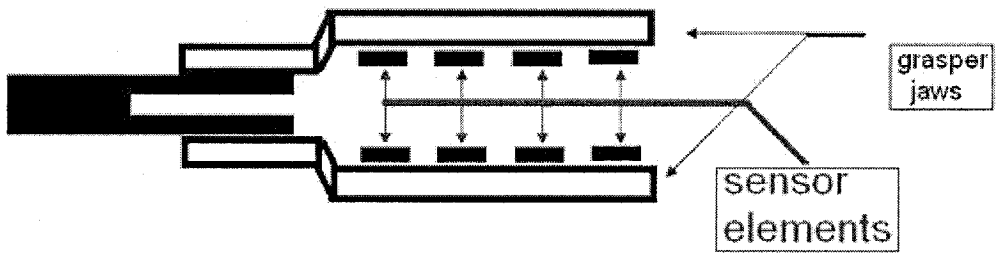

Figure 5-5 Endoscopic Grasper

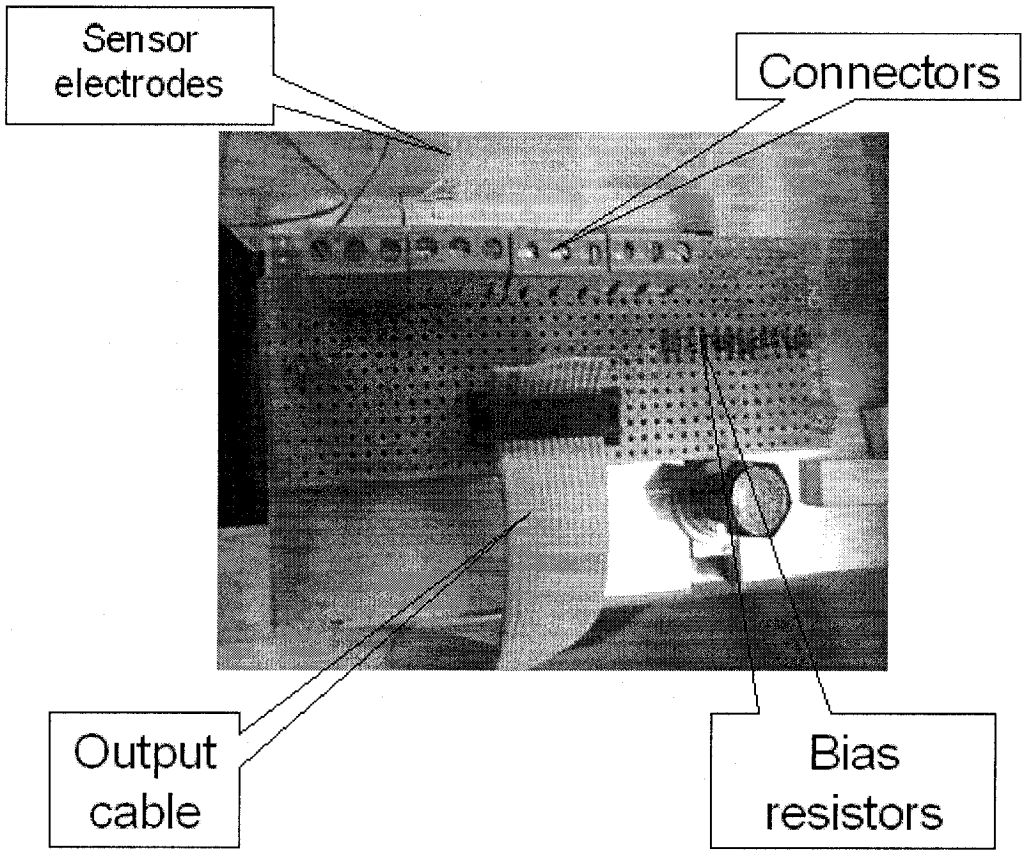

Figure 5-6 - Connectors and Bias Resistor Board

In Figures 5.6 the bias resistors board is shown. Sensors electrodes are connected to this board are interfaced with the DAQ by a flat cable.

The complete experimental set up with all the electronic components and the display unit is shown in the Figure 5.7.

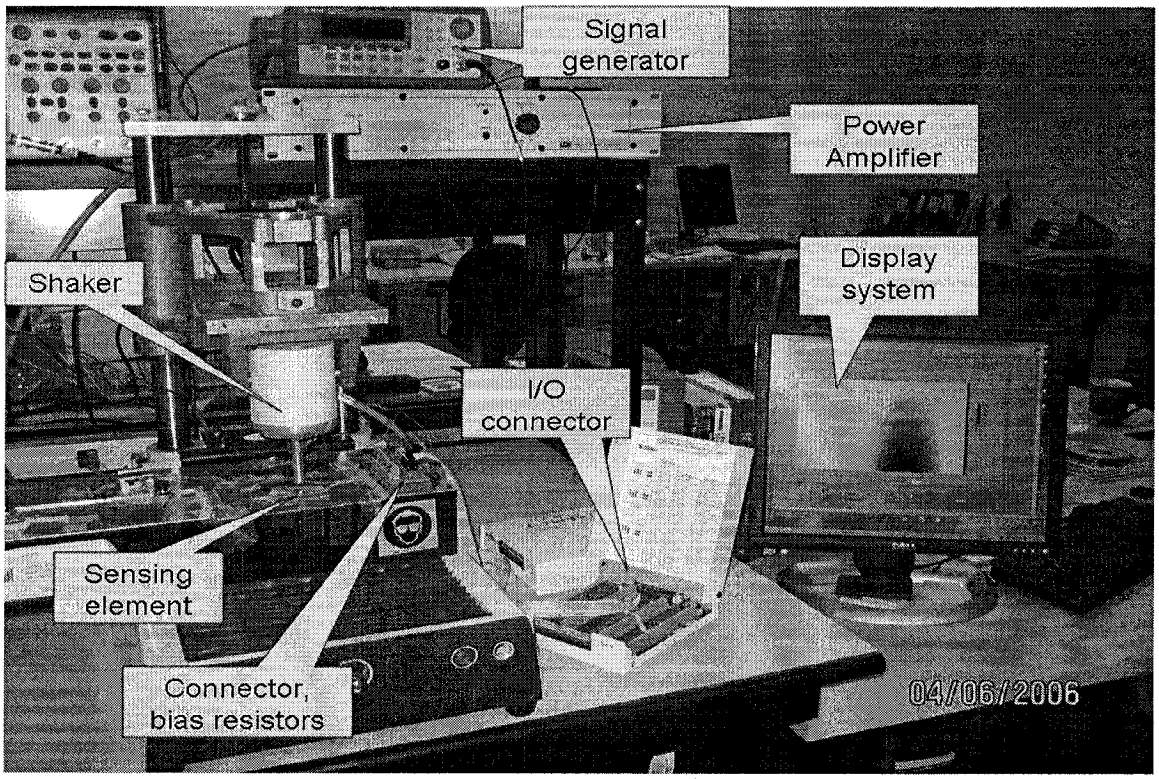

Figure 5-7 Photograph of the complete setup

The tactile sensor is positioned under a probe. A dynamic load was applied by the shaker which was activated by a power amplifier and a signal generator. The output of the sensor was fed to the connector box via the bias resistors. The data was then transferred to the data acquisition card inside the computer. The block diagram of the data acquisition system is shown in Figure 5.8.

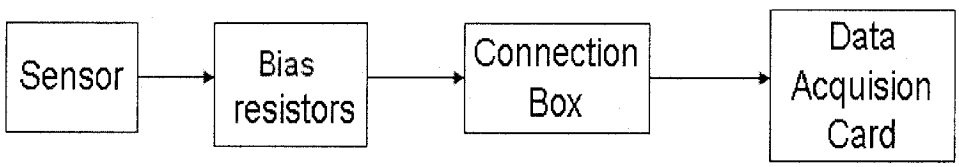

Figure 5-8 Block diagram of the Data Acquisition System

5.4 Results

The approach used to investigate the prototype tactile sensor is to apply a dynamic load and measure the voltage outputs. As mentioned earlier, two different designs were tested. The first one was a single sensor element and the second one is an array of tactile sensors. The test samples are sliced in the form of rectangles using a hot and thin metal string foam cutter. Three elastomers, each having a different Modulus of elasticity, were chosen for the testing and were supplied by PROFOM, Canada whose values are shown in Table 5.1.

Table 5-1 Young's Modulus value of each material supplied by the manufacturer

Material#1	Material#2	Material#3
MPa	MPa	MPa
170	22	15

This material is placed between a cylindrical probe and the sensor. A sinusoidal force is applied using a force transducer. The test frequency is kept at 10 Hz and the voltages in each case are recorded. Based on the test materials, the rigid and compliant element of the sensor will carry different forces, and hence the PVDF under the rigid and compliant cylinder will generate different voltages. These voltages are fed into a computer using an A/D converter and a Data Acquisition System from which Lab view 7.1 software is used to process the signals. The signals from the PVDF contain considerable noise which is removed using a low pass filter at a cut-off frequency of 45Hz. The voltage outputs V_1 and V_2 from the rigid and soft cylinders correspond to F_1

and F_2 respectively with an amplification factor of 10mV/lbf. Hence the voltage ratio corresponds to the force ratio. The voltage ratios are monitored on the computer screen and the different results for different tests are obtained and recorded.

5.4.1 Calibration

Calibration is defined as the process of quantitatively defining the system response to known, controlled signal inputs. Prior to performing the experiments on objects, the sensor assembly was calibrated and the resulting curve is shown in Figure 5.9. A known force was applied to the sensor using the force and the output voltage from the sensor was measured. As can be seen, between the force ranges of. 0.1N to 1 N, a good linear relationship exists between the output voltage from the sensor and the applied load.

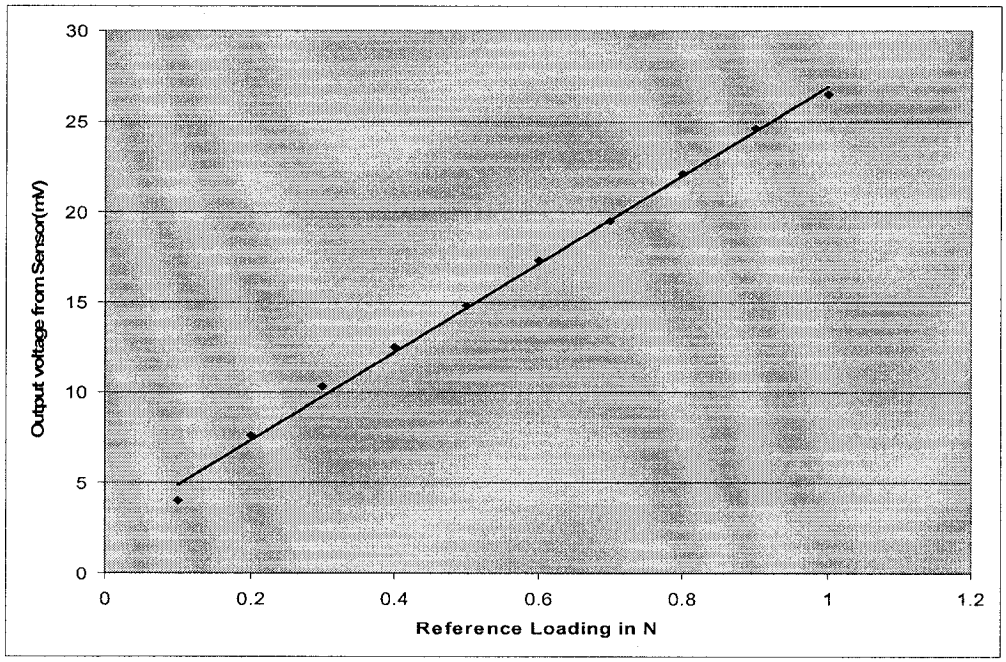

Figure 5-9 Calibration curve for the tactile sensor

5.4.2 Testing

The dynamic response of the sensor was observed by applying a sinusoidal load (at a frequency of 10Hz) on the tooth of the sensor. The measured peak-to-peak voltage ratio values are plotted against the applied force for different materials.

5.4.2.1 Single Sensor Testing using Material#1

Figure 5.10 shows the output of the sensor when Material#1 was tested under a sinusoidal input force of 1.77V at frequency of 10Hz. We can see the signals from the rigid and the outer PVDF in terms of volts as well as their voltage ratio V_1/V_2.

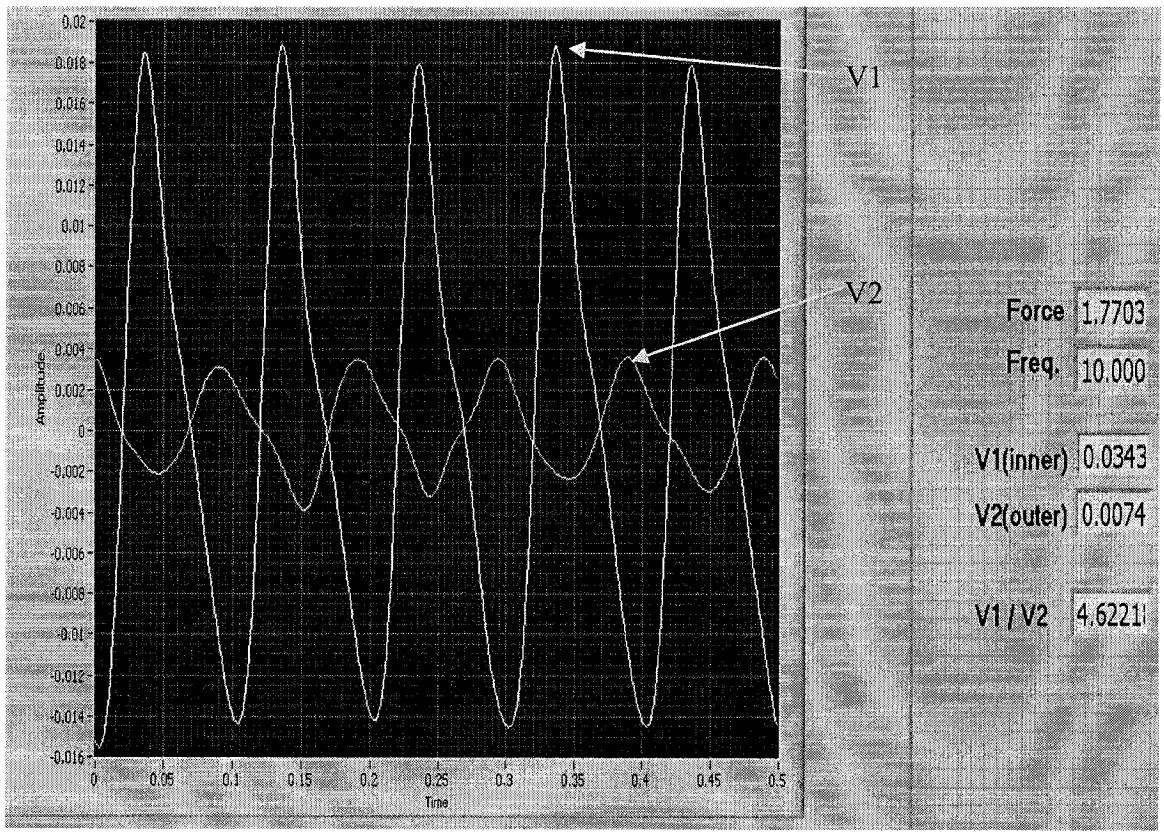

Figure 5-10 Single sensor output for Material#1

Material #1 was tested at different input forces and the corresponding voltage ratio was recorded as shown in Table 5.2.

Table 5-2 Single sensor input and output signals for Material#1

Input Signal (Volts)	Voltage ratio (V_1/V_2)
0.2	1.23
0.4	1.56
0.6	1.9
0.8	2.2
1	2.5
1.1	2.74
1.2	3.1
1.3	3.4
1.4	3.75
1.5	4.1
1.6	4.4
1.7	4.62
1.8	4.66

Figure 5.11 shows the plot of force versus peak-to-peak voltage output from PVDF films for the prototype Design-1 using Material#1. It can be seen from the plot that with the increase in force on the tooth of the sensor, the peak-to-peak voltage ratio outputs from the PVDF film increases linearly. The input signal is the sinusoidal force interpreted in terms of voltage from the force transducer.

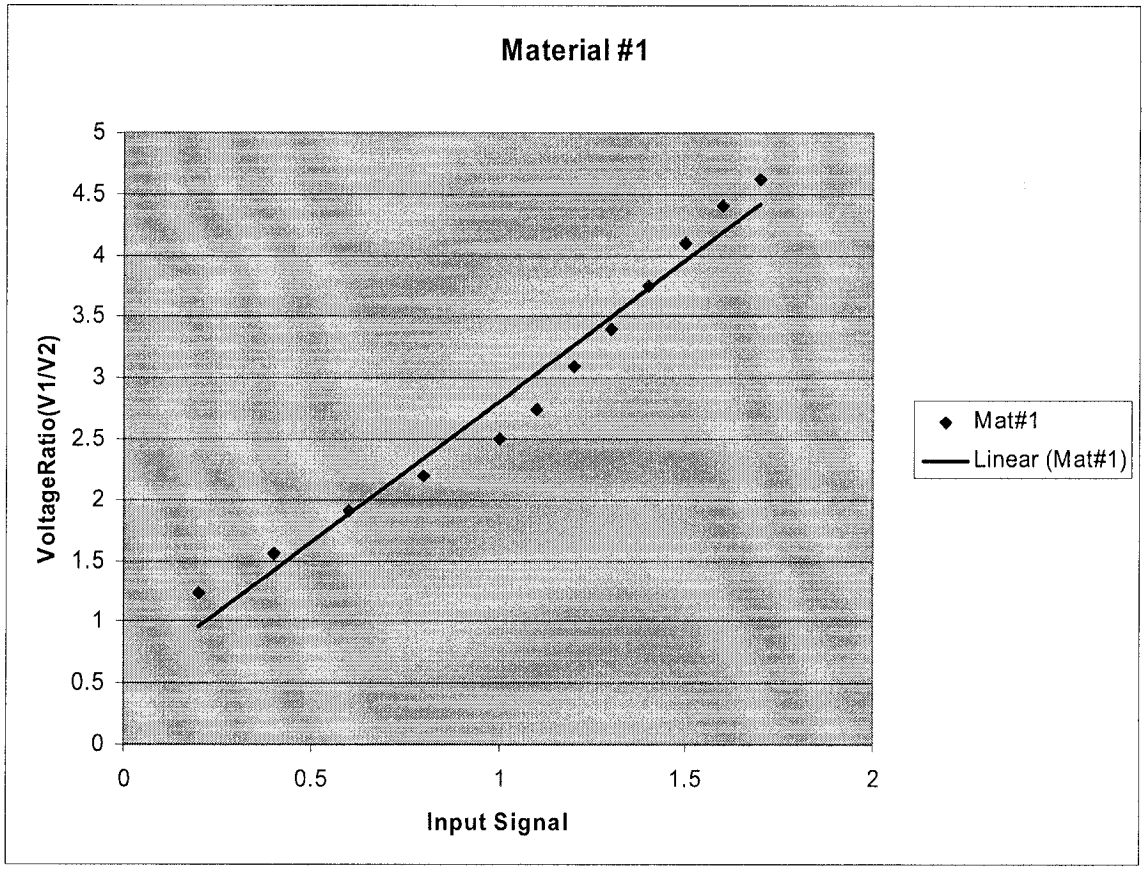

Figure 5-11 Single sensor plot of force versus peak-to-peak voltage

5.4.2.2 Single Sensor Testing using Material#2

Figure5.12 shows the output of the sensor when Material#2 was tested for a sinusoidal force of 1.79V at frequency of 10Hz. We can see the signals from the rigid and the outer PVDF in terms of volts as well as their voltage ratio V_1/V_2 which, in turn, is proportional to the force ratio.

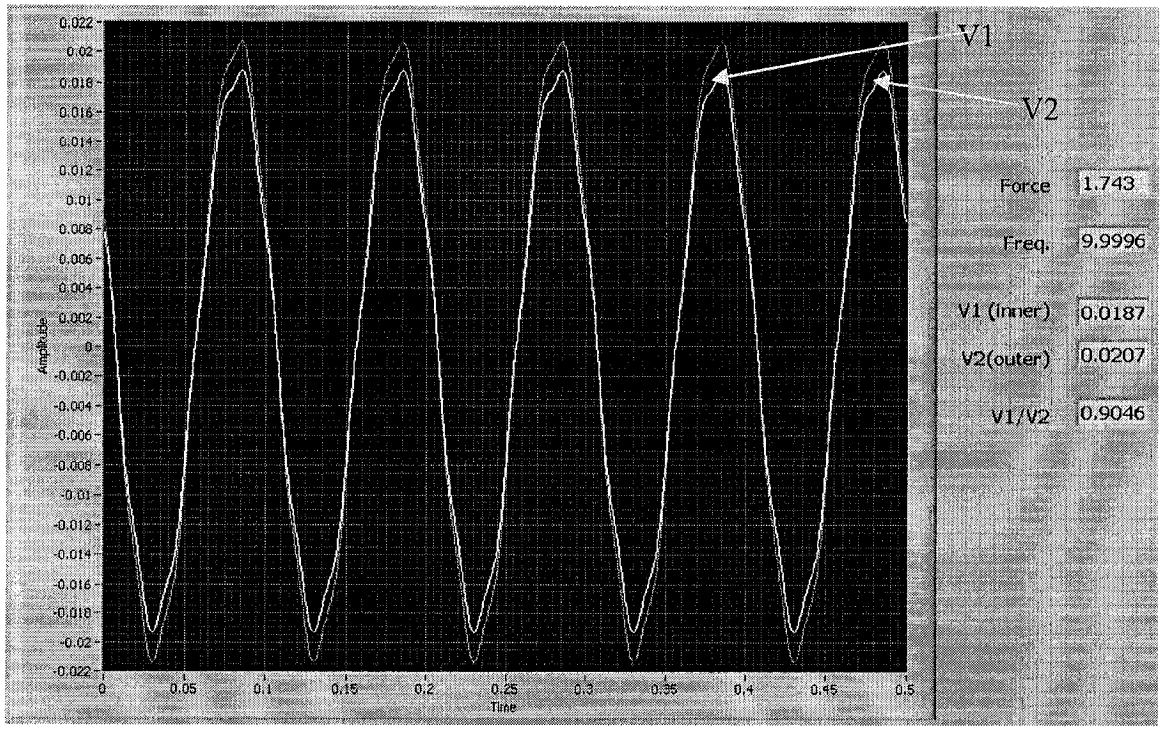

Figure 5-12 Single sensor output for Material#2

Material#2 is tested at different input forces and their corresponding voltage ratios were recorded and summarized in Table 5.3.

Table 5-3 Single sensor input and output signals for Material#2

Input signal (Volts)	Voltage Ratio (V_1/V_2)
0.4	0.277
0.8	0.38
1	0.48
1.2	0.59
1.4	0.7
1.6	0.82
1.8	0.91

Figure 5.13 shows the plot of force versus peak to peak voltage output from PVDF film for the prototype Design-1 using Material#2. It can be seen from the plot that as the input force increases, the peak to peak voltage output from the sensor PVDF film increases linearly and also the voltage ratio.

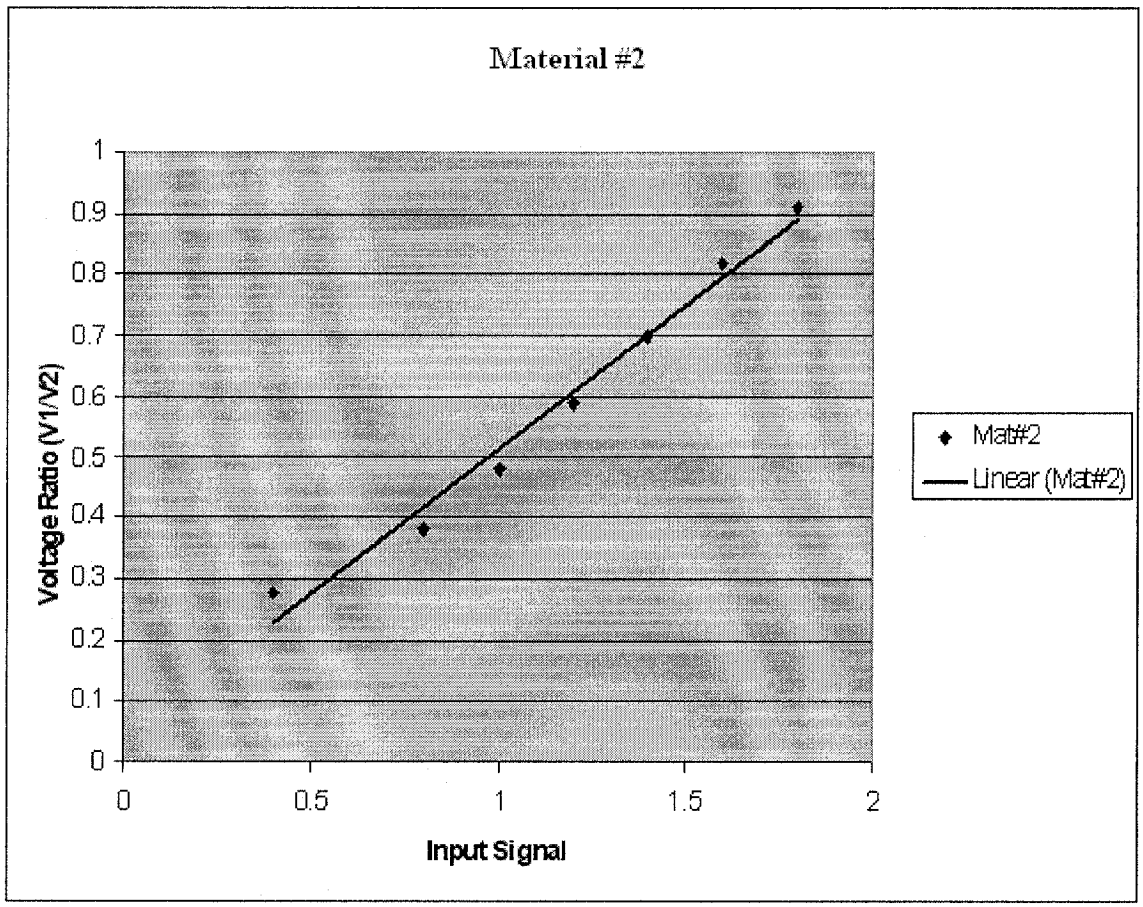

Figure 5-13 Single sensor plot of force/peak-to-peak voltage for Material#2

5.4.2.3 Single Sensor Testing using Material#3

Figure5.14 shows the output of the sensor when Material#3 was tested using a force of 1.73V at a frequency of 10Hz. We can see the signals from the rigid and the outer PVDF in terms of voltage as well as their voltage ratio V_1/V_2 which, in turn, is proportional to the force ratio.

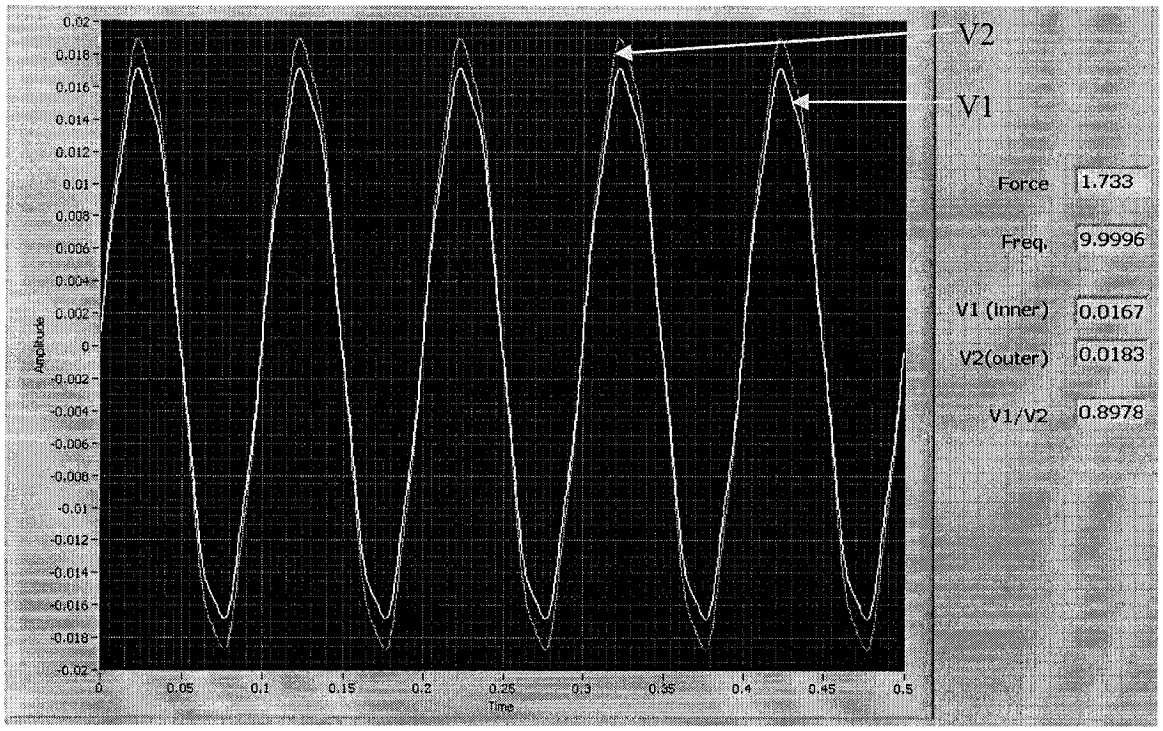

Figure 5-14 Single sensor output for Material#3

Material#3 was tested for different input forces and the corresponding voltage ratios were recorded and summarized in Table 5.4.

Figure 5.15 shows the plot of force versus peak to peak voltage output from PVDF film for the prototype Design-1 using Material#3. It can be seen from the plot that with the increase in force on the tooth of the sensor, the peak to peak voltage output from the PVDF film increases linearly and also the voltage ratio.

Table 5-4 Single sensor input and output signals for Material#3

Input Signal (Volts)	Voltage Ratio (V_1/V_2)
0.4	0.37
0.8	0.44
1	0.54
1.25	0.61
1.4	0.72
1.7	0.81
1.8	0.87

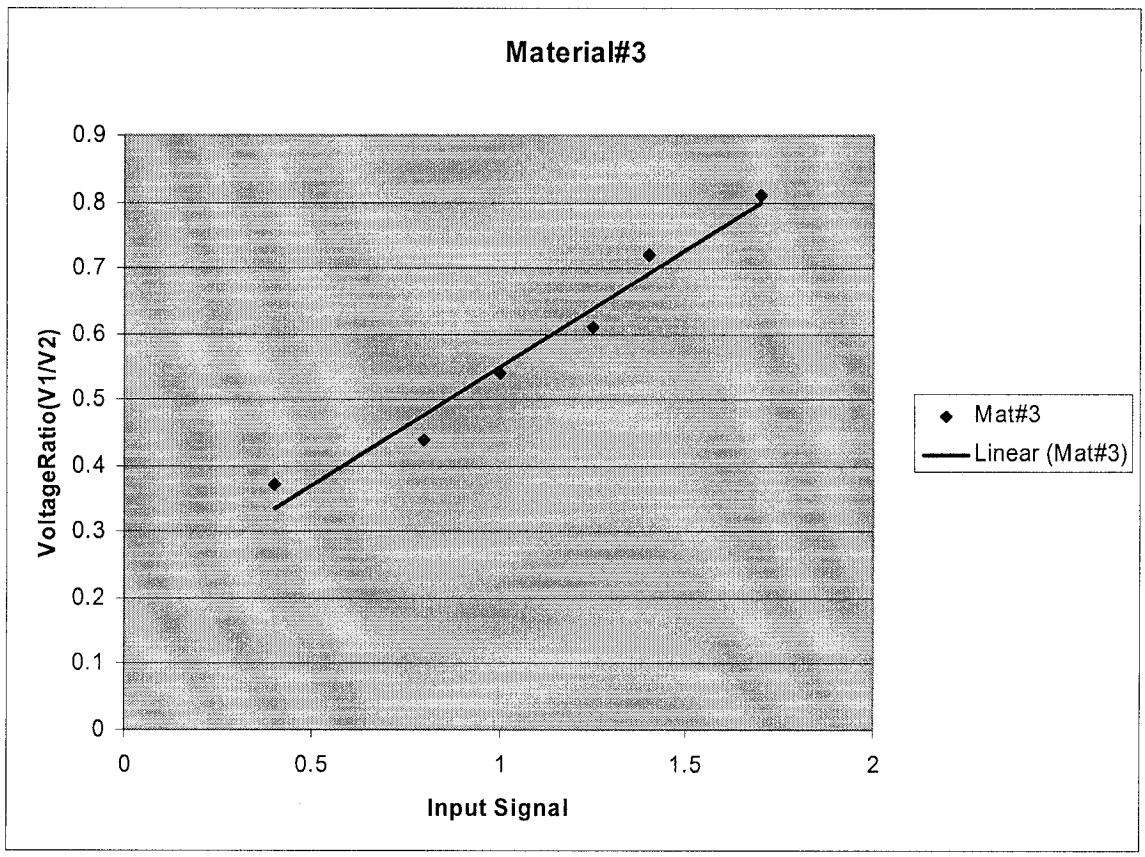

Figure 5-15 Single sensor plot of force/peak-to-peak V for Material#3

5.4.2.4 Single Sensor Testing using all Material

Table 5.5 shows the recorded values for all three materials tested. The values are recorded for each increased force value. From the this table, it can be seen that the values of the voltage ratios for Material#1, Material#2 and Material#3 increases with the input force value. Also we can see that the voltage ratios of Material#2 and Material#3 are almost identical as both the materials have similar softness properties.

Table 5-5 Single sensor input and output signals for Material#1, #2 and #3

Input Force V	Material#1	Material#2	Material#3
0.2	1	0.27	0.21
0.4	1.23	0.37	0.277
0.6	1.56	0.4	0.3
0.8	1.9	0.44	0.38
1	2.2	0.54	0.48
1.1	2.5	0.57	0.51
1.2	2.74	0.61	0.59
1.3	3.1	0.66	0.63
1.4	3.4	0.7	0.72
1.5	3.75	0.75	0.74
1.6	4.1	0.82	0.77
1.7	4.4	0.87	0.81
1.8	4.66	0.91	0.87

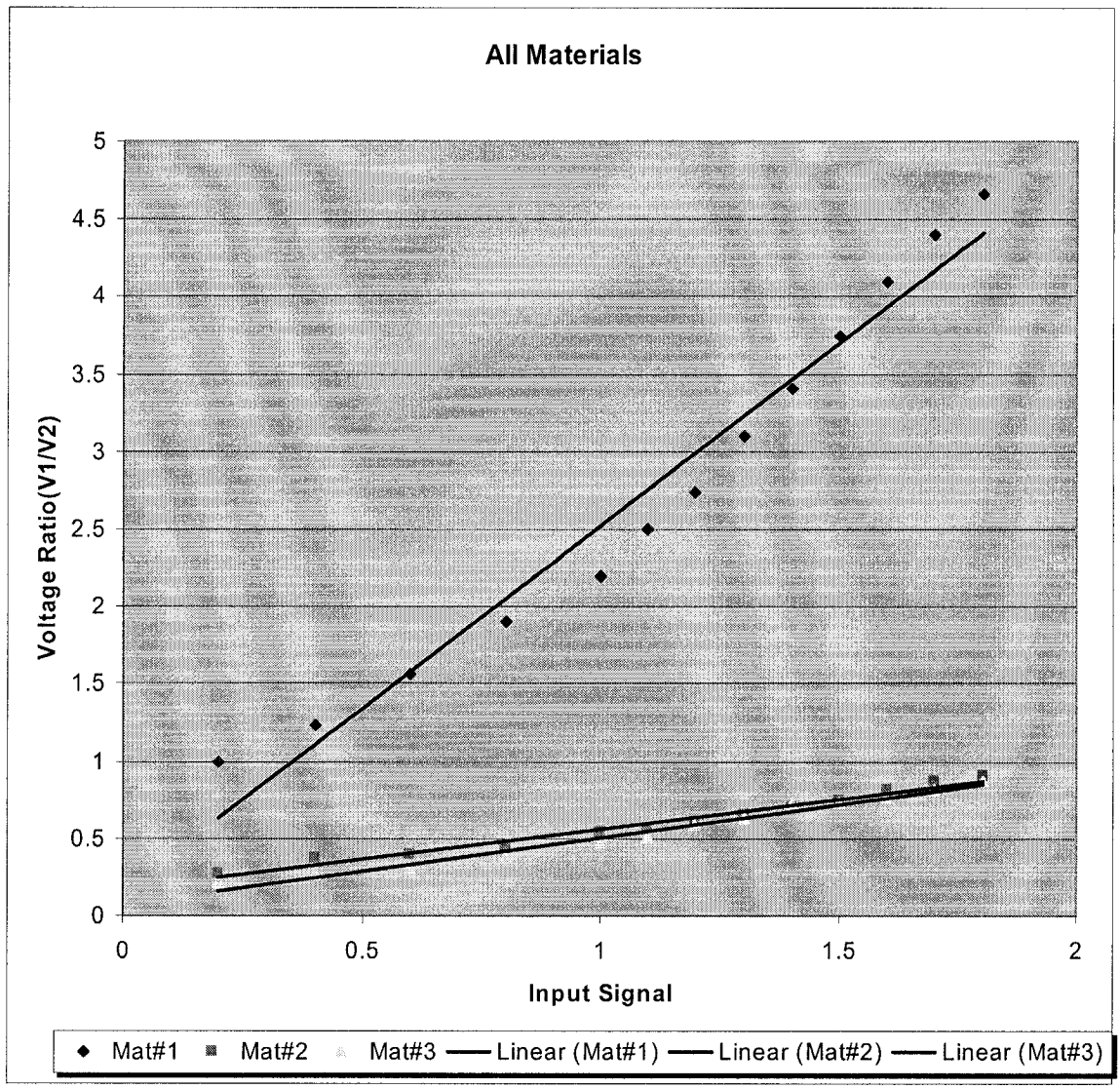

Figure 5-16 Single sensor plot of force versus peak to peak V for all material

The graph displayed in Figure 5.16 shows the output voltage ratio of all material for the same input forces. It can be seen that for all material, the output voltage ratio increases linearly with the input force.

5.4.3 Four-Sensor Testing

After the single sensor was tested, an array of sensors were fabricated and were tested for the same set of materials having the same thickness but having greater length than that used for single sensor testing. This is done so that the sensed material completely covers the four-sensor array. All the three materials were tested for the same frequency and same load as the single sensor and their values were recorded. The applied load, in terms of voltage, was 1.8V and the tested frequency was 10Hz. The sensor array, together with the connections and the material being tested, are shown in Figures 5.17.

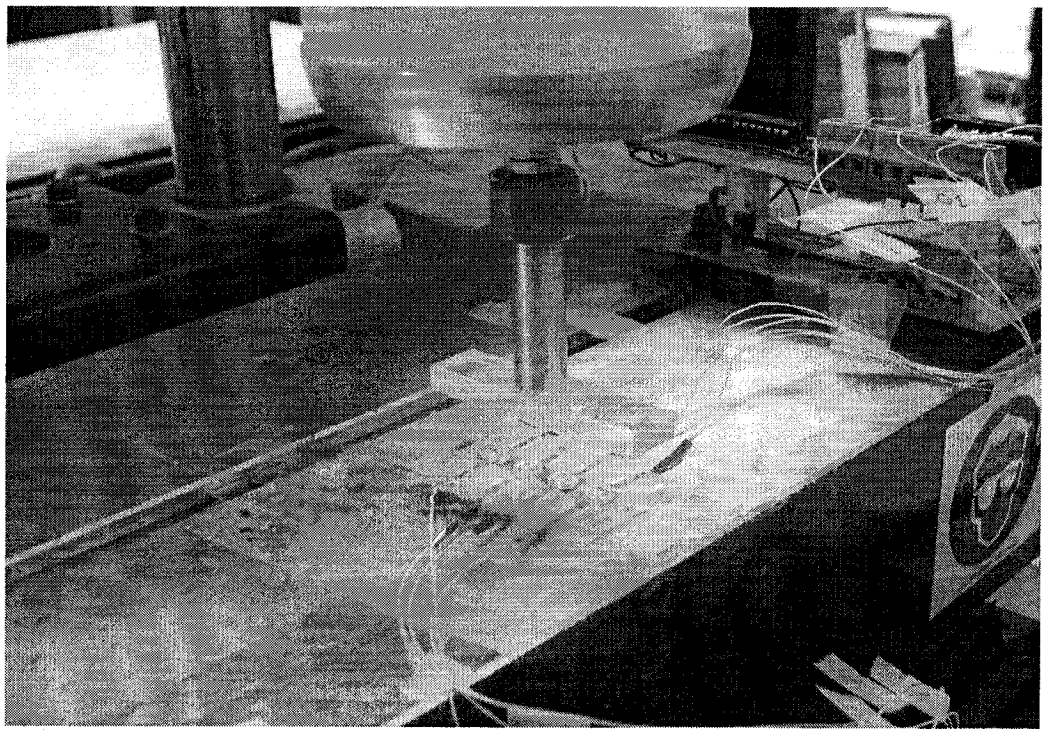

Figure 5-17 Array of sensors with the test probe in contact with the material

5.4.3.1 Four-Sensor Testing using Material#1

Material#1 was tested by placing it on top of the array of sensors and applying a sinusoidal load of 1.8V at 10Hz. The readings from the PVDF under the rigid cylinder and the PVDF under the outer cylinder were recorded and tabulated. In the figures shown below, I1, I2, I3 and I4 denote the voltages (in millivolts) from the PVDF under the inner cylinder and O1, O2, O3 and O4 denote the voltages (in millivolts) from the PVDF under the outer cylinder and n1, n2, n3 and n4 denote the ratio between the inner and outer PVDF. As it can be seen, the ratios from the four sensors are quite similar and in conformance with the one tested for the single sensor.

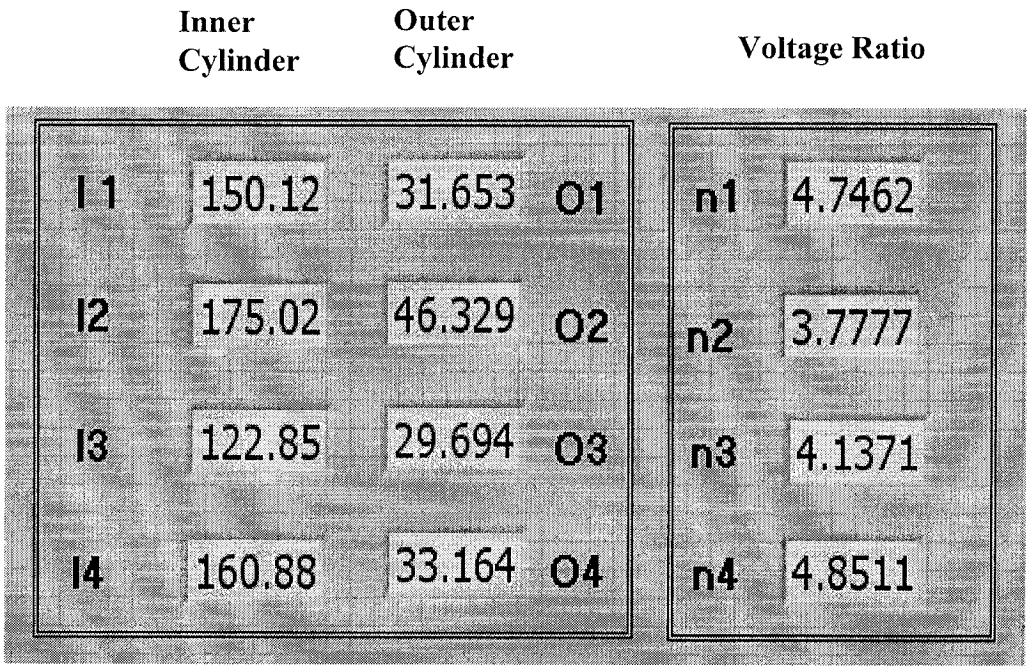

Figure 5-18 Four sensor design output for Material#1

5.4.3.2 Four-Sensor Testing using Material#2

Material#2 was tested using the same input signal of 1.8V at 10Hz and the voltage readings from the inner and outer PVDF were recorded and tabulated as shown below. Similar values are recorded for all the four sensors and were in conformance with the single sensor test.

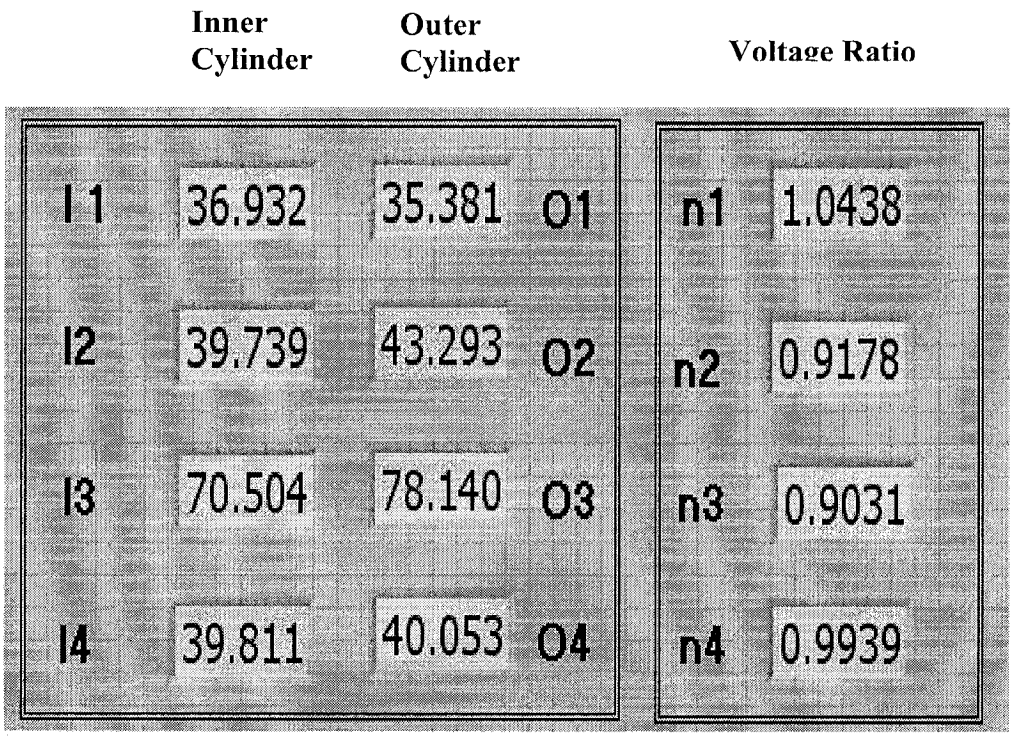

Figure 5-19 Four sensor design output for Material#2

5.4.3.3 Four-Sensor Testing using Material#3

Material#3 was tested using the same input signal of 1.8V at 10Hz and the voltage readings from the inner and outer PVDF were recorded and tabulated as shown in Table 5.6. Similar values are recorded for all the four sensors and were in conformance with the single sensor test.

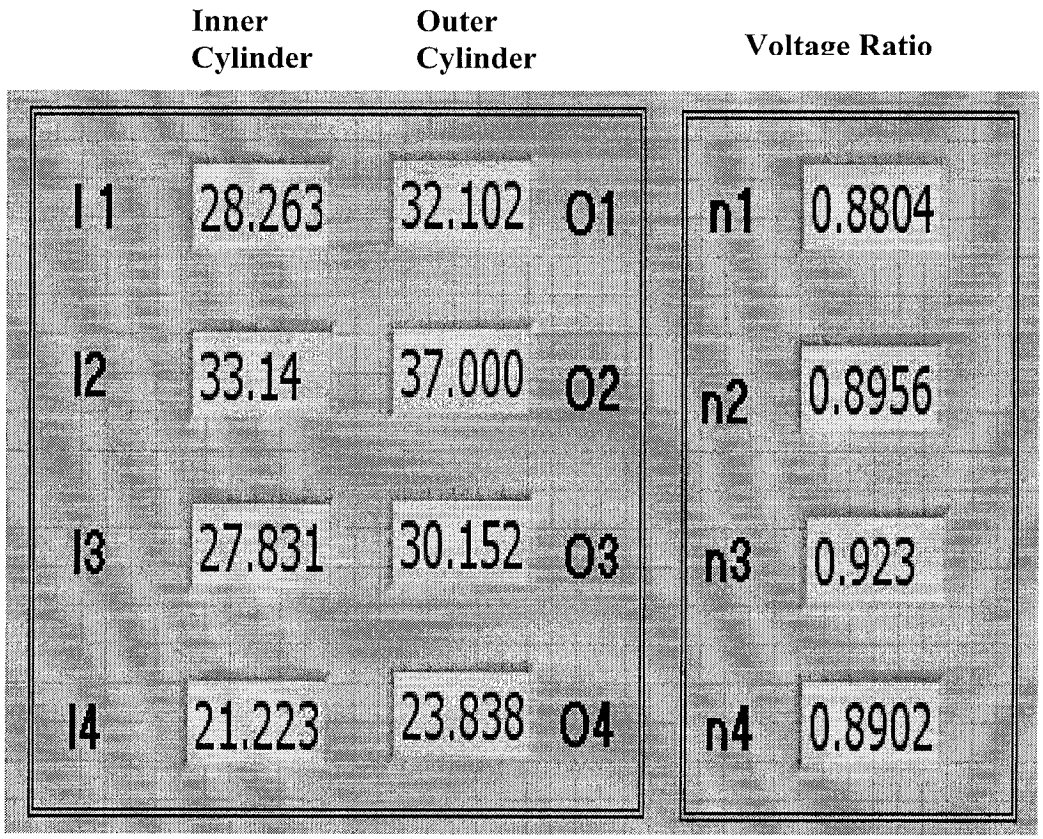

Figure 5-20 - Four sensor design output for Material#3

The results of the array of sensors are summarized in Table 5.6 which also shows the average value taken from the four sensors.

Table 5-6 Comparison of voltage ratio for all three materials for each sensor of the array

Voltage Ratio of inner and outer PVDF of each Sensor			
Sensor	Material#1	Material#2	Material#3
1	4.75	1.04	0.88
2	3.77	0.91	0.89
3	4.13	0.90	0.92
4	4.85	0.99	0.89
Average	4.37	0.96	0.89

5.5 Comparison of Results between a Single Sensor and an array of Sensors

The results obtained for the Single sensor design and the array of four sensor design was compared for an input signal of 1.8V at 10Hz. The voltage ratio for all the three materials were tabulated and found to be in close conformance as shown in Table 5.7.

Table 5-7 Comparison of voltage ratio between the single and four sensor design

Material	Single Sensor	Four Sensor	% Difference
#1	4.66	4.37	6.6
#2	0.91	0.96	5.5
#3	0.87	0.89	2.3

5.6 - Young's Modulus Experimental Value

Three samples were tested and their E values calculated by the force ratio values derived from the test and then used in Equation (27) derived in Chapter 4:

$$\frac{F1}{F2} = \frac{Aa}{Ab}\left[1 + \frac{E_1 T_2}{E_2 T_1}\right]$$

The value of Aa, Ab, T_1, T_2 and E_2 are all known values as described in Chapter 2 and the unknown value E_1, the Young's modulus of the test object, is calculated from the above equation. The force ratio value is equal to the output voltage ratio values obtained from the experiments. E values obtained from the single sensor design and four sensor designs are compared as shown in Table 5.8 which shows a variation of between 5% and 10% compared to the actual value of elasticity supplied by the manufacturer.

Table 5-8 Young's modulus value comparison between single and four sensor designs

Material	Thickness	Single sensor voltage ratio	Four-sensor voltage ratio	Area Ratio	Single Sensor	Four-Sensor
	mm				MPa	MPa
#1	2.8	4.6	4.37	0.45	183.33	173.18
#2	3.0	0.91	0.96	0.45	21.77	24.13
#3	2.5	0.87	0.89	0.45	16.56	17.35

5.6.1 Comparison of Elasticity value with the Manufacturer's value

The values of Young's modulus obtained from the Single sensor design and the four sensor design are compared with the actual value supplied from the manufacturer as shown in Table 5.9 and Table 5.10. We found a percentage deviation of between 1 and 15% though this differential may be attributable to the difference in testing conditions arising due to noise..

Table 5-9 Single sensor value compared to actual value

Material	Single Sensor value	Actual value	% Difference
	MPa	MPa	
#1	183.33	170	7.8
#2	21.77	22	1.3
#3	16.56	15	10.4

Table 5-10 Four-sensor evaluation compared to actual value of elasticity

Material	Four-Sensor value	Actual Value	% Difference
	MPa	MPa	
#1	173,18	170	1.8
#2	24.13	22	9.68
#3	17.35	15	15.66

5.7 Force Ratio comparison between the Experimental and Finite Element model

This section enumerates the relative comparison between the actual experimental testing results of the sensor and the finite element results of the sensor using the ANSYS software program. Very careful steps were taken to model the sensor in close concurrence with actually built sensor. Due to the difficulty in meshing the different parts of the sensor in ANSYS, a quarter-size model was built and the results are tabulated. As seen in the analytical model, the force ratio equals the voltage ratio. The force experienced at the different nodes in the PVDF under the Inner rigid cylinder, and the PVDF under the outer soft cylinder, are tabulated and the force ratios are found for the average of these values. These force ratio values are compared for the known values of the material for a single sensor design in ANSYS with the voltage ratio values obtained from the experiment for both the single sensor and four-sensor designs. The force values at different nodes are tabulated in Chapter 4 and the comparison is tabulated in Table 5.11 which shows the force ratio comparison between the ANSYS, Single sensor and the four sensor design. It shows that all the three values are within 10% of each other.

Table 5-11 Comparison of force ratio between ANSYS and the two-sensor model

Material	ANSYS	Single Sensor	Four Sensor
#1	4.63	4.6	4.37
#2	1.016	0.91	0.96
#3	0.933	0.87	0.89

In Chapter 5, we summarized all the experiments performed on the single and four sensor designs by comparing the values obtained from experiments with those supplied by the manufacturer. In addition to these values conforming, we also demonstrated that the force ratio values from the ANSYS analysis, when compared to the experimental voltage ratio values, were found to be within an acceptable range.

6. CHAPTER

CONCLUSION AND FUTURE WORK

The major thrust of this thesis is to design and fabricate a micro-piezoelectric tactile sensor for measuring the softness of tissues during Minimal Invasive Surgery (MIS) using the phenomenon of relative deformation. The sensors were designed in such a size to justify theoretical and experimental results. In this final chapter, we will summarize the work presented in Chapters 3 and 4 on tactile sensing design and analysis and its testing in Chapter 5 and suggest possible extensions and future work.

6.1 Summary

Research work is summarized as follows:

1. The design of the single sensor and an array of sensor.
2. Micro fabrication process developed for the sensor.
3. An analytical approach showing the magnitude of variation of elastic and viscoelastic properties of materials at different loading unloading conditions.
4. A mathematical equation was derived showing the relationship between the force ratios and the Young's modulus of the elastic materials.
5. Experimentation was carried out for different loads for single sensor design and four sensor design.
6. The voltage ratio output for the single sensor design and the four sensor design were obtained experimentally and compared.

7. Elastic modulus of different test samples were found using experimental and analytical formulation for single and four-sensor design and its comparison to the value supplied from the manufacturer.
8. The force ratio obtained for the single sensor design for different materials was compared with corresponding voltages ratios output from the experiments, for the same material.

6.2 Discussion and Conclusion

In this section, the complete discussion and conclusion of this thesis is presented.

1. It is shown that using the prototype micro machined piezoelectric tactile sensor, it is possible to characterize various soft objects with reasonable accuracy.
2. An analytical expression derived shows the magnitude variation of the elastic and viscoelastic properties of the materials at different loading and unloading times. This expression shows that the fast loading and unloading is very important to characterize the viscoelastic properties. The derived expression is employed to characterize the viscoelastic material.
3. Another feature of the designed prototype involves the polarization characteristics of the PVDF polymers. It is widely known that, in PVDF polymers, polarization can be changed both by mechanical stresses and by temperature variation. The former is associated with the piezoelectric property and the latter is associated with the pyroelectric property. In this particular design, care was taken to eliminate or reduce the effect of pyroelectricity by sandwiching the PVDF films between a substrate and the cylinders.

4. In the design of the sensor, a gap of 0.5mm was allocated between the rigid and the compliant cylinders. The reason for this gap is to eliminate the friction between the two cylinders and hence to make the sensors operate more smoothly.
5. One of the major benefits of the designed system is its miniaturized form. As a result, it could be mass-produced at low cost and even be disposable.
6. The reason for testing and comparison of a single sensor as well as an array of sensor is to show that for the same material it array of sensors exhibits similar outputs. This is mainly used for local softness sensing during the grasping of tissues and hence the output from each sensor is important in characterizing the tissue being grasped during MIS.
7. This modulus of elasticity value calculated from the experimental and analytical formulation were compared with the modulus of elasticity of the materials given by the manufacturer and it was found to be within an acceptable percentage difference of between 5% and 20%.
8. The finite element analysis of the single sensor was undertaken using ANSYS. The force ratio output values were in conformance with the voltage ratio values for all the three materials tested experimentally within a deviation of about 10%.
9. Theoretical results were obtained by static loading while the experimental testing was done by dynamic loading. This could account for the difference in the compared value.
10. The sensor structures were assembled using non-conductive glues. These glues provide excellent strength to the sensor structure and the PVDF films did not undergo any deformation due to the gluing properties.

6.3 Future work

As with most designs, one learns a great deal from each generation of prototypes. The sensor design concept presented in this thesis has evolved considerably since their conception. However, it is clear that many improvements can still be made. The following subsection outlines suggested improvements and possible future work in these areas.

The future work can be extended to different directions. More work is required on the miniaturization aspect, fabrication methodology and packaging. Proper packaging and protection from the environment is also required for more effective functioning of the sensor. Future micro-machined sensors can be fabricated on an electronic chip which results in high precision measurements.

The second main aspect of the design of the sensor is to consider the effect of fluids on the sensor because, in reality, the sensors mounted to endoscopic graspers which interact with fluids inside the body. The leakage of charges from the PVDF and wires will affect the performance of the sensor and hence proper insulation and protection from the fluid should be considered in any further work.

More work is also required for proper assembly of each sensor and appropriate provisions should be made for cleaning and sterilization. The effect of shear on the sensor could be considered in future analysis in order to determine the roughness and slip of tissues from the endoscopic grasper. The sensor was susceptible to noise during the experiment. Proper shielding should be installed so that the sensor output does not become affected by the noise signals.

BIBLIOGRAPHY

1. Tendick F., Sastry S.S., Fearing R.S. and Cohn M., "Applications of micromechatronics in minimal invasive surgery," IEEE Trans. Mechatron., vol. 3, pp. 34-42, Mar. 1998.
2. Karl Storz GmbH & Co, Tuttlingen, Germany website, " http://www.karlstorz.com/"
3. http://concave.concordia.ca/people/endoscopic.shtml
4. Webster J.G., "Tactile sensors for robotics and medicine", A Wiley-Interscience Publication, New York, 1988.
5. Melzer A., Buess G., Cuschieri A., "Instruments and Allied Technology for Endoscopic surgery", Operative Manual of Endoscopic surgery 2, Springer-Verlag, New York, pp. 1-69, 1994.
6. Dargahi J. and Najarian S. "Analysis of a membrane type polymeric based tactile sensor for biomedical and medical robotic applications" journal of Sensors and Material, vol. 16, pp.25-41, 2004.
7. Nagarajan N.B., "Design, Fabrication and testing of a novel micromachied piezoelectric tactile sensor to measure softness of biological tissues", Poster presentation, IRIS-Precarn conference, Ottawa, 2004.
8. Dargahi J., "An endoscopic and robotic tooth-like compliance and roughness tactile sensor", J Mech Design, vol. 124, pp. 576-582, 2002.
9. Tai-Ran Hsu, "MEMS and MICROSYSTEMS Design and Manufacture", McGraw-hill, Inc, 2002.
10. Rebello K. J., "Applications of MEMS in surgery," Proceedings of the IEEE, vol. 92, no. 1, pp. 43-55, 2004.

11. Cohn M.B., Lam N., Fearing R.S., "Tactile feedback for teleoperation. in Telemanipulator Technology", SPIE Proc., Boston, pp. 240–254, November 1992.
12. Dario P., "Tactile sensing–technology and applications", Journal of Sensors and Actuators A—Phys, vol. 26, pp. 251–256, 1991.
13. Bicchi A., Canepa G., DeRossi D., Iacconi P., Scilingo E.P., "A sensorized minimally invasive surgery tool for detecting tissutal elastic properties", In: IEEE Int. Conf. on Robotics and Automation, Minneapolis, MN, pp. 884–888, 22–28 April 1996.
14. Cohn M.B., Crawford L.S. and Wendlandt J.M., "Surgical application of milli-robots. Robotic Systems", Journal of Robotics Systems, vol. 6, pp. 401–416, 1995.
15. Fischer H., Heilig R., Trapp R., Brhel K., "Tactile optical sensor for use in minimally invasive surgery", Langenbecks Archiv Fur Chirurgie, pp. 1290, 1996.
16. Dizaji M., Dizaji, R. M., "Detection of internal displacement of tissues in ultrasound images using image registration technique", IEEE CCECE, Canadian conference, 2002.
17. Picinbono G., Delingette H., Ayache N., "Nonlinear and anisotropic elastic soft tissue models for medical simulation", proc. ICRA. IEEE , 2001.
18. Gladilin E., Zachow S., Deuflhard P., Hege H., "A biomechanical model for soft tissue simulation in craniofacial surgery", International workshop on Medical Imaging and Augmented Reality, shatin, hong kong, china, 2001.
19. Tritto G., Pirlo G., Tritto M. C., "Soft tissues expanders: computer- assisted simulation of elastic mesh deformation and fractal vascular geometries in controlled skin expansion", Proc. of the Annual International Conf. of the IEEE Engineering in Seattle, WA Vol. 6, pp. 1951-1952 , 1989.

20. Dario P., Carrozza M.C., Lencioni L, Maganani B., D'Attanasio S., "A micro robotic system for colonoscopy", IEEE Int. Conf. on Robotics and Automation, Albuquerque, New Mexico, pp. 1567–1572, 1997.

21. Kontarinis D.A., Son J.S., Peine W., Howe R.D., "A tactile shape sensing and display system for teleoperated manipulation". IEEE Int. Conf. on Robotics and Automation, Nagoya, Japan, pp. 641–646, 21–27 May 1995.

22. Josivaldo G.S., Carvalho A.A. and Silva D.D.," A strain gauge tactile sensor for finger mounted applications", IEEE Trans. On Instrumentation and Measurement, Vol.51, No.1, February 2002.

23. Shinoda H., Ando S., " A tactile sensor with 5-d deformation sensing element" IEEE Int. Conf. on Robotics and Automation, Minneapolis, MN, pp. 7–12, 22–28 Apr 1996.

24. Dargahi J., "A three sensing element piezoelectric tactile sensor for robotic and prosthetic applications", J. Sensors Actuators A Phys, vol. 80, pp.23-30, 2004.

25. Ohka M., Mitsuya Y., Takeuchi S., Kamaekawa O., Ishihara H., "A 3-axis optical tactile sensor—(FEM contact analysis and sensing experiments using a large-sized tactile sensor)", IEEE Int. Conf. on Robotics and Automation, Nagoya, Japan, pp. 817–824, 21–27 May.

26. Obana F.Y., Carvalho A.A., gualda and Silva G.J.,"A Semiconductor strain gauge tactile transducer", IEEE Instrumentation and Measurement technology Conf, Budapest, Hungary, pp.429-432, May 21-23, 2001.

27. Howe, R. D., "Tactile sensing and control of robotic manipulation", Journal of Advanced Robotics vol.8 no. 3, pp. 245-261, 1994.

28. Fearing, R. S., "Tactile sensing mechanisms", International Journal of Robotics Research, Vol.9 (3), pp. 3-23, 1990.

29. Faraz, S. Payandeh, and A. Salvarinov, "Design of haptic interface through stiffness modulation for endosurgery: Theory and experiments," IEEE International Conf. Robotics and Automation, Leuven, Belgium, May 1998

30. Petter, E., Biehl, M., Meyer, J., "Vibrotactile palpation instrument for use in Minimal invasive surgery", Engineering in Medicine and Biology society, Bridging Disciplines for Biomedicine. Proc. of the 18th Annual International Conf. of IEEE, 1996.

31. Ryan, A., Beasley, T., Robert, D., "Tactile Tracking of Arteries in Robotic Surgery" International Conf. on Robotic & Automation, proc. of IEEE. Washington, DC, May2002.

32. Youngping, Z., Arthur, F., Mak, T., "Effective Elastic properties for Lower Limb Soft Tissues from Manual Indentation Experiment", IEEE Transactions on rehabilitation Engineering, Vol. 7. N). 3, September 1999.

33. Gray BL, Fearing RS. A surface micromachined microtactile sensor array. In: IEEE Int. Conf. on Robotics and Automation, Minneapolis, Mn, 22–28 April 1996. IEEE, Robot and Automat Soc, 1996. pp. 1–6.

34. Metha M., "A Micromachined Capacitative Pressure Sensor for Use in Endoscopic Surgery", MSc thesis, School of Eng. Sci., Simon Fraser University, BC, Canada, 1996.

35. Dargahi J., Parameswaran M., Payandeh S.M., "A micromachined piezoelectric tactile sensor for an endoscopic grasper-theory, fabrication and experiments", Journal of Microelectromechanical Systems, Vol. 9, Issue 3, pp.329-335, Sep 2000.

36. Dario P., Bergamasco M., and Sabatini A., "Sensing body structures by an advanced robot system," Proc. 1988 IEEE Int. Conf. Robotics and Automation, vol. 3, pp. 1758-1763.

37. Maria C. C., Eisinberg A., Menciassi A., Campolo D., Micer S. and Dario P., "Towards a force-controlled microgripper for assembling biomedical microdevices", Journal of Micromechanics and Microengineering, pp. 271-276, 2000.

38. Sugiyama S., Kawahata K., Yoneda M., Igarashi I., "Tactile image detection using a 1K-element silicon pressure sensor array" Journal of Sensors and Actuators A, vol. 22, pp. 397-400, 1989.

39. Beebe D. J., Hsiesh A. S., Denton D., Radwin G., "A Silicon force sensor for robotics medicine", Sensors and Actuator A, vol. 50, pp. 55-56, 1995.

40. Gray B. L., Fearing R. S., "A Surface micromachined microtactile sensor array", Proc.1996 IEEE Int. Conf. On Robotics and Automation, pp 1-6, 1996.

41. Leineweber M., Pelz G., Schmidt M., Kappert H., Zimmer, G., "New Tactile Sensor chip with silicone rubber cover", Journal of Sensors and Actuators A, vol. 84, pp. 36-45, 2000.

42. Kolesar E. S., Dyson C. S., "Object imaging with a piezoelectric robotic tactile sensor", Journal of Microelectromechanics, Syst., vol. 4, pp. 87-96, 1995.

43. Reston R. R., Kolesar E. S., "Robotic tactile sensory array fabricated from a piezoelectric polyvinylidene fluoride film", Proc. IEE NAECON, Vol. 3, pp 1139-44, 1990.

44. Jonathan E., Jack C., Chang L., Bruce R., "Development of polyimide-based Flexible Tactile Sensing Skin", Proc.Mat. Res. Soc. Symp. Vol. 736.

45. Kane B. J., Cutkosky M. R., Kovarcs T. A., "A traction stress sensor array in high-resolution robotic tactile imaging", Journal of Microelectromech. Syst., vol. 9, pp.425-434, 2000.

46. Shinoda H., Ando S., "Ultrasonic emission tactile sensor for contact localization and characterization", IEEE International conference on Robotic and Automation, proc. 1994.

47. Reston R. R., Kolesar E. S., "Robotic tactile sensory array fabricated from a piezoelectric polyvinylidene fluoride film", Proc. IEE NAECON, Vol. 3, pp 1139-44, 1990.

48. Beebe D., Denton D., Radwin R., and Webster J., "A silicon-based tactile sensor for finger-mounted applications," IEEE Trans. Biomed. Eng., vol. 45, pp. 151-159, 1998.

49. Lord Industrial Automation, "Tactile Sensing System", ser. Lord Series 210 Covy, NC, 1987.

50. Suzuki K., Najafi K., and Wise K. D., "A 1024-element high-performance silicon tactile imager," IEEE Trans. Electron Devices, vol. 37, pp. 1852-1859, 1990.

51. Samaun., Wise K. D, and Angell J. B., "An IC piezoresistive pressure sensor for biomedical instrumentation," IEEE Trans. Biomed. Eng., vol. BME-20, pp. 101-109, 1973.

52. Lee Y. S. and Wise K. D., "A batch-fabricated silicon capacitive pressure transducer with low temperature sensitivity," IEEE Trans. Electron Devices, vol. ED-29, pp. 42-48, 1982.

53. Tanigawa H., Ishihara T., Hirata M., and Suzuki K., "MOS integrated silicon pressure sensor," IEEE Trans. Electron Devices, vol. ED-32, pp. 1191-1195, 1985.

54. Atkinson, G.M. Pearson, R.E. Ounaies, Z. Park, C. Harrison, J.S. Midkiff, J.A., " Piezoelectric polyimide tactile sensors", Proceedings of the 15th Biennial University/Government/Industry Microelectronics Symposium, pp. 308-311, 2003.

55. Mei T., Li W. J., Ge Y., Chen Y., Ni L. and Chan M. H., "An integrated MEMS three-dimensional tactile sensor with large force range" Journal of Sensors and. Actuator A, vol. 80, pp. 155-162, 2000.

56. Despont, M., "A comparative study of bearing designs and operational environments for harmonic side-drive micromotors", In. proc. of MEMS, pp. 171-176, 1992.

57. Crowder R.M., "Sensors: Touch, force, and torque", Handbook of Industrial Automation, New York, NY, Marcel Dekker, pp. 377–392, 2000.

58. Rao N.P., Dargahi J., Kahrizi M., and Prasad S., "Design and fabrication of a microtactile sensor," in *Proc. Can. Conf. Elect. Comput. Eng.*, Montreal, Que., May 2003.

59. Good Fellow Corporation, US ,"http://www.goodfellow.com/csp/active/gfHome.csp"

60. Dargahi J., Eastwood A. and Kemp I. J., "Combined force and position polyvinylidene fluoride (PVDF) robotic tactile sensing system", Proc. of SPIE Int. Conference, Orlando, USA, pp 20-25, 1997.

61. Dargahi J., Sokhanvar S. and Packirisamy M., "Theoretical and Experimental Techniques in Using Polyvinylidene Fluoride (PVDF) Films as a Transducer in Sensor Systems" Transactions of the Canadian Society of Mechanical Engineering, Vol 28(2B), pp 291-307, 2004.

62. Dow Corning Electronics "Division Information about Dow Corning Brand Silicone Encapsulants", U.S.A, 2003.

63. Wilhelm Flugge, "Viscoelasticity", Springer-Verlag , New York, Berlin, 1975.

64. Johnson K. L. "Contact Mechanics", Cambridge University press, Cambridge, U.K, 1985.

65. Mase G. T. and Mase G. E., "Continuum Mechanics for Engineers", 2nd ed CRC Boca Raton, 1999.

66. Fu G., "Theoretical study of complete contact indentations of viscoelastic materials", Journal of Materials Science, vol. 38, pp. 2877-2886, 2004.

67. Findley W. N., Lai J. S. and Onaran K., "Creep and Relaxation of Nonlinear Viscoelastic Materials", Dover Mineola, 1989

68. Fung Y. C., "Biomechanics: Mechanical Properties of Living Tissues", Springer-Verlag ,New York, 1981.

69. http://www.today.uidaho.edu/photos%5Couterspace2.jpg

70. http://www.parallax.com/detail.asp?product_id=28026

71. http://www.memunity.com/rf_mems.htm

72. http://www.uwnews.org/photos.asp?articleID=3485&spid=3486

73. Cady W.G., "Piezoelectricity", 1st ed., McGraw-Hill Inc., New York, 1946.

74. Toupin R.A., "A Dynamical theory of elastic dielectrics," International Journal of Engineering Science, Vol. 1, pp. 101-126, 1963.

75. Toupin R.A., "The Elastic dielectric," Journal of Rational Mechanical Analysis, Vol. 5, No. 6, pp. 849-915, June 1956.

76. Tiersten H.F., "Coupled magneto mechanical equations for saturated insulators," Journal of Mathematical Physics, Vol. 5, No. 9, pp. 1298-1318, 1964.

77. Allik H., Hughes T.J.R., "Finite element method for piezoelectric vibration", International Journal for Numerical Methods in Engineering, Vol. 2, pp. 151-157, 1970.

78. Peelamedu S., Naganathan G., Barnett, A., Rao, D. " Finite element approach to model and analyze piezoelectric actuators", American Institute of Aeronautics and Astronautics (AIAA) Journal, Feb 1999.

79. Peelamedu S., Niemeyer S., Naganathan G. and Rao D., "Piezoceramic array actuator system for deformable mirror applications", Journal of Smart Materials and Structures, Dec 1999.

80. John B.and Neil W., "Intelligent Sensor systems", IOP publishing Ltd, 1996.

81. Peter E., "Sensors for measurement and control", Pearson Education Ltd, 1998.

82. Ren C. L., "Sensor Technologies and Microsensor Issues for Mechatronics Systems", IEEE/ASME Transaction on Mechatronics, vol.1 Issue1, pp.39-49, 1996.

83. Harmon, L.L., "A high resolution imaging tactile sensor", Int. J.robotics Res., vol. 1, p.33, 1982.

84. Tse F.S. and Morse E.I., "Measurement and instrumentation in engineering", Marcel Dekker Inc, New York, 1989.

85. Narayanan N.B., Bonakdar A.' Dargahi J., Packirisamy M. and Bhat R., "Design and analysis of a micromachined piezoelectric sensor for measuring viscoelastic properties of tissues in minimally invasive surgery", Journal of Smart Materials and Structures, vol.15, pp. 1684-1690, 2006.

A.1 APPENDIX – 1

Piezoelectric Effect

Piezoelectric substances are new materials used for sensor and actuators with the help of micro electromechanical systems technology. When external force is applied to piezoelectric materials it generates charge on the surface, which is proportional to applied mechanical stress. The converse effect is also there, applied voltage generates deformation in the materials. Similarly ferroelectric type of material is one which exhibits a spontaneous polarization in one or more direction of the crystal over a definite temperature range. Piezoelectric must not be confused with the ferro electricity, which is the property of a spontaneous or induced electric dipole moment. All ferroelectric materials are piezoelectric, but the contrary is not always true. Piezoelectricity relates to the crystalline ionic structure. Ferro-electricity instead relates with electron spin.

A simplified model of piezoelectricity entails the motion of anions (-) and cations (+) moving opposite directions under the influence of an electric field and mechanical force. The force generated by this motion cause lattice deformation for non-Centro symmetric crystals due to presence of both high and low stiffness ionic bonds. As results, all piezoelectric materials are anisotropic, in case of central symmetry; an applied force does not yield an electric polarization. The effect for quartz is shown below in Figure A.1, positive and negative charges are formed. It is important to remember that the piezoelectric materials are function of the continuously changing mechanical deformation. Therefore dynamic forces are used in practical situations.

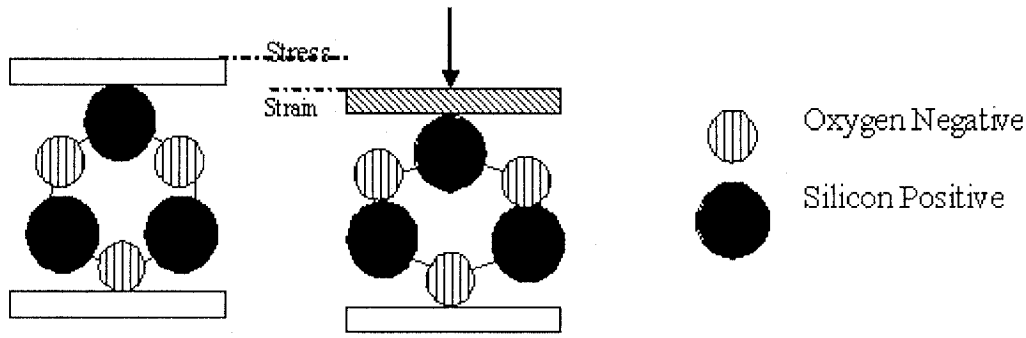

Figure A-1 Piezoelectric in ionic crystals such as quartz, ion position in quartz lattice with and without applied stress.

A1.1 Piezoelectric Materials

The most extensively used natural piezoelectric materials are crystals (quartz and tourmaline). In synthetic piezoelectric, ceramics formed by many tightly compacted monocrystals (1μ in size) are most popular. These Ceramics, such as Lead Zirconate titanate (PZT), barium titanate is ferroelectrics. To align the dipoles to monocrystals in same direction, they are subjected to strong electric field during their manufacturing process. The applied electric field to crystal above the Curie temperature to align the dipoles. Then cool the crystal while maintaining the field. This process makes crystal permanent electric polarized. When electric field is removed, the crystalline cannot reorder in random from because of mechanical stresses accumulated, resulting in permanent electric polarization. The problem with these materials relates to their temperature sensitivity and aging when approaching the curie temperature.

Polymers such as polyvinylidene fluoride (PVDF) also display piezoelectric properties and have pyroelectric features, i.e. change the electrical charge with change in

temperature. PVDF are not central symmetry i.e. it display piezoelectric properties. Compared to quartz and ceramics, piezo-film is more pliant and lighter in weight. In addition to this it is rugged, inert and low cost. Secondly urethane and epoxy adhesive are used for gluing PVDF. The use of epoxy and urethane adhesives depends upon the strength requirement of the structure.

In smart structures, piezo ceramics are typically used as actuators, polymeric piezoelectric materials are typically tactile sensor, temperature and stain sensors. It is common practice to embed piezoelectric sensors into prototypes because these sensors can be manufactured with strength and dimensional characteristics that do not degrade the structural integrity of the material from which the prototype device is made. Piezoelectric ultrasonic motors and piezoceramic sensors are currently being built into commercial products such as camera lens drives and automotive engine control systems. In many cases, thin layers of piezoceramic composites are bonded to other structural material surfaces. When thermal effects are generated through either friction or direct exposure to significant temperature gradients, the reliability of the electrode layer in these piezoceramics can completely dominate the performance of the device.

Many efforts have been done for mathematical modeling of piezoelectric phenomenon. The researcher efforts in piezoelectricity carried out in the past produced in our work. Cady [73], gave comprehensive description of development in the theory of piezoelectricity. Toupin [74-75], involved in development of the governing equation using energy methods and dynamics theory. Tiersten [76], made several approximations and developed linear equation of piezoelectricity using Hamiltonian mechanics and variation techniques. Allik and Hughes [77] developed the general equation of motion for

piezoelectric materials in a matrix form. The S. Peelamedu [78-79], combined the work together to formulate finite element solution for piezoelectric structure.

Basic Constitutive Equations [76] are expressed in matrix notation as

$$\begin{aligned} [T] &= [c]\{S\} - [e]^T \{E\} \\ [D] &= [e]\{S\} + [\varepsilon]\{E\} \end{aligned} \qquad \text{(A1.1)}$$

The first and second equation represents structural and electrical constitutive of piezoelectric material, respectively. Where as the entire matrix are given as

{T} = Stress vector (N/m^2)

{D} = Electric flux density (C/m^2)

{E} = Electric Field Vector (V/m)

{S} = Strain vector (dimensionless)

[c] = Elasticity Matrix (N/m^2)

[e] = Piezoelectric matrix at constant stress(C/m^2)

$[\varepsilon]$ = Dielectric Matrix

A1.2 Piezoelectric Coefficients

Most of piezoelectric coefficients have double subscript that links electrical and mechanical quantities. The first subscript gives the direction of the electrical field associated with voltage applied and second subscript gives the direction of the mechanical stress or strain.

A1.2.1 D – Coefficients

The piezoelectric constant relating the mechanical strain produced by an applied electric field are termed the strain constant or'd' coefficients or piezoelectric strain matrix. Conversely the coefficient may be viewed as relating the charge collected on the electrodes, to the applied mechanical stress. The unit of'd' coefficient is C/N.

d = charge density/applied mechanical stress.

A1.2.2 E – Coefficients

The piezoelectric constant relating the electrical field produced by applied mechanical stress at constant strain is known as stress constant or 'e' coefficient or piezoelectric stress matrix. The unit of 'e' coefficient is C/m^2. There is relationship between [e] and [d] matrix and it is given as

$$[e] = [d] [c] \qquad \text{(A1.2)}$$

For 3D analysis Z-axis are considered as polarized axis and size of array [e] and [d] is 6x3. If we are considering the 2D analysis then we use Y- axis as polarized axis and order of array [e] and [d] is 4x2. Similarly for [ε] matrix size are different for 3x3 and 2x2 for 3D and 2D model respectively.

A1.2.3 G Coefficients

The piezoelectric constants relating the electric field produced by a mechanical stress are termed the voltage constants, or the "g" coefficients. The units are then expressed as volts/meter per Newton/square meter.

$$g = \frac{ElectricField}{Applied\ Mechanical\ Stress} \tag{A1.3}$$

High g_{ij} constants favor large voltage output, and are sought after for sensors. The relationship between the [d] and [g] matrix is given as $[d] = [K]^T[g]$ (A1.4)

A1.2.4 Dielectric Constants

The relative dielectric constant is ratio of the permittivity of material, ε, to the permittivity of free space, ε_o, in the unconstrained condition. ($\varepsilon_o = 8.9 \times 10^{-12}$ farad/meter).

$$K = \frac{Permittivity\ of\ materail}{Permittivity\ of\ free\ space} = \frac{\varepsilon}{\varepsilon_o} \tag{A1.5}$$

A1.2.5 Capacitance

Capacitance is a quantity dependent on the type of materials and its dimensions. Unit of capacitance is Farad. Capacitance is expressed by following formula

$$C = \frac{K\varepsilon_o A}{t} \tag{A1.6}$$

where as 'A' area of electrodes, 't' is gap between the electrodes.

A1.2.6 Young's Modulus

Young's Modulus is ratio of stress (force per unit area) to strain (change in length per unit length). Unit of young Modulus is N/m^2.

$$Y = \frac{Stress}{Strain} \tag{A1.7}$$

A1.2.7 Density

The ratio of the mass to volume in the material, expresses in Kg/m^3

$$\rho = \frac{mass}{volume} \tag{A1.8}$$

A1.2.8 Curie Temperature

The Temperature at which the crystal structure changes from a non-symmetrical (piezoelectric) to a symmetrical (non- Piezoelectric) form, expresses in degrees Celsius.

A1.2.9 Pryoelectricity

Piezoelectric materials are also pryoelectric. They produce electric charge as they undergo a temperature change. When their temperature is increased, a voltage develops having the same orientation as polarization voltage. The change in electric field due to a temperature change is given as.

$$E_{pyro} = \frac{\alpha \Delta T}{K_3 \varepsilon_o} \tag{A1.9}$$

where as, E is the induced electrical field (volts/meter), α is the pyroelectric coefficient in Coulomb/$^0Cm^2$, ΔT is temperature difference in ^0C.

A1.3 Analytical Approach

The analytical method is demonstrated in this section. In this section relation between the voltage generation and force applied are discussed. The force F is applied to the rectangular piezoelectric plate of size L x T x W. The Figure A.2 demonstrates the

working of the rectangular piezoelectric plate. The voltage and charge develop by this force is given as

$$Q = F\, d_{33} \tag{A1.10}$$

$$\frac{V}{T} = \frac{F g_{33}}{LW} \tag{A1.11}$$

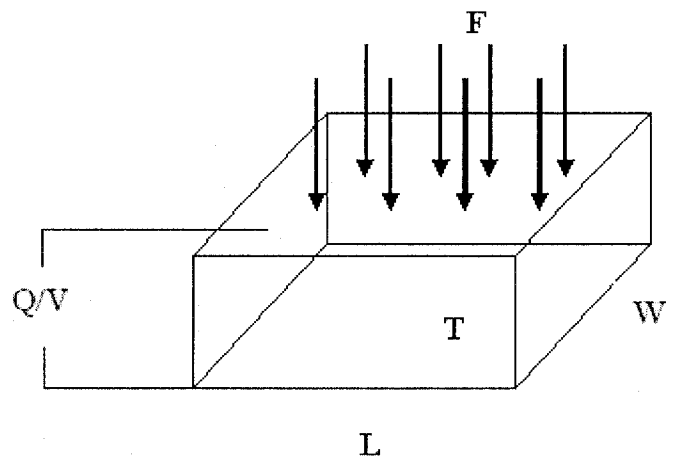

Figure A-2 voltage generation by piezoelectric substance

For ordinary solids, a stress σ merely causes a proportional strain ε, related by an elastic modulus, $\sigma = \varepsilon E$. Piezoelectricity is the additional creation of an electric charge by the applied stress. This is the direct piezoelectric effect. The charge is proportional to the force, and it is therefore of opposite sign for compression and tension. In terms of dielectric displacement **D** (charge **Q** per unit area) and stress σ, we may write

$$\mathbf{D} = \mathbf{Q/A} = \mathbf{d}\,\sigma \text{ (d expressed in coulombs/Newton)} \tag{A1.12}$$

There is also a converse effect. An applied electric field produces a proportional strain ε, expansion or contraction depending on polarity.

$\varepsilon = \mathbf{d}\, V$ (**d** expressed in meters/Volt) (A1.13)

For both effects, the proportionality constant is the piezoelectric constant **d**, which is numerically identical for both direct and converse effects.

$$\mathbf{d} = D/\sigma = \varepsilon/V \quad \text{(A1.14)}$$

High **d** constant is desirable for materials intended to develop motion or vibration, such as sonar or ultrasonic cleaner transducers. Another frequently used piezoelectric constant is **g** which gives the voltage produced by a stress. Its usual units are meter volts/Newton, simplified from (Volt/meter) /(Newton/square meter).

The **g** constant is related to the d constant by the permittivity $\mathbf{g} = \mathbf{d}/\varepsilon' = \mathbf{d}/K\varepsilon_0$ ($K = \varepsilon'/\varepsilon_0$, the relative dielectric constant, is the ratio between the charge stored on a electroded slab of material brought to a given voltage and the charge stored on a set of identical electrodes separated by vacuum. It is usually referred as dielectric constant, and is dimensionless)

High **g** constant is desirable in materials intended to generate voltages in response to a mechanical stress, as in a phonograph pickup.

On the other hand we have from hook's law: $\sigma = \varepsilon E$ then we can write: $\sigma = \mathbf{d}\, V\, E$, so $V = \sigma / \mathbf{d}\, E$ where E is the Young's modulus of the piezoelectric material. The piezoelectric coefficient d depends on piezoelectric crystals will be given by the manufacturer.

A.2 APPENDIX-2

SENSOR CHARACHTERISTICS

Before proposing the viable solution that could enhance tactile sensation, it is realized that the potential force sensing modalities has to be explored properly. Force can be measured by the alteration of the properties of the sensor. In some sensors the structural and electrical properties have been used as a parameter to measure force. Electrical Resistance might increase or in some the current may be generated. As the size of the sensor is small it is difficult to measure the structural deformation of the sensor, and hence the structural properties are measures using the changes in the electrical properties. Sensor has to be part of the transducer system before these properties changes can be realized. A transducer system is a device that senses either the absolute value or changes in some physical quantity such as force or strain, which converts into an electrical signal that can be used for measurement. The characteristics of the sensor currently used for measuring force, pressure and their corresponding quality are discussed in this section

A2.1 Quality of sensor

Choosing a sensor for a measurement or control system depends on several factors, such as cost, availability, and environmental factors. When choosing a sensor it is important to match its characteristics to the quality of output required. The best sensor for any job is one that has sufficient quality for the job, has adequate durability. The present study is mainly concerned with the sensing force between the endoscopic grasper and

tissue. This is very important since the artificial tactile sensing is going to augment the human dexterity. Some important specification were used to evaluate the tactile sensing, like signal to noise ratio, frequency response, spatial resolution, temperature drift, Sensitivity, dynamic range , linearity

The following section discusses what these terms mean. Theses characteristics can be applied to the whole measurement system and all components within a measurement system, including the sensor, signal conditioning unit, and display or recording device. There are different ways of expressing all of them, but usually they are stated as a percentage or as a maximum and minimum value, depending on the nature of the system and measurand, and the manufacturer's preference.

A2.1.1 Accuracy

The accuracy of a device or system is the extent to which any value it creates could be wrong, or the maximum error it may produce [80]. With a sensor, it is how close the output value is to the actual value of the measurand. In practice, every device will produce an error, however small, and will have some degree of accuracy rating. It may be expressed in terms of the measurement units involved. Alternatively it may be expressed as a percentage error of the range of the device.

Accuracy is related to absolute error. Absolute error, ε, is defined as the difference between the true value applied to a measurement system and the indicated value of the system (i.e. during calibration process)

ε = true value-indicated value,

From which the percent of accuracy is found by:

A= (1-lεl /true value) *100

A2.1.2 Calibration

Calibration refers to the units the scale of a sensor display or recorder is labeled in [81]. For example, our type of sensor measuring the force ratio of the sensed object generates an electrical output. The ratio of this voltage is proportional to the force ratio. Thus we can say that the sensor is calibrated in terms of the voltage ratio it measures.

A2.1.3 Drift

Drift is the natural tendency of a device, circuit, or system to alter its characteristics with time and environmental changes [81]. There is a change in the output characteristics while the inputs to the device have not changed, which affects accuracy. Drift occurs over different time scales for different reasons. One of the most common and influential drift inducing effects is a change in ambient temperature. This is why the specifications of many sensors state the effect of temperature on various characteristics of the device. On an older device drift may be caused by ageing affects on the materials it is made of, such as oxidation of metal elements. It can also be caused by the mechanical wear or self- heating of components in a system.

A2.1.4 Hysteresis

Hysteresis causes the difference in the output of a sensor when the direction of the input has been reversed. This produces error and so affects the accuracy of a device.

Not all sensors or measurement systems suffer from hysteresis. It is caused by various factors, particularly mechanical strain and friction.

A2.1.5 Signal-to-Noise ratio (SNR)

It is the ratio of the amplitude of the desirable signal to the amplitude of the noise signal (undesirable signal) at a given point of time. SNR is expressed as 20 times the logarithm of the amplitude ratio, or 10 times the logarithm of the power ratio. SNR is usually expressed in dB and in terms of peak values for impulse noise and root-mean square values of random noise. In defining or specifying the SNR, both the signal and noise should be characterized, e.g. peak-signal-to-peak-noise ratio, in order to avoid ambiguity. Sensors can be characterized by electrical impedance [82]. The performance of the sensor depends on the noise signal embedded in the signal. This is one of the fundamental parameters of sensor performance.

A2.1.6 Linearity

The linearity of a sensor is the amount by which the graph of its input against output is near to being a straight line [84].

The ideal transducer is one that has an output exactly proportional to the variable it measures (within the sensor's quoted range). No transducer's output is perfectly proportional to its input. However, the sensor user must be aware of the extent of the failure to be linear is often quoted on spec sheets as a +/- value for the sensor's output signal.

It may be quoted as being linear for a range of input values, as shown in Figure 1.13

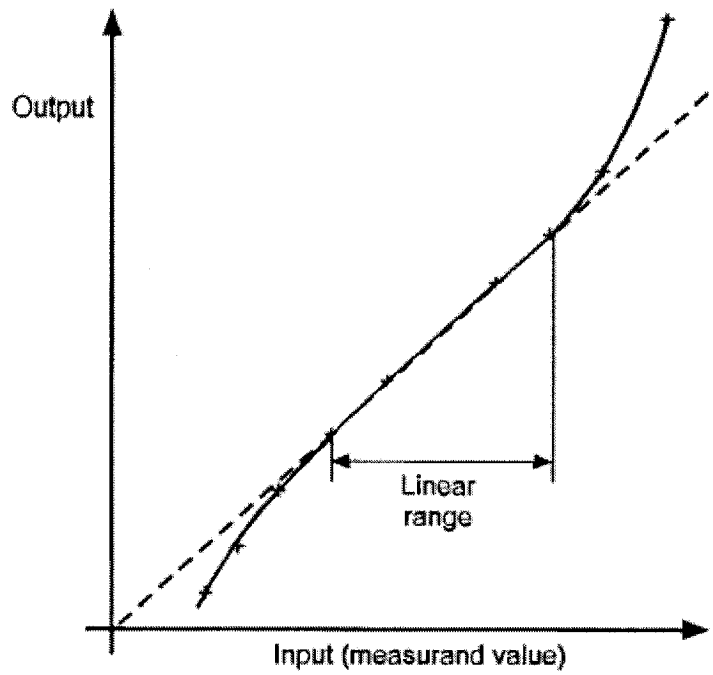

Figure A-3Linearity curve of a sensor

It may also refer to the maximum amount by which the graph deviates from being a straight line, quoted as a percentage of the operating range.

A2.1.7 Precision

The precision of a device is the degree to which it produces similar results for the same input on a number of occasions. Precision is often used in everyday language to mean accuracy, and hence the two are sometimes confused. However, in measurement terminology a sensor can be precise; giving a very similar output a number of times when measuring a fixed quantity, but, if there is a large error in the output it is not accurate. On a specification, precision is usually quoted in general terms (such as a high precision instrument). Repeatability (reproducibility) is a quantified measure of precision, and more likely to be quoted on a specification.

A2.1.8 Range

The operating range of a device is a statement of the limits in which it can function effectively. The operating range or "span" of a sensor is usually specified as the lowest and highest input values (measured variables) which it is capable of measuring. For example the range of operation of the tactile sensor that was fabricated is 10Hz-40Hz. It is important not to exceed these ranges because not only may the device fail to operate effectively, it could also damage other components of the system.

A2.1.9 Rating

The rating of a device relates to the recommended conditions, electrical or mechanical, under which it will successfully or safely operate. A description of the type of rating is usually given, for example maximum temperature rating, or average load rating.

A2.1.10 Reliability

The reliability of a device is similar to its operating life, and may often be quoted instead, depending on its nature. Reliability is the ability of a device to perform its function under specified conditions for a stated period of time, or a stated number of operations, whilst remaining within its specification.

A2.1.11 Repeatability

Values quote a sensor's repeatability or 'Reproducibility' indicates the range of output values that the user can expect when the sensor measures the same input values several times. In the other word it is a measurement of the ability of a device to produce identical indications or responses, for repeated applications of the same value of the physical quantity to be measured. It may be given as 6 a maximum percentage of the

reading, or within stated limits of each reading. For Example the sensor which was fabricated here and tested produced repeated results even after span of 6 months.

A2.1.12 Resolution

The resolutions with which a device senses or displays a value relates to the smallest input or change in input it is able to detect or, is the largest change in a measured value that will not result in a change in the sensor's output. Put more simply, the measured value can change by the amount quoted as resolution, without the sensor's output changing. It is usually expressed in terms of the smallest increment, which can be measured or sensed. The higher the resolution of a display, the smaller the increment it is able to measure. For example, a five-digit display which can measure a quantity to 0.0001 units has a higher resolution than a four-digit display measuring to 0.001 units. It is usually expressed as a percentage.

A2.1.13 Sensitivity

Sensitivity is the relationship (under fixed conditions) between changes in the output of a device to the change in input. The sensitivity of a sensor is the difference in its output values over a given range divided by the change in the value of the measurand. That is,

Sensitivity = (Maximum output value – minimum output value) /

(Maximum input value –minimum input value)

The units in which sensitivity is expressed are defined by the above equation and consequently vary depending on the nature of the device and measurand. Higher the

sensitivity greater is the precision and resolution power to the sensor. Sensitivity values generally required for tactile sensor are between $0.5 \times 10^{-2} - 1 \times 10^{-2}$ N [83].

If the relationship between the measurand and the output is linear, then the sensitivity will usually be expressed over this whole range. If it is non-linear, the sensitivity characteristics of the device will vary for different values, and so the sensitivity will usually be quoted for several ranges.

A2.1.14 Spatial Resolution

In tactile sensing, a space constraint plays a significant role in the design of the sensor. The sensor should be attuned to the space available without compromising the results. The thickness of the single tactile sensor is generally 1-2 mm

A2.1.15 Frequency Response

The frequency or the dynamic response in another property that need to be considered for the selecting a sensor. When the input or the applied force to the sensor is not static and it varies with time it is called dynamic input, In that case the sensor must be compatible to measure the dynamic responses. By using dynamic response of sensor vein pulse can be located and thus the damaging of veins could be avoided. Piezoelectric sensors are very sensitive to dynamic response. The ideal frequency response for any sensor would be from DC to 30Hz [4]. The sensors with good static and dynamic response are preferred.

A2.1.16 Temperature Variation

The variation of temperature caused changes in the properties of the transducers, which gives erroneous results. So the sensor output is required to be independent from

the temperature drift. Mostly the sensors are designed for the temperature of application. It is preferred to design a sensor in such a way that even a small change in the temperature would not affect the sensor functional drastically

All the above properties are discussed while focusing on the functionality of the sensor. But the viability of the sensor also depends on the physical shape, ruggedness, installation and financial constraints. Summarizing the requirements of the sensor, it can be concluded that sensor should be inexpensive, reliable and durable.